Sampling of Surface Metals Using Minimally Invasive Approaches and Spectroscopy

by

Kimberly Dawn Marie Charleton

Submitted to the Faculty of Graduate Studies of
The University of Manitoba

in partial fulfillment of the requirements of the degree of

Master of Science

Department of Chemistry
University of Manitoba
Winnipeg

THE UNIVERSITY OF MANITOBA

FACULTY OF GRADUATE STUDIES

*****

COPYRIGHT PERMISSION

Sampling of Surface Metals Using Minimally Invasive Approaches and Spectroscopy

BY

Kimberly Dawn Marie Charleton

A Thesis/Practicum submitted to the Faculty of Graduate Studies of The University of Manitoba in partial fulfillment of the requirement of the degree

MASTER OF SCIENCE

ACKNOWLEDGEMENTS

I would like to thank my supervisor, Dr. Goltz, for his continuous guidance and encouragement. Dr. Goltz has showed me different ways to approach research problems and was always there for academic and emotional support. I am especially grateful to my lab-mate and best friend, Tyler Buffie, for his ongoing love and support throughout my time as a Graduate student. I would also like to thank my friends and family for their unconditional support and encouragement to pursue my interests, for listening to my complaints and frustrations and for believing in me. This work would also have not been possible without the help of the following people, they are all gratefully acknowledged for access to materials and technical assistance: Cathy Collins (Winnipeg Art Gallery), Rob Ridgen and Ainsley Walton (Manitoba Archives), Ed Cloutis (University of Winnipeg), Sergio Mejia and Debbie Armstrong (University of Manitoba) and Eno Busse (Parks Canada). Funding for this research was provided by the Natural Sciences and Engineering Research Council of Canada and the Canadian Foundation for Innovation.

ABSTRACT

Minimal surface damage is essential for the analysis of valuable samples (e.g. cultural objects and painted artwork). In this work, different approaches were used to sample minute quantities of metals prior to analysis using spectroscopy. Pigments were sampled by contacting the cellulose from a cotton bud to a painted surface. The cotton bud was then digested in concentration HNO_3 prior to analysis. Identification of metals in pigments is extremely useful for art attribution and conservation. Pigment identification using Raman spectroscopy was also investigated. Microsampling using low power electrocorrosion was explored for identifying alloys. Rapid surface oxidation of alloys was carried out by applying potential (9 – 18V) between a metal alloy and a cellulose electrode that was made conductive using an aqueous solution of NH_4NO_3 or KCl. Metal ions diffuse into the cellulose as rapid surface oxidation of the metal occurs. Steel (316L, SRM 663), brass and aluminum alloys were used as test samples. For both techniques metals were determined using graphite furnace atomic absorption spectroscopy and electrothermal vaporization inductively coupled plasma mass spectrometry. The small sample size requirement and high sensitivity of these instruments made them very suitable for analyzing the samples. Solution nebulization (SN) ICP-MS was also used for obtaining a mass scan for most elements in the periodic table.

LIST OF FIGURES

LIST OF TABLES

1.0 INTRODUCTION

The need for sensitive, minimally-invasive, elemental analysis was the stimulus for this research. Several features of the analysis must be considered, including sensitivity, specificity, interference and damage to the surface of the object under investigation. With these attributes in mind, analytical chemists are constantly improving their techniques or adapting them from related fields. The present study will demonstrate the feasibility of microsampling techniques that are complementary to current analytical techniques.

This thesis is divided into two chapters. Chapter 1 presents work related to microsampling painted surfaces for pigment identification. Chapter 2 presents work related to electrocorrosion for rapid, minimally invasive sampling of alloys.

Inorganic pigments are used in paint for their opacity and colour[1]. The most stable pigments often occur naturally as minerals[2-5]. For example, metal oxides such as red ochre (Fe_2O_3) or chromium oxide (Cr_2O_3) can withstand even the harshest conditions of an outdoor environment. Other stable pigments consist of metal carbonates (azurite, $Cu_3(CO_3)_2(OH)_2$), sulphides (cadmium red, CdS) or sulphates (blanc fixe, $BaSO_4$). Numerous approaches are available to the conservator for identifying metals or pigments used in paintings, illuminated manuscripts and other cultural objects. Visual inspection and optical microscopy are useful for qualitatively identifying pigments. Obvious difficulties can arise with this approach because visual inspection is incapable of differentiating between chemically and structurally similar materials. As a result, spectroscopic techniques have become some of the most important tools used by

conservators for examining artwork and identifying pigments[6], including atomic spectroscopy, X-ray spectroscopy and Raman spectroscopy.

Pigment identification may be a tool that art historians can use for attribution or dating artwork by determining the *post quem*, earliest date, and *ante quem*, latest date, which gives a period of time based on the date pigments were introduced or manufactured[5]. Art historians are also interested in identifying pigments to illuminate artistic working methods; for example, the pigments an artist mixed to create specific hues. Perhaps the most worthwhile reasons for pigment identification are restoration and conservation. There is a significant role of the analytical chemist in the study of painted objects because pigment identification can be an important step prior to preservation and conservation. Pigments are affected by humidity, light, heat, gaseous atmospheric pollutants and storage conditions. Effects will vary depending on the type of pigments used for the artwork. Pigment identification can be used to identify restored areas from the original or if restoration is required, pigment identification can be used to determine the correct pigment for restoration. Touching up a painting may have negative visual effects if the new pigment is chemically incompatible with, or different from, the original[7-9].

The primary objective of the first chapter was to demonstrate that microsampling with a cotton bud[8,10] could be used together with atomic spectroscopy to determine metals and ultimately identify pigments found in paint. A second objective was to examine the possibility of using Raman spectroscopy for semi-quantitative analysis of mixed pigments. Finally, the application of this approach to painted artwork was investigated. For this project, a number of approaches were used in the analysis including: graphite

furnace atomic absorption spectroscopy (GFAAS), solution nebulization inductively-coupled plasma mass spectroscopy (SN-ICP-MS), electrothermal vaporization (ETV) ICP-MS and Raman spectroscopy.

The second chapter presents work related to microsampling for the determination of metals in alloys using low power electrocorrosion, a technique developed by our laboratory. Metallic objects of historical and cultural importance include metal statues, precious metals (e.g. jewelry) and utilitarian objects (e.g. cutlery). Identifying the metals present in these objects can be used for artist attribution and to determine artifact origins. For example, detailed isotope ratios can yield information used for geographical attribution of coins. Metal identification can also be useful for conservation as different alloys require specific welds based on the composition of the alloy.

The first objective was to investigate some of the properties and to examine the feasibility of using electrocorrosion for identifying metals in various alloys (e.g. brass, silver, steel, aluminum). A second objective was to illustrate the effect of low power electrocorrosion on the surface of an alloy. Finally, this methodology was applied to identify metals in an unknown alloy (museum object). For this project, a number of approaches were used in the analysis including: GFAAS, SN-ICP-MS, ETV-ICP-MS and scanning electron microscopy (SEM). Each chapter presents a feasible and promising approach for sampling valuable objects with high sensitivity.

1.1 Studying Valuable Objects

When examining valuable objects analytical techniques are typically employed to identify materials, assess the state of conservation (e.g. pigment darkening), and to determine appropriate restorative actions[11]. Analysis of cultural objects requires approaches that are either non-destructive or minimally-invasive. These remove minimal amounts of material and do not significantly modify the appearance of the object. To determine the appropriate method it is necessary to consider the requirements of the analysis, such as the type of information required (qualitative or quantitative) and the value of the object under investigation.

There are several approaches from experimental physics and analytical chemistry that can be applied to the analysis of cultural objects. Minimally-invasive spectroscopic techniques include X-ray fluorescence (XRF), proton-induced X-ray emission (PIXE), and neutron activation analysis (NAA). Microscopic techniques such as light microscopy are also used, as well as vibrational techniques such as Raman spectroscopy. Graphite furnace AAS, flame AAS (FAAS), ICP-MS and laser-induced breakdown spectroscopy (LIBS) can also be used but they tend to be more destructive and require samples to be removed from the object.

In most cases the application of a wide range of techniques is employed to obtain complementary results[12-13]. Several research groups have published articles using two methods of analysis for a single sample. For example, Malmqvist[14] and Johansson[15] have compared PIXE and XRF for the analysis of ancient metal objects. X-ray fluorescence is generally less sensitive than PIXE, but is better suited to heavy elements. Using a combination of both techniques would provide accurate results for a larger number of

elements. Other groups have described the use of various spectrometric methods to investigate painted artwork[16-17]. Ortega-Aviles et al.[16] report that there is a relationship between sampling a valuable object and the information that can be obtained from the analysis. Other groups have also investigated multi-analytical approaches. Andalo et al.[18] have examined a combination of non-destructive techniques, PIXE and Raman spectroscopy, for pigment identification in valuable painted artwork. Paternoster et al.[19] studied the use of XRF and micro-Raman spectroscopy to identify pigments in Roman era mural paintings. Sampling cultural objects becomes feasible when a large amount of information can be obtained from the sample; this is one of the main advantages of a multi-technique approach[16-17]. The literature illustrates that analytical techniques can be complementary rather than competitive.

It is important to consider many factors when developing an analytical technique. For example, the speed of analysis, as a rapid analysis can show general trends in the data and also allow multiple analyses of the same object or the analysis of a range of objects quickly[12,20]. High instrument sensitivity is required for trace elemental analysis and multi-elemental techniques allow many elements to be determined in a single measurement[7,20]. Also, mobile sampling and instrumentation that can function in an open air environment is beneficial because cultural objects may be large or irregularly shaped and transporting the object to the lab may be problematic.

1.2 Atomic Spectroscopy

Metal analysis can be carried out using spectroscopic methods such FAAS, GFAAS and ICP-MS, which typically require the target analyte to be dissolved in a dilute aqueous solution. Therefore, sample dissolution, usually in acid, may be required prior to analysis. Apart from traditional acid digestion, many sample preparation methods are useful for sample dissolution, including: microwave digestion, pressure ashing, ultrasonication, and anodic electrodissolution. The major drawback of these methods is that they will damage the object under investigation and may not be suitable for valuable samples, such as cultural objects and painted artwork, where the integrity of the object must be maintained.

1.2.1 Conventional Dissolution

Conventional dissolution is often carried out using acid mixtures or fusion mixtures of salts and peroxides[21,22]. The choice of sample preparation method depends on the nature of the sample as well as the analytical method. It is often best to use the mildest solution that will digest the sample, as stronger acids are more likely to increase the blank measurements[21]. Acid digestion uses mineral or oxidizing acids and an external heat source to decompose the sample matrix. Typically, samples are dried, weighed, and placed in an open container. After the addition of the digestion reagent, the vessel is covered and placed on a hot plate or other heat source. The sample is brought to a gentle boil and solution may be added during the digestion in order to prevent the sample from drying, which may result in the formation of less soluble species. After complete digestion the solution is then diluted to the appropriate volume for analysis. At this point,

filtration may be required to remove any insoluble material. Conventional dissolution may be a time-consuming step as some alloys may require several hours for complete dissolution[21].

1.2.2 Microwave Dissolution

Several methods have been developed to overcome some of the physical drawbacks of acid digestion such as contamination and loss of analyte due to sample volatility; these include microwave digestion[23-28], pressure ashing[23,28,29] and ultrasonication[30,31]. Microwave digestion was developed to increase the speed of dissolution by controlling temperature and pressure. The digestion occurs in an open or closed container made of temperature resistant polymers, which minimize contamination and loss of analyte. When closed containers are used they eliminate possible contamination from the lab atmosphere. Sealed containers also reduce evaporation, which minimizes the amount of acid required and the loss of volatile analyte species[24,25]. Current microwave ovens also have the benefit of automated electronics to control pressure and temperature, reducing instrumental variability from run to run and decreasing the attention required by the operator. Borszeki et al.[32] examined the use various pressurized devices for quantitative sample preparation of metal alloys. Hinds et al.[33] have reported that closed-vessel microwave dissolution reduces the amount of time and solvent required for metal dissolution when compared to conventional wet dissolution. Other groups have also compared wet and microwave dissolution and demonstrated that comparable results could be achieved between the two[34]. Ultrasonication uses an ultrasound probe or bath to vibrate the solution slurry;

however, it is usually limited to organic matrices such as biological samples[30,31]. Pressure ashing is another alternate method used to digest samples. The sample is weighed and placed in a quartz container with the appropriate acid solution. The containers are sealed and placed in a closed heating block, and nitrogen gas is used to pressurize the apparatus. Pressure ashing offers advantages similar to microwave digestion, as there is no loss of volatile species, sample preparation is rapid and contamination is minimized[28]. Wet digestion, microwave digestion and pressure ashing all prepare the sample separate from the analysis. To avoid the two-step analysis as well as the problems associated with wet digestion, electrodissolution has been developed.

1.2.3 Electrodissolution

Anodic electrodissolution has been studied as an alternative for rapid metal dissolution for the purpose of identifying surface metals in alloys[35,36]. Several groups have used electrodissolution for rapid metal analysis[35-40]. In electrodissolution the conductive metal sample acts as the anode. The metal sample and a cathode are immersed in an electrolytic solution, usually 0.5 – 1.5 M HNO_3. Typically, a current of 2 – 5 A (current density 1.6 – 5 A cm^{-2}) is applied. Sampling intervals are short, usually being less than 10 s and dissolution occurs via electrolysis or anodic stripping. A corrosion mechanism has been suggested by Stansbury and Buchanan[41] and is as follows: $M + nH_2O \rightarrow M^{n+} + nOH^- + n/2\ H_2$ and $M^{n+} + nOH^- \rightarrow M(OH)_n$. After electrolysis the electrodissolved sample can be determined using either voltammetry or spectroscopy. Electrodissolution is not useful for samples that cannot be immersed in an electrolytic solution such as large or irregularly shaped objects[37,40,42].

It is also possible to use electrodissolution for on-line sample preparation, thus eliminating the need for a two step analysis. For example, Packer et al.[39] investigated on-line electrolytic dissolution for metal identification using isotope dilution ICP-MS. Sample dissolution was obtained by using a 1.5 M HNO_3 electrolytic solution and applying a current intensity of 2.5 A for 4 s (current density 5 $A \cdot cm^{-2}$). The electrodissolved solution was filtered through wool glass to remove any solid particles generated during electrolysis. Other groups have also explored electrodissolution for on-line dissolution of alloys such as steel[42-47]. For example, Bergamin et al.[43] dissolved alloys for the determination of Al and Mn using flow injection analysis. Several groups have analyzed steel[44] and aluminum[46] samples using electrolytic dissolution with FAAS.

In many cases, it is necessary to avoid a destructive sample preparation technique. Several analytical techniques are available to the analyst that can be performed without prior sample preparation; these include laser ablation (LA) ICP-MS, LIBS, XRF, PIXE, and NAA. These techniques tend to be less invasive and have been used extensively for the study of valuable objects.

1.3 Laser Ablation

Laser ablation (LA) ICP-MS offers low detection limits, wide linear dynamic range, spatial resolution, and small sample size (μg)[48]. A sample is usually placed in a small chamber and, as the ablation takes place a carrier gas transports the ablated material to the ICP-MS. Typically, ablated craters are invisible to the naked eye and so LA can be considered virtually non-destructive for small spot sizes. Coupling solid sample introduction to techniques such as ICP-MS is extremely useful because it offers quasi-simultaneous multi-element analysis in one acquisition[48]. For larger objects (> 3 cm), a fragment of the material must be removed to fit into the sample chamber but this is not always possible. As a result, Devos et al.[48] investigated LA-ICP-MS for the analysis of large silver objects using a laboratory built instrument that enclosed the plume of ablated material but not the entire sample.

1.4 Laser Induced Breakdown Spectroscopy

Laser induced breakdown spectroscopy is a rapid, minimally invasive, atomic emission technique for performing elemental analysis of materials such as painted objects and alloys[49]. A Nd-YAG laser is used to excite the atoms on the surface of a cultural object and the excited atoms produce an emission pattern, which is indicative of the metals present[9,49]. Damage to the painted surface can be minimized by focusing the laser on a small area (1 μm^2)[49-54]. This method is characterized by high sensitivity and selectivity and small sample sizes (< 1 μg). An added benefit of LIBS is that depth profiling of different paint layers can be achieved by measuring successive pulses at the

same spot[9,49]. To monitor and safeguard against possible damage, LIBS is commonly used during laser cleaning. Anglos et al.[49] examined the use of LIBS for in situ analysis of pigments in painted artwork and report craters 30 – 60 μm in diameter and less than 10 μm deep. Quantitative analysis can be hampered by the matrix effect in the spark, sample inhomogeneities and multiple paint layers. Colao et al.[55] investigated LIBS for the semi-quantitative analysis of various artworks. They used a Nd:YAG laser emitting at 355 nm with a 10 ns pulse width. The pulse energy was set between 10 – 25 mJ depending on the artifact and the laser beam was focused using a 150 mm focal length lens. The study was aimed at improving data repeatability and enhancing the ability to identify minor elements.

1.5 X-Ray Fluorescence

X-ray fluorescence is one of the most common methods for analysis of cultural objects[11,20,8,56-59]. The sample is bombarded with X-rays with sufficient energy to excite the inner shell electrons. A secondary X-ray beam is emitted as the electrons from outer shells drop down into the vacant inner-shell positions; this is known as the fluorescence signal. The fluorescence signal is characteristic for each element and is detected by an X-ray spectrometer with collimators, a Bragg crystal or an X-ray detector. The elemental composition of the sample can be calculated from the wavelength and intensity of all the spectral lines[8]. Traditional X-ray spectrometers use scintillation or gas-flow detectors which determine the spectrum sequentially (~ 1 h). Energy dispersive XRF uses a solid-state Si-semiconductor detector and the results are processed simultaneously by a pulse-height analyzer. The energy of the peak is used for metal identification and the

abundance is proportional to peak intensity. For artwork, fluorescence can originate from surface contamination such as varnish (e.g. shellac), the ground layer (e.g. $CaCO_3$) or the support (e.g. canvas)[60]. Aloupi et al.[61] examined various X-ray spectrometric techniques for the analysis of pigments in painted objects. Milazzo et. al.[59] examined quantitative energy dispersive (ED) XRF analysis of ancient coins and have developed methods for the accurate quantitative XRF analysis of cultural objects that have irregular shapes and non-geometric reliefs on their surface.

A range of XRF instruments exists from synchrotron beamlines to portable spectrometers. Synchrotron sources are generally not useful for analyzing metallic objects because of the high primary intensity of the microbeam[20]. In general, XRF can have low measurement sensitivity for lighter elements ($Z < 13$)[11]. Quantification errors occur when XRF is applied on curved metal surfaces and as a result, the use of conventional XRF instruments (large beam diameter) for quantitative analysis is limited. Micro-XRF offers better lateral resolution because small beams allow sampling on locations that resemble flat surfaces[20]. When a small beam diameter is employed for both XRF (and PIXE) specific site analysis and elemental mapping is possible[62].

The major drawback of many spectroscopic techniques is that in order to fit into the sample chambers of some instruments, samples must be removed from the original object and in many cases this is not possible. Several portable XRF instruments have been reported; however, these instruments suffer from poor sensitivity (100 ppm vs. 10 ppm for benchtop models)[60]. To overcome this problem, total reflection XRF (TXRF) has been developed and applied to the analysis of pigments in the painted artwork[60,63] and illuminated manuscripts[64]. Traditional XRF excitation geometry is 45°/45° whereas

in TXRF the X-rays from the source are totally reflected at a glancing angle of only 0.1° relative to the sample[8]. Total reflection can occur as radiation travels from one medium to another with a smaller refractive index. When X-rays are being reflected, any solid medium has a smaller refractive index than air so total reflection is generally possible[65]. Total reflection XRF is characterized by high line intensities and low backgrounds because the primary beam is totally reflected and the incident X-ray beam has minimal interaction with the carrier. An energy dispersive detection system such as a Si(Li) detector is placed at right angles to where the reflected X-rays contact the sample. For many elements the required sample size is on the order of a few picograms, which makes TXRF extremely useful for micro, trace and surface layer analysis[8,10,65]. Samples can also be quantified by the addition of an internal standard. The main advantage of TXRF is that the analysis is non-destructive and the sample can be measured repeatedly. It also has multi-element capabilities and high detection power for heavier elements. One drawback of TXRF is that the pigment particle size must be restricted to a few micrometers; this may be a problem for pigments with large particle sizes such as lead white and cerulean blue (10 – 30 μm)[3,4]. Other disadvantages include the requirement for a clean, dust-free, lab environment; TXRF is unsuitable for organic pigments and typically XRF measurements are not sensitive for elements with atomic mass less than 13[10,65].

Central to the success of TXRF is the sampling approach used for valuable objects, specifically paintings. Typically, a very small amount of pigment is gently removed using a cotton bud by rubbing the paint surface. Since only a microgram quantity of pigment is required, there is minimal, if any, physical damage to the paint

surface. When approaches using atomic spectroscopy are combined with molecular spectroscopy (i.e. Raman spectroscopy) they become extremely powerful tools for identifying most inorganic pigments that are used in paint[63,64]. Klockenkamper[8] and Devos[10] have examined the use of sampling with a cotton bud and TXRF for the analysis and characterization of inorganic pigments and inks. They report that there is no visible damage from the contact with the cotton bud and that the cotton is versatile, easily transported and conservators are accustomed to using cotton buds for art restoration. Because the sampling method removes a small quantity of paint, it is possible to sample a greater number of areas on the painted surface and sampling is not restricted to damaged or marginal areas, which is often the case for invasive techniques[10]. Sampling with a cotton bud is also not limited to painted artwork; it can be applied to all painted objects such as sculptures, illuminations, coloured characters in manuscripts and printed books, painted leather, textile and paper[60]. The drawback of sampling with a cotton bud is that the painted surface needs to be free of varnish and other surface treatments.

Much of the work on pigment sampling using a cotton bud involves XRF; however, some work has been carried out using GFAAS[60]. The disadvantage of using GFAAS is that analysis can be slow as only one element can be determined at a time. Fortunately, for most samples there are a limited number of elements (< 3) that correspond to a specific pigment. Furthermore one potential advantage of GFAAS over TXRF is its greater sensitivity.

1.6 Proton Induced X-Ray Spectroscopy

Proton induced X-ray emission uses a charged particle beam of protons as a means of X-ray production for non-destructive trace element analysis[20,66-71]. X-ray spectroscopic methods are multi-elemental and this best illustrated by PIXE. For example, one irradiation of about ten minutes can yield reasonable detection limits over a wide interval of atomic numbers, whereas with secondary target XRF two or three irradiations with different target materials are usually required[15]. A study by Johansson et al.[72] demonstrated that PIXE could be used to detect many elements simultaneously with good sensitivity while using a high resolution Si(Li) photon detector and MeV proton beams. One drawback of using PIXE analysis for cultural objects is that the size, shape or nature of the object may not be compatible with the vacuum and the small sample enclosures of the instrument. The limit of detection of proton probe techniques can be as low as a few ppm; this is 2-3 orders of magnitude better than electron induced techniques (e.g. XRF) but orders of magnitude poorer than NAA and AAS[73]. Swann's research group has been investigating PIXE for the analysis of art and archaeology for the past two decades and have reported problems detecting Ca, Pb and Fe[74-76]. This is significant as Pb and Fe are present in a number of alloys and pigments and Ca in matrices (e.g. plaster). It is also difficult to obtain quantitative results because the analysis requires standards of similar composition and the results obtained for the surface may not reflect the bulk composition[69]. The penetrating range of PIXE is approximately 30 μm for 2.5 – 3.0 MeV protons[77] and when PIXE is used with variable proton energy it is possible to obtain an elemental depth profile. When PIXE is combined with the Rutherford backscattering (RBS) technique, composition of the surface relative to the

bulk can be determined[61]. A serious drawback of PIXE analysis is the possibility of energy deposition, which may damage the surface of the object. According to a report by Malmqvist[14], some damage is unavoidable. Gyodi et al.[69] describe the use of an external beam PIXE for the analysis of a metal statuette and the painted surface of a wooden relief. Hajivaliei et al.[66] used PIXE analysis to determine the provenance of ancient Indian coins and Demortier et al.[70] have investigated the use of external beam PIXE to study gold jewelry.

Surface sampling techniques (< 100 μm depth), such as XRF and PIXE, may be affected by the presence of surface corrosion and contamination because the depth of analysis is usually less than the patina thickness[68,76]. For example, aged silver typically has a patina with a thickness ranging from a few micrometers to hundreds of micrometers. This can be a result of artificial enrichment with Ag after the minting process, or due to naturally selective corrosion phenomena[59]. The presence of a patina makes it very difficult to achieve quantitative results through direct, non-destructive surface analysis because it is not always possible to remove the patina due to curatorial concerns[74]. Metals can be pre-treated to remove the surface corrosion; however, surface treatments tend to be destructive in nature. Swann et al.[74] have also demonstrated that surface treatments do not ensure that the area is corrosion-free. They have reported that the visible appearance alone is not sufficient to indicate complete removal of surface contamination. In many cases however, exhaustive quantitative analysis is not required in order to achieve material identification. For example, differentiating between brass, bronze, silver or tin alloys is possible using qualitative analysis.

1.7 Neutron Activation Analysis

Neutron activation analysis offers good sensitivity (ppb) and is especially useful for the determination of some trace elements (e.g. Pb and Fe)[78,79]. A compound nucleus forms in an excited state when a neutron interacts with the target nucleus via a non-elastic collision. The excitation energy of the compound nucleus is due to the binding energy of the neutron with the nucleus. Almost instantaneously the compound nucleus will relax into a more stable configuration through emission of one or more characteristic gamma rays. In most cases, this new configuration yields a radioactive nucleus which also decays by emission of one or more characteristic gamma rays, but at a much slower rate according to the unique half-life of the radioactive nucleus. Depending upon the particular radioactive species, half-lives may vary from fractions of a second to several years. Instrumental NAA is a multi-element technique that can be used on a sample with or without sample preparation; however, typically, it is not possible to irradiate the entire object and so samples must be removed prior to analysis and used either as a powder or a pellet[71]. To determine larger numbers of elements with good sensitivity it is necessary to use multiple irradiations with different decay times, which can last up to one month. Since the number of samples is limited the irradiations are usually performed on a single sample, leading to error. Similar to other techniques, NAA can suffer from interferences among some elements (e.g. ^{76}As and ^{122}Sb)[80] and routine applications of NAA can be limited by the availability of a reactor[79]. Several groups have demonstrated that NAA can be used to characterize cultural objects[78-80]. Carrot et al.[80] report small sample size requirements (100 mg); however, this is large relative to other techniques such as X-ray emission and atomic absorption.

1.8 Raman Spectroscopy

Raman spectroscopy has emerged as an important technique for the identification of pigments on manuscripts, paintings and other works of art by identifying the chemical structure of pigments in paint[18,54]. An incident laser beam is focused on individual pigment particles using a microscope objective. The same objective collects the scattered light and directs the light to a beam splitter in the optical path to the monochromator and then to the detector. The beam splitter reduces the overall efficiency of the system creating the need for high power lasers to balance the loss of the Raman signal[9]. A pinhole is used to reduce the amount of unwanted light collected from outside the focal point of the laser beam; however it also reduces the efficiency of collection. The efficiency is increased by using high-sensitivity CCD detectors and wavelength specific holographic edge filters that block unwanted Raleigh scattering. The principal advantage of CCD detectors and edge filters is that lasers can be low-power and air- cooled, which makes these instruments more compact, less expensive and easier to operate and maintain. A Raman spectrometer can also be interfaced with a fiber-optic probe enabling the user to obtain spectra from large irregularly shaped objects that would not fit onto a microscope stage[9].

Unlike atomic spectroscopy, Raman spectroscopy can be used to identify organic as well as inorganic pigments. For example, Raman spectroscopy has been used to determine the presence of indigotin ($C_{16}H_{10}N_2O_2$), a common organic dye[16]. The technique has high spectral (1 cm^{-1}) and spatial (1 μm) resolution, can be performed *in situ* and is non-destructive, has high sensitivity and high reproducibility. A drawback of Raman spectroscopy is the possibility of broadband fluorescence, that can overwhelm

Raman signals (especially for oil and varnished paintings)[63]. Most contemporary Raman spectrometers include a fluorescence background correction feature. Raman spectra also require interpretation but spectral databases are readily available, such as the libraries of Raman spectra of various painting materials including pigments[81-87]. Civici et al.[63] investigated Raman spectroscopy as a tool to identify organic pigments and confirm inorganic pigments following metal identification using atomic spectroscopy. Several samples were removed by scalpel from areas, which were already damaged, for Raman analysis. Identification of pigments was performed by comparing the measured spectra with the data in Raman libraries. Bruni et al.[88] examined the use of vibrational microscopy and TXRF for the analysis of pigments in Italian frescoes. Other groups have also reported using Raman on painted manuscripts[89] and artwork[90].

2.0 EXPERIMENTAL

2.1 Chemicals

All solutions were prepared using de-ionized water (18 MΩ cm^{-1} Milli-Q). Standard metal solutions were prepared by appropriate dilution from 1000 μg ml^{-1} standards (SCP Science). High purity AR Select® Plus HNO_3 (Mallinckrodt) was used for acid dissolution and solution matrix matching; HCl (Mallinckrodt), HF (Mallinckrodt) and H_2SO_4 (ACP) were used to optimize acid dissolution; KCl (Aldrich) and NH_4NO_3 (Aldrich), were reagent grade. All glassware, including Petri dishes and glass scintillation vials, were pre-soaked in 50% HNO_3 for at least 24 h and rinsed with de-ionized water prior to use.

2.2 Commercial Artist Paints

A number of commercially available oil (Grumbacher) and water colour (Grumbacher) paints were sampled to demonstrate that sampling with a cotton bud could be applied to a variety of pigments with different properties such as composition and pigment particle size. Table 2.2.1 includes a list of artist paints as well as the chemical name and formula. The target metal for each pigment is also indicated.

Table 2.2.1: Inorganic pigments

White Pigments	Chemical Name	Formula	Target Metal
Flake White	basic lead(II) carbonate	$2PbCO_3 \cdot Pb(OH)_2$	Pb
Chinese White	zinc oxide	ZnO	Zn
Lithophone	zinc sulfide, barium sulfate	$ZnS, BaSO_4$	Zn, Ba
Green Pigments			
Olive Green	Cr(III) oxide	Cr_2O_3	Cr
Blue Pigments			
Cobalt Blue	Co(II)-doped alumina glass	$CoO \cdot Al_2O_3$	Co
Prussian Blue	Fe(III) hexacyanoferrate(II)	$Fe_4[Fe(CN)_6]_3 \cdot 14\text{-}16H_2O$	Fe
Cerulean Blue	Co(II) stannate	$CoO \cdot nSnO_2$	Co
Red/Brown Pigments			
Cadmium Red	Cd(II) sulfide	CdS	Cd
Red Lead	Lead(II,IV) oxide	Pb_3O_4	Pb

2.3 Metal Samples

Several ferrous and non-ferrous alloys were used as test samples in various experiments. Bulk and trace elemental compositions can be found in Tables 2.3.1 through 2.3.5. Standard reference material (SRM) 663 (Table 2.3.3) was used for semi-quantitative analysis. The samples studied were obtained from Welders Supplies. The advantage of using this type of sample was that their approximate composition was known and they were readily available. The surfaces were treated prior to their first use by filing and polishing the surface and rinsing with de-ionized water.

Table 2.3.1: Composition of Allegheny Ludlum Type 316L Stainless Steel.

Component	Wt. %	Component	Wt. %
C	0.03	N	0.1
Cr	16-18	Ni	10-14
Fe	62-69	P	0.045
Mn	2	S	0.03
Mo	2-3	Si	0.75

Table 2.3.2: Composition of Austenitic Standard Type 304L Stainless Steel.

Component	Wt. %	Component	Wt. %
C	0.03	Ni	8-12
Cr	18-20	P	0.045
Fe	Balance	S	0.03
Mn	2	Si	0.75
N	0.10		

Table 2.3.3: Composition of SRM 663 Stainless Steel.

Component	Wt. %	Component	Wt. %
Al	0.24	Mn	1.50
Co	0.048	Si	0.74
Cu	0.098	V	0.31
Pb	0.0022	Cr	1.31
Ni	0.32	C	0.57

Table 2.3.4: Composition of Aluminum 6061-T6.

Component	Wt. %	Component	Wt. %
Al	98	Mn	< 0.15
Cr	0.04-0.07	Si	0.4-0.8
Cu	0.15-0.4	Ti	< 0.15
Fe	< 0.7	Zn	<0.25
Mg	0.8-1.2		

Table 2.3.5: Composition of 2xxx Type Aluminum.

Component	Wt. %	Component	Wt. %
Al	Balance	Si	> 0.4
Cu	4 - 5.75	Zn	> 0.3
Bi	0.2 - 0.9		
Sn	0.12 - 1.0		
Fe	< 0.7		

2.4 Instrumentation

Absorption spectroscopy was carried out using a PerkinElmer 3100 flame atomic absorption spectrophotometer (FAAS) and a PerkinElmer AAnalyst 800 graphite furnace atomic absorption spectrophotometer (GFAAS) equipped with an AS800 autosampler (Fig. 2.4.1). Instrumental parameters for the GFAAS and FAAS can be found in Tables 2.4.1 and 2.4.2 respectively. For GFAAS, Zeeman Effect background correction was used for all measurements. A Pd modifier (500 ppm $Pd(NO_3)_2$) was also employed for the analysis of Mn. External calibrations and the method of standard addition were used for quantitative analysis.

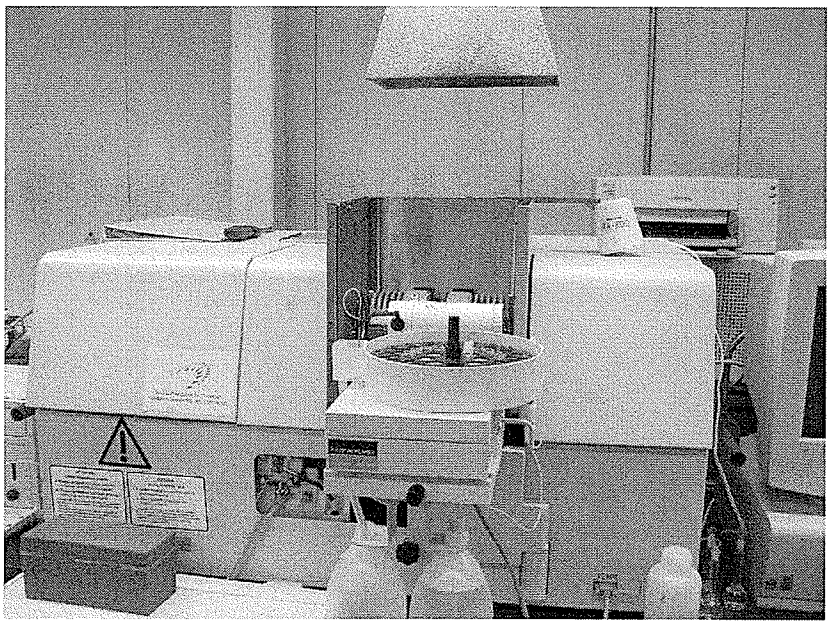

Figure 2.4.1: Perkin-Elmer AAnalyst 800 Graphite Furnace Atomic Absorption Spectrophotometer (GFAAS) with Zeeman Effect background correction equipped with a L'vov furnace.

Table 2.4.1: Furnace heating program for the PerkinElmer AAnalyst 800 GFAAS.

Element	Step Temperature (°C)			
	Dry	Char	Atomize	Clean-out
Ag	110	800	1700	2450
Cr	110	1500	2300	2450
Cu	110	1200	2000	2450
Fe	110	1400	2100	2450
Ni	110	1100	2300	2450
Mn	110	800	2200	2450
Pb	110	850	2000*	2450
Co	110	1400	2400	2450
Zn	110	700	1800	2450
Cd	110	500	1500	2450
Ramp (s)	1	10	0	1
Hold (s)	30	20	5	3

* changed from standard furnace conditions

Table 2.4.2: Instrumental operating parameters of the PerkinElmer AAnyalyst 800 GFAAS and the PerkinElmer 3100 FAAS.

Element	Ag	Cr	Cu	Fe	Ni	Mn	Co	Cd	Zn	Pb
Wavelength (nm)	328.0	232.0	324.7	248.3	232.1	279.5	242.5	228.8	213.9	283.3
GFAAS slit (nm)	0.7	0.2	0.7	0.2	0.7	0.2	0.2	0.7	0.7	0.7
FAAS slit (nm)	0.7	0.2	0.7	0.2	0.7	0.2	0.2	0.7	0.7	0.7
Flame Type*	R	R	L	L	L	L	L	L	L	L

*R, rich/reducing; L, lean/oxidizing

A PerkinElmer Elan DRC II inductively coupled plasma mass spectrometer (ICP-MS) with solution nebulization was also used for metal identification (analyses performed by Debbie Armstrong at the University of Manitoba, Winnipeg, Manitoba), while an ETV-ICP-MS was used for pigment analysis (analyses performed by Patricia Grinberg at Chemical Metrology, Institute for National Measurement Standards, National Research Council of Canada, Ottawa, Ontario). Experimental parameters for the ICP-MS instruments are indicated in Tables 2.4.3 and 2.4.4. With ETV-ICP-MS the multi-elemental analysis used a temperature program (Table 2.4.4), which required compromise conditions for vaporizing more than one element. To reduce spectral interferences from ArO, Fe was also analyzed in DRC mode using NH_3 with a gas flow rate of 0.3 ml $minute^{-1}$.

Table 2.4.3: PerkinElmer Elan DRC II SN-ICP-MS instrumental operating and data acquisition parameters.

ICP Mass Spectrometer	
RF power	1100 W
Coolant Ar flow	15.0 l $minute^{-1}$
Auxiliary Ar flow	1.4 l $minute^{-1}$
Carrier Ar flow	1.0 l $minute^{-1}$
ICP-MS Data Acquisition	
Lens setting	auto lens
Dwell time	50 ms
Scan mode	peak hopping
Signal measurement	average counts

Table 2.4.4: Instrumental operating and data acquisition parameters of the ETV-ICP-MS.

Step	Temperature (°C)	Ramp (s)	Hold (s)	Ar Flow Rate (ml min^{-1})
Dry	120	10	60	300
Char	400-800	10	30	300
Atomization	2000-2400	0	5*	150
Clean out	2400	0	5	300

* read step; masses monitored: Pb, Zn, Ba, Ti, Fe, Cr, Cu, As

A Cambridge Stereoscan 120 Scanning Electron Microscope equipped with a 4-quadrant semi-conductor back scattered electron detector and a Kevex 7000 energy dispersive spectrometer was used to collect SEM images and ED-XRF data (analyses performed by Sergio Meija at the Univeristy of Manitoba, Winnipeg, Manitoba).

2.5 Raman Spectroscopy Instrumentation

Raman spectroscopy was employed for confirmation of pigment identity. Two spectrometers were used, a DeltaNu Advantage 200A™ and a DeltaNu Rockhound™ each with a different sampling procedure.

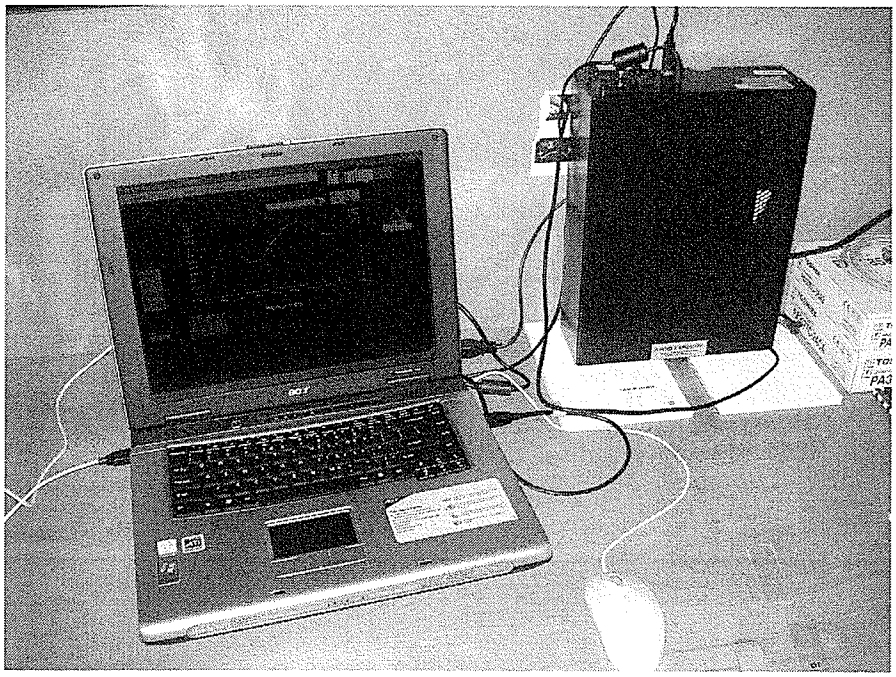

Figure 2.5.1: DeltaNu Advantage 200A^{TM} Raman spectrometer.

A DeltaNu Advantage 200A^{TM} (Fig. 2.5.1) was used without the sample holder in order to obtain spectra from flat surfaces. The Raman was held vertical and optimal signals were obtained when the instrument was less than 1 cm from the surface. The sampling area was approximately 1 mm^2. Typical measurement intervals for each spectrum were 5 – 10 accumulations of data collected over a time interval of 30 – 59 s each. Each spectrum was corrected for background optics signal and fluorescence was minimized through background correction. Whenever possible, ambient light was kept to a minimum to avoid extraneous radiation. Spectra were processed using DeltaNu software and Microsoft Excel.

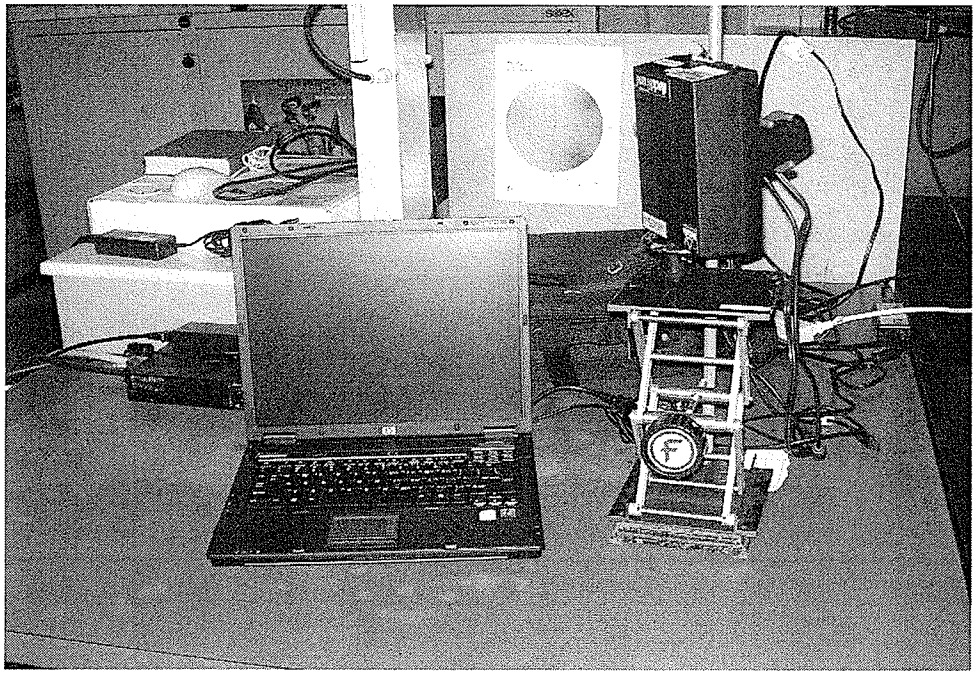

Figure 2.5.2: DeltaNu Rockhound™ Raman spectrometer.

The DeltaNu Rockhound™ (Fig. 2.5.2) was designed to be used in-situ and so it was not necessary to remove the sample holder. The instrument was held in position using a ringstand and a labjack was used to maneuver the sample relative to the probe. With this probe, optimal signals were obtained when the instrument was less than 1 mm from the surface. Typical measurement intervals for each spectrum were 5 – 10 accumulations of data collected for 1 s. Background correction and experimental condition where the same as for the Advantage 200A™.

Table 2.5.1: DeltaNu Raman spectrometer operating and data acquisition parameters.

	Advantage200A™	Rockhound™
Laser power	3 mW	100 mW
Laser wavelength	633 nm HeNe	785 nm solid state diode
Spectral Range	200 – 3400 cm^{-1}	100 – 2000 cm^{-1}
Resolution	10 cm^{-1}	8 cm^{-1}
Acquisition time	30 – 59 s	1 s
Accumulations	5 – 10	5 – 10

Table 2.5.2: Library of selected Raman bands[52,87].

Pigment	Wavenumbers[a] (cm^{-1}) and relative intensities[b]	Excitation wavelength (nm)
Flake White	665 vw, 687 vw, 829 vw, 1050 vs	514.5
Chinese White	331 w, 383 w, 438 vs	514.5
Lithophone	216 w, 276 vw, 342 m, 453 m, 461 w(sh), 616 w, 647 w, 988 vs	514.5
Olive Green	221 vw, 308 w, 349 w, 552 vs, 611 w	514.5
Cobalt Blue	203 vs, 512 vs	514.5
Prussian Blue	282 vw, 538 vs, 2102 m, 2154 vs	514.5
Cerulean Blue	495 m(sh), 674 vs	514.5
Cadmium Red	136 w, 239 m, 335 vw(br), 988 s	1064[52]
Iron Oxide	224 vs, 291 vs, 407 m, 494 w, 608 m	632.8
Red Lead	65 w, 122 vs, 144 m, 148 m, 150 m, 224 w, 232 vw(sh), 314 w, 391 w, 456 vw, 477 vw, 550 vs	1064[52]

[a] ± 1 cm^{-1}

[b] s, strong; m, medium; w, weak; v, very; (sh), shoulder; (br), broad.

2.6 Pigment Removal with a Cotton Bud

A cotton bud was gently contacted with a painted surface to remove small amounts of paint (~ 1 μg) (Fig. 2.6.1). After sampling, the cotton bud was placed in a 25 ml glass vial and 2 ml of HNO_3 was added. The vial was then placed on a hotplate at low temperature to evaporate most of the acid (~ 1 h). The cotton swab stick was removed once the cotton had decomposed; the stick was rinsed with a small volume (100 μl) of the HNO_3 in order to ensure pigment was not being removed from the vial. After heating, the vials were removed from the hotplate and allowed to cool. The remaining acid was then diluted with de-ionized water. Dilution volumes were dependent on the pigment and the analysis method. After dissolution there was no cotton left remaining in the vial and as a result centrifugation and/or filtration was not required. Analysis was performed using FAAS or GFAAS and metals were quantified using matrix-matched standards.

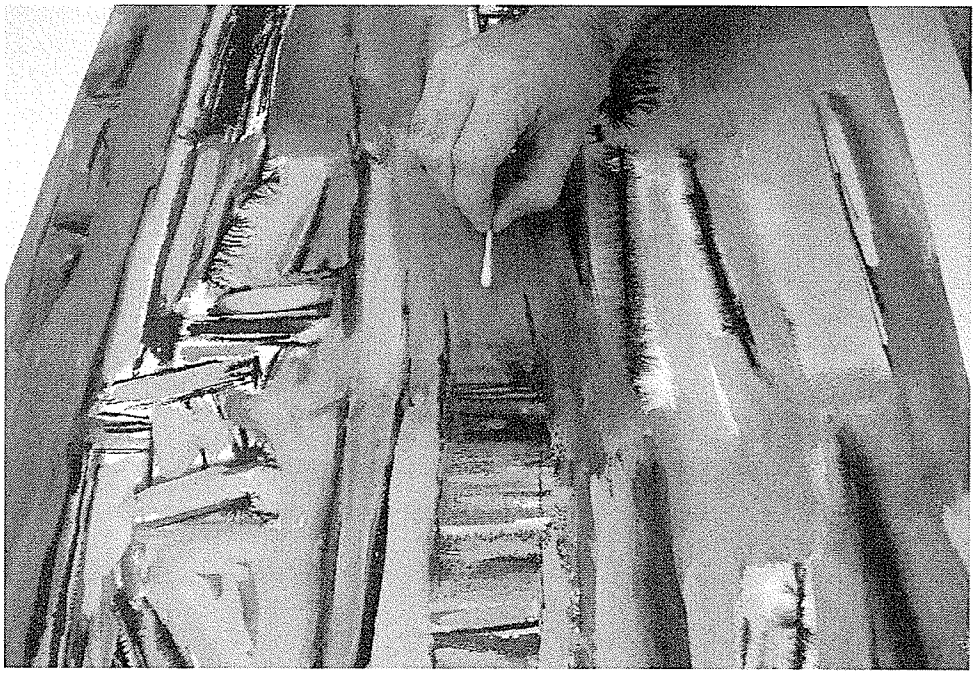

Figure 2.6.1: Pigment removal by contact with a cotton bud.

2.7 Paint Digestion Optimization

A small amount (25 μg) of dried artist paint was weighed into a glass scintillation vial and various acid combinations were added to each vial. Cotton buds were also added to the vials to simulate actual sampling conditions. The vials were heated on a hotplate at low temperature for approximately one hour or until there was minimal acid left in the vial (1 ml or less). Prior to analysis, all solutions were mixed at the same time and were allowed to sit for approximately 1 h; this allowed the undigested material to settle to the bottom of the vial. The rest of the procedure was the same as for pigment removal with a cotton bud. Analysis was performed using FAAS.

2.8 Low Power Electrocorrosion

Several 9 V and 1.5 V (AA) batteries were used in series to generate 3 – 27 V of applied potential. Filter paper (VWR 5.5 cm) was sectioned in approximately 1 cm x 2 cm pieces using tweezers wrapped in Parafilm® wax to minimize metal contamination. Filter paper was chosen because it is flexible and was found to be free of transition metals. Flexibility was required to sample curved surfaces and small spaces. The filter paper was attached to the anode of a 9 V battery by wire and alligator clip. The paper was partially submerged into a 0.3 - 2.4 M aqueous solution until the solution diffused through the cellulose. The paper was then placed on the bottom of a Petri dish (Fig. 2.8.1). The metal sample was attached to the cathode of the 9 V battery by wire and alligator clip. The metal was then placed on top of the filter paper in the Petri dish for a specified time interval, typically 10 to 120 s. After corrosion, the filter paper was torn away from the alligator clip with tweezers and placed into a polystyrene cup. The portion

of paper in contact with the alligator clip was discarded. Metals were extracted using concentrated HNO_3 in pre-weighed disposable 1.5 ml polystyrene cups, which were not pre-treated prior to use. The site of analysis on the Petri dish was washed with 50 µl of de-ionized water, which was then removed and added into the polystyrene cup. Approximately 2 ml of de-ionized water was added to dilute the contents of the cup, which was then weighed a final time. Prior to analysis by GFAAS, the solution was mixed vigorously. Dilutions, if required, involved pipetting a volume, typically 200 – 500 µl, into a new, pre-weighed, 1.5 ml polystyrene cup. The cup was diluted with 2 ml of de-ionized water, weighed and mixed vigorously prior to analysis.

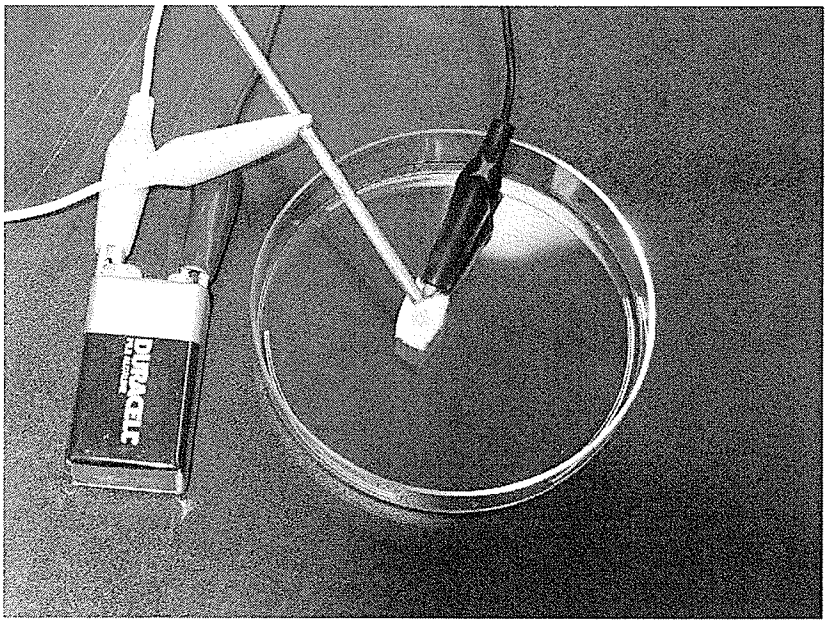

Figure 2.8.1: Low power electrocorrosion of 316L Stainless Steel using a 9-V battery as a power source.

The choice of acid used in the digestion of the paper may have a significant impact on the analysis. For example, if HCl was used, the presence of large amounts of Cl^- in the sample can cause chemical interferences for some elements (e.g. Cr, Cd, Ag) with GFAAS[91]. For ICP-MS analysis, Cl^- in the sample may also cause spectral interferences. For example Cl^- can recombine to form $^{40}Ar^{35}Cl^+$, overlapping with the only isotope of $^{75}As^+$ which has been found as an impurity in antique silver. For these reasons HNO_3 was chosen for the extraction of all the samples.

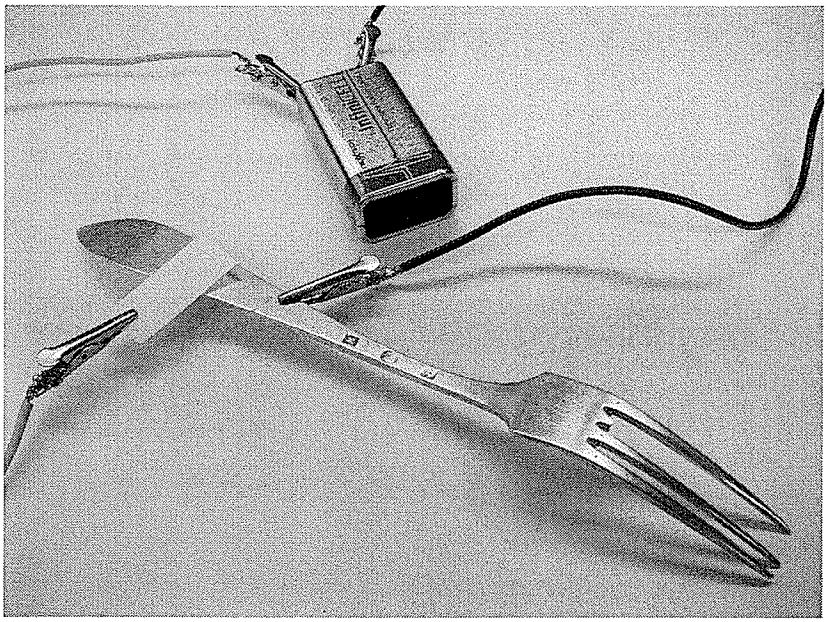

Figure 2.8.2: Low power electrocorrosion of a museum object using a 9-V battery as a power source.

The procedure for electrocorrosion of a museum object was similar; a sectioned filter paper was attached to the anode of a 9 V battery by wire and alligator clip and soaked with aqueous solution (Fig. 2.8.2). The cathode of the 9 V battery was attached directly to the object's surface. The paper was then placed on the surface of the metal for

a specified time interval (10 – 120 s). After corrosion, the cellulose was treated as before. In order to ensure consistent sampling, the distance between the edge of the object and the cathode was maintained constant. This minimized the effect of paper resistance and as a result current density remained similar for all trials. A similar procedure was used when the anode was a cotton bud.

For conventional acid dissolution a silver alloy was partially submerged in 5 – 15 ml of environmental grade HNO_3 for approximately 40 s. The alloy was then removed and the solution was quantitatively transferred to a 100 ml volumetric flask and diluted with de-ionized water. The flask was mixed vigorously prior to analysis using FAAS.

3.0 RESULTS AND DISCUSSION CHAPTER 1: MICROSAMPLING FOR PIGMENT INDENTIFICATION USING SPECTROSCOPY

To test the feasibility of using GFAAS for detecting various metals in pigments using a cotton bud for solid sampling, several experiments were carried out on commercially available watercolour and oil paints with known metal content as listed in Table 2.2.1. The goal of these initial experiments was simply to compare signal intensities of pigment metals relative to signal intensities of metals that may be present as minor constituents in the paint. Each of the paints was applied to the surface of a microscope slide using a glass rod to avoid contamination of the commercial paint with trace metals. A clean cotton swab was contacted gently with each of the dried paints and placed in a 1.5 ml polystyrene beaker; 100 µl of concentrated HNO_3 was then added to extract the pigment metals prior to analysis using GFAAS. A typical absorbance signal obtained from 1.5 ml solution containing extracted Cr from Olive Green is shown in Figure 3.0.1. This experiment illustrates that it is possible to identify the primary pigment metals (Cr) relative to other metals that may be present as minor components or as impurities (Cu and Co) by using the low detection limits and high sensitivity of GFAAS.

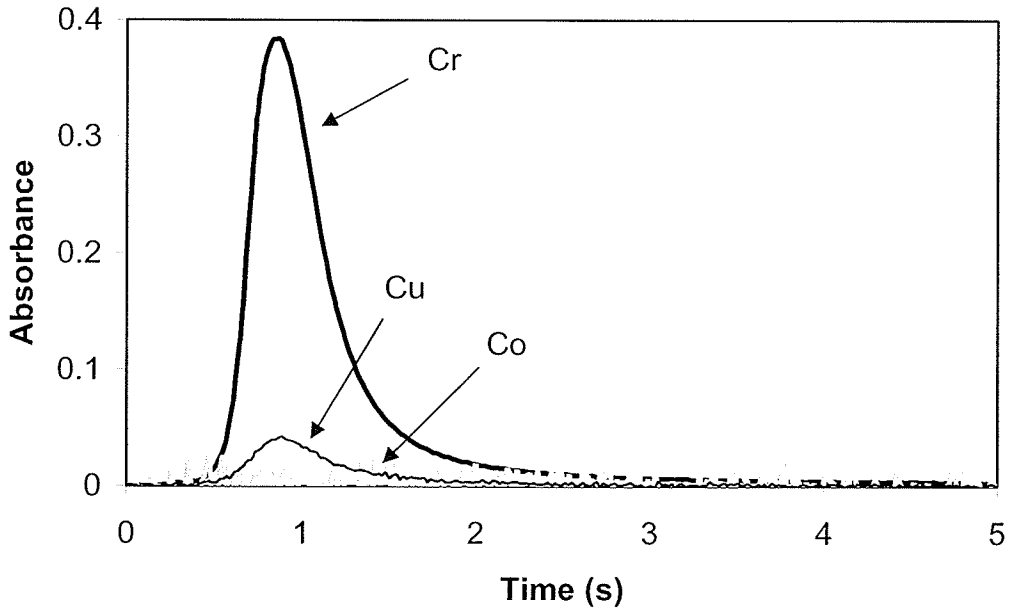

Figure 3.0.1: Typical absorbance signals generated using Olive Green watercolour paint.

Previous experiments in our laboratory illustrated the practicality of using a cotton bud to sample painted surfaces[92,93]. Pigment particles are suspended in the paint binding agent (oil or water) and applied to a support (e.g. canvas, paper). As the binding agent dries the pigments remain as a layer on the support where the top layer of pigment is loosely bound. The effect of sampling the same surface repeatedly revealed that the first contact picks up the bulk of the loosely bound surface pigment particles. Successive contacts in the same location with a new cotton swab appeared to pick up less paint[92]. Devos et al.[10] have reported that sampling error of about 10% is acceptable and that the repeatability of sampling by contact with a cotton bud is limited by the surface homogeneity of the pigment layer and pigment particle size. If sampling errors are low, comparisons can be made between pigment concentrations in different areas of a painted surface.

3.1 Effect of Sampling Force

Perhaps the most important parameter associated with sampling a painted surface using a cotton bud is the mass of metal or pigment removed. Clearly, there is a relationship between the amount of pigment removed and the amount of damage that may be sustained by the painted surface. For painted surfaces of valuable artwork, any damage to the surface would be unacceptable. In a previous study[92], painted surfaces were sampled by hand with a cotton bud and it was estimated that the amount of pigment removed is approximately 1 μg. To acquire a better estimate of the mass of pigment that is typically removed with a cotton bud during sampling, an experiment was designed to quantify the mass of pigment removed with respect to the contact force. In this experiment a series of microscope slides were painted using a glass rod and allowed to dry. The paint was sampled by placing the microscope slide on a pan balance. A cotton bud was secured with a clamp and carefully lowered onto the paint surface. The pan of the balance was rotated 10 – 20 times in both clockwise and counter clockwise directions. This allowed the pigments on the paint surface to be removed in a reproducible manner. The force on the paint surface was determined by mass. Periodically, the clamp securing the cotton bud was adjusted to ensure that the mass remained within 10% of the desired value. Some fluctuations were inevitable since the cotton bud would compress somewhat as more force was exerted on it from the painted surface. At higher forces sampling was also affected by bending of the cotton swab stick. Since a fresh paint surface was sampled for each determination, error bars on the vertical axis represent the measurement uncertainty of the instrument (i.e. ± 5%).

Figures 3.1.1 through 3.1.4 summarize the relationship between contact force of the cotton bud and the mass of pigment metal extracted for various oil and watercolour paints. Pigments suspended in oil are more likely to dry to a smooth finish because the oil dries via a complex oxidation process unlike watercolours, which dry by evaporation[4]. Initially, solvents (e.g. turpentine) evaporate; this is followed by a long oxidation phase where the oil paint absorbs atmospheric oxygen. The oil polymerizes and the polymers cross-link to form a stable paint surface. Over time, the polymer network may undergo further change as functional groups in the polymer become ionized. The network can transform from a system dominated by non-polar covalent bonds to a system held together by primarily ionic forces between the polymer functional groups and the metal ions present in the pigment. As such the surface of oil paints will differ according to pigment, type of oil and manufacturing additives. For example, Cobalt Blue will produce grainy or crystalline paints whereas Flake White tends to react to form smooth, buttery, paints[3]. This is evident from the range of masses removed for each pigment sampled. The difference between oil and watercolour paints is illustrated by Chinese White (Fig. 3.1.1); greater amounts of pigment were removed from the watercolour when compared to the oil paint, which indicates that pigment particle size may also affect pigment sampling. Particle sizes can range from 1 – 20 μm, where the larger particles (20 μm) will feel gritty and be more susceptible to removal. As a result, much higher masses (an order of magnitude) of Zn were obtained from the watercolour, even when gentle pressure (< 0.5 N) was applied to the paint surface. A similar trend was observed for Cadmium Red paint (Fig. 3.1.4).

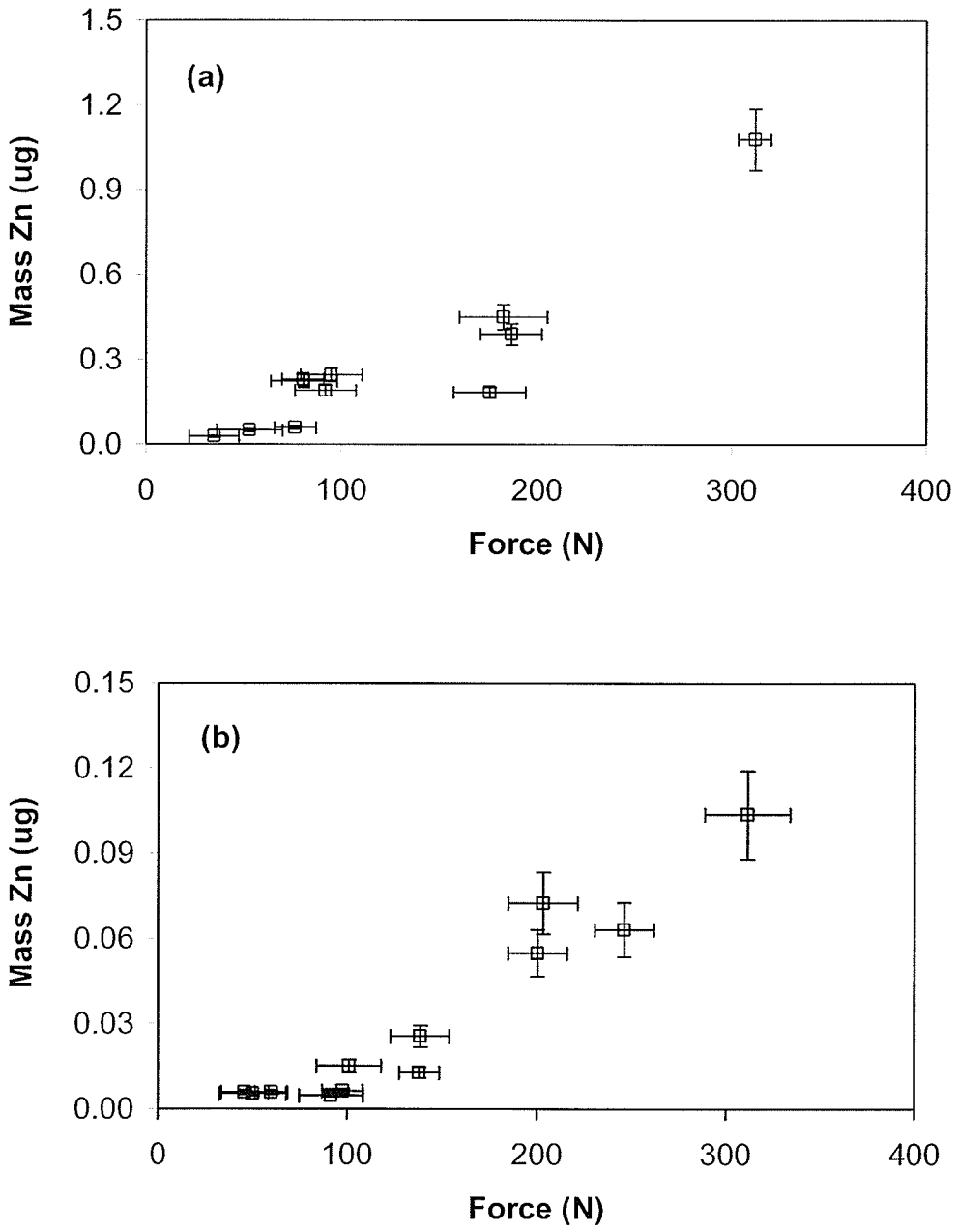

Figure 3.1.1: Relationship between the mass of metal removed and the applied force of the cotton bud for Zn extracted from Chinese White (ZnO) (a) oil paint and (b) watercolour paint.

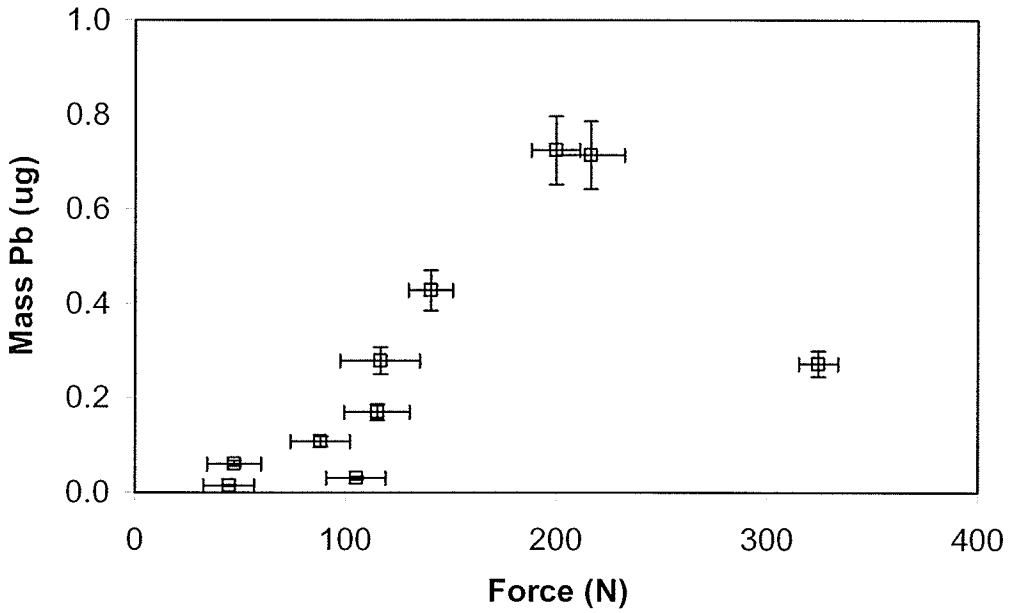

Figure 3.1.2: Relationship between the mass of metal removed and the applied force of the cotton bud for Pb extracted from Flake White ($PbCO_3$) oil paint.

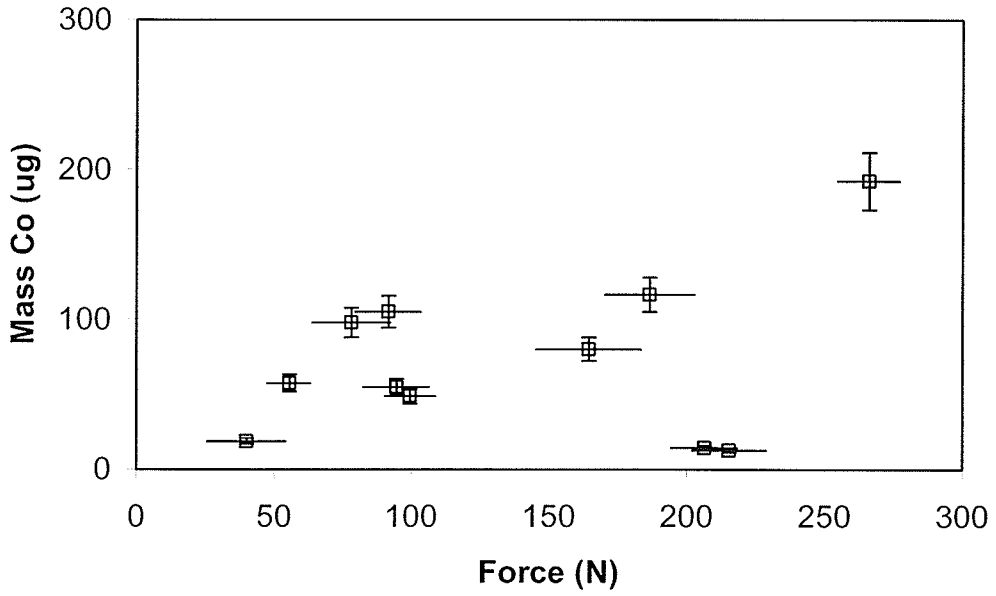

Figure 3.1.3: Relationship between the mass of metal removed and the applied force of the cotton bud for Co extracted from Cobalt Blue ($CoO{\cdot}Al_2O_3$) watercolour paint.

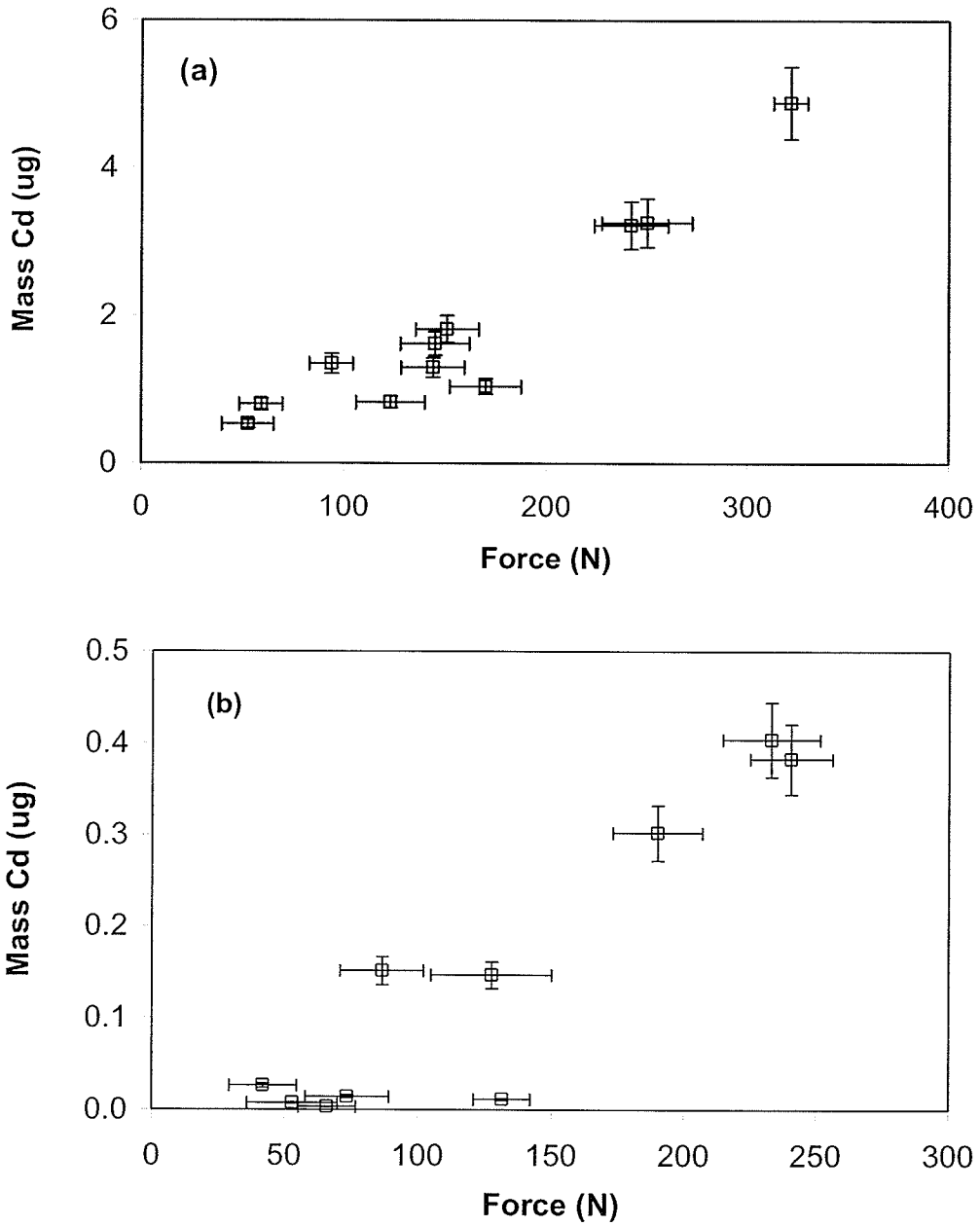

Figure 3.1.4: Relationship between the mass of metal removed and the applied force of the cotton bud for Cd extracted from Cadmium Red (CdS) (a) oil paint and (b) watercolour paint.

Although this experiment differed in many ways from the manual approach to pigment sampling of paint, it was useful for understanding how the surface of a painting could be affected. The amount of pressure applied was certainly subjective, however it was possible to make an estimate of the pressure exerted on the surface of a painting. For most paints this amount of force would have negligible effect on the surface. A larger amount of force (> 0.3 N) could cause a dent to the oil paint surface, which would be both harmful to the appearance of the paint and unnecessary for obtaining a representative paint sample.

3.2 Reproducibility of Sampling by Hand

Since it will generally not be possible to measure the amount of contact force applied to painted artwork, it was necessary to demonstrate that sampling by hand was comparable to sampling using the pan balance. Two commercial paints were selected, Flake White ($PbCO_3$) oil and a Chinese White (ZnO) watercolour.

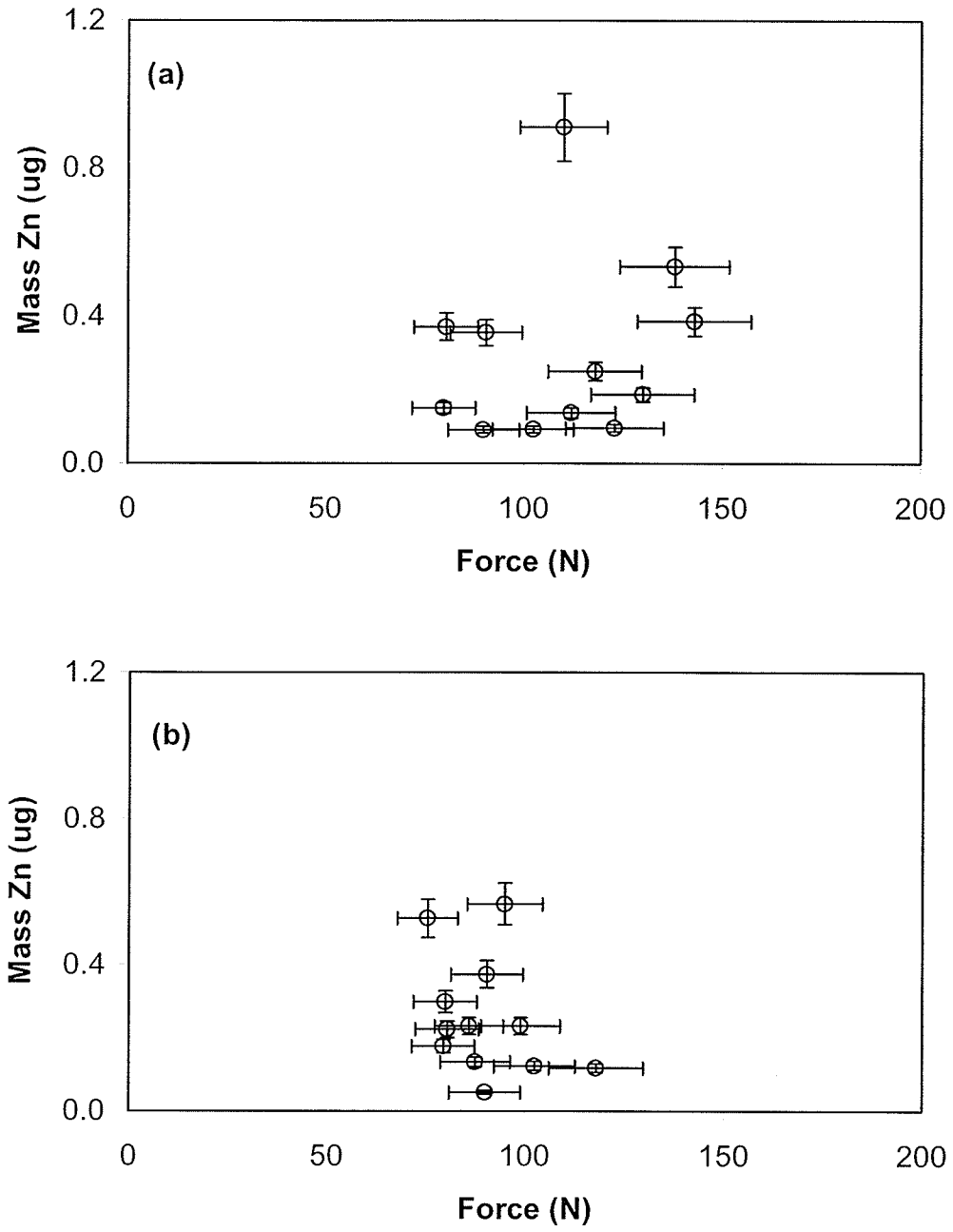

Figure 3.2.1: Chinese White (ZnO) watercolour paint sampled, (a) by hand and (b) using a pan balance.

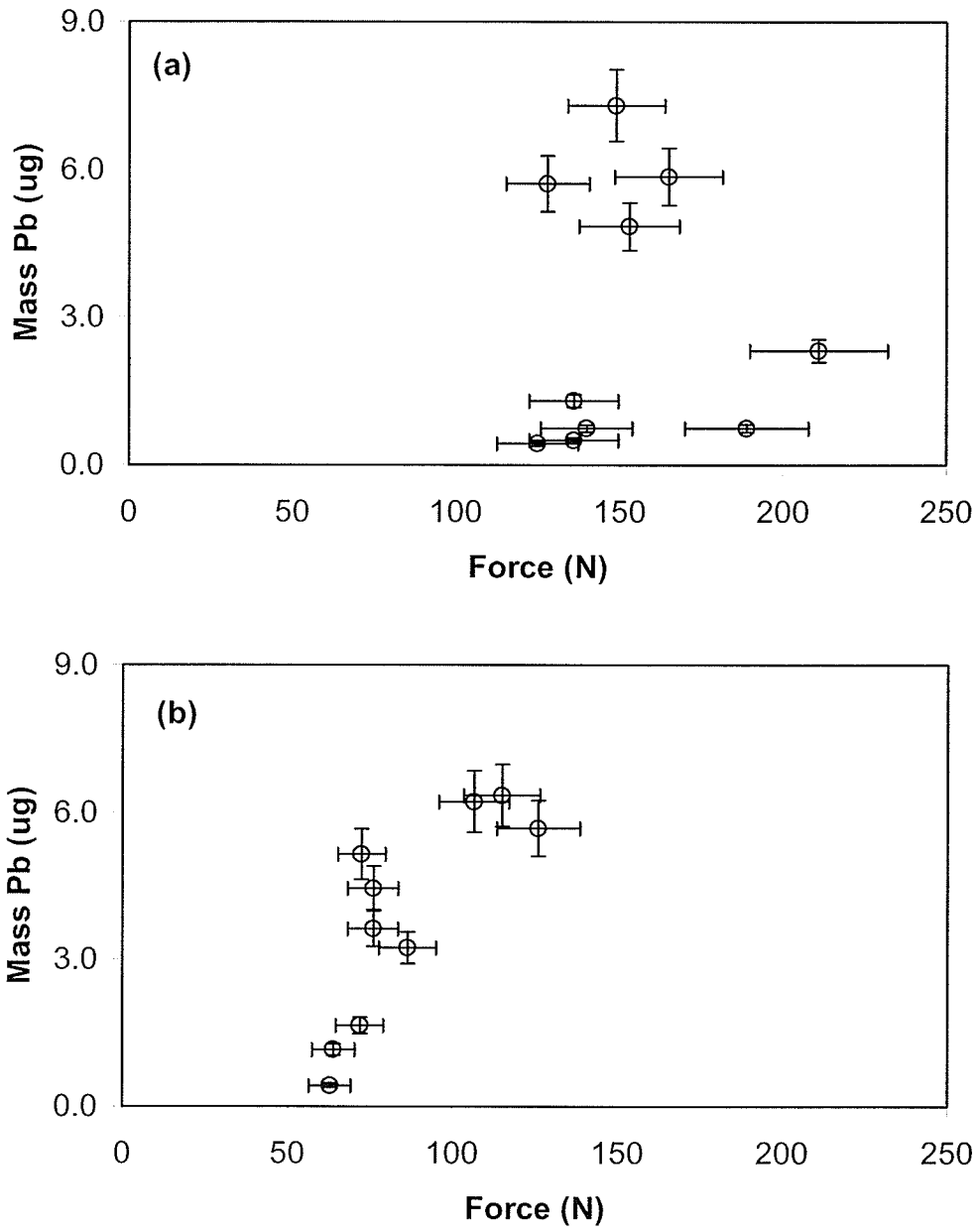

Figure 3.2.2: Flake White ($PbCO_3$) oil paint sampled, (a) by hand and (b) using a pan balance.

Figures 3.2.1 and 3.2.2 illustrate that sampling by hand removed similar amounts of metal when compared to sampling using the pan balance. When paints were sampled by hand there was a broader range of forces that corresponded to varying amounts of metal indicating that sampling by hand was less precise. Typically, Flake White paint contains pigment particles that are approximately 10 μm whereas Chinese White pigment particles are 0.1 μm. A larger quantity of pigment was removed from the Flake White sample which suggests that pigment particle size may affect pigment removal. It is important to note that, in this experiment, there was no visible damage to the surface of either of the paints, regardless of the amount of material removed. There was lower precision when sampling the oil paint, which may have also been due to particle size. Decreased precision will affect the ability to compare pigments from different locations as well as determining mixtures of pigments from the same location.

3.3 Paint Digestion Optimization

It was necessary to develop a decomposition procedure that would maximize dissolution and that could be used for a variety of pigment types. The optimal conditions for each pigment may differ slightly due to the presence of a variety of organic as well as inorganic compounds, for example, binders and drying agents. However, it was necessary to choose compromise conditions so that one digestion procedure could be used for paint mixtures. Pigments such as Cobalt Blue ($CoO \cdot Al_2O_3$) may not be digested by an oxidizing acid such as HNO_3 because the Co is present in an alumina glass matrix. For this reason, it was hypothesized that HF may be required to digest these pigments because it is an extremely corrosive fluorinating agent that dissolves glasses.

Many of the studies involving paint decomposition employ microwave digestion; for example, Paudyn and Smith[1] used microwave assisted digestion to digest commercial paint before analysis with ICP-AES. Paint scrapings were ground and placed on the bottom of the digestion vessels prior to microwave digestion. Solvents were initially evaporated by microwaving uncovered glass digestion vessels for 1 minute at 130 W. The samples were then covered and microwave digested in a mixture of 5 ml HNO_3 and 2 ml HF. After digestion the samples were diluted and transferred to 100 ml polytetrafluoroethylene (PTFE) beakers and evaporated on a hotplate. The authors noted that if a sample accidentally dried, 1 ml of HNO_3 was added and the sample was gently heated on a hot plate to dissolve the salts. Evaporating samples to approximately 1 ml on a hotplate after microwave digestion generally took up to 2 – 3 h; however, evaporation on a hotplate may lead to contaminated samples. Adding boric acid to deactivate the HF eliminated the evaporation step but at the cost of matrix effects for elements measured by ICP-AES in the UV region[1]. Adding boric acid increases the overall salt concentration of the solution and when using pneumatic nebulizers for ICP-MS the total dissolved solids should remain below 0.2%[94]. The authors concluded that a mixture of HNO_3 and HF was suitable for the microwave assisted decomposition of a variety of paints; they also investigated microwave digestion under high pressure using aqua-regia, HNO_3, and HNO_3 with perchloric acid but the digestion was not significantly improved[1].

For this investigation a small amount (~25 μg) of dried artist paint was weighed into a glass scintillation vial and the appropriate acid combination was added. A cotton bud (Q-tip) was also added to each vial in order to simulate actual sampling conditions. The vial was then placed on a hot plate and heated at low to medium heat for

approximately 1 h or until there was minimal acid left in the vial (>1 ml). Once the cotton was dissolved the Q-tip stick was removed and rinsed with the appropriate acid mixture to ensure that pigment was not being removed from the vials. After digestion, the vials were removed from the hotplate and allowed to cool. Samples were then diluted with de-ionized water. The solutions were all mixed at the same time and allowed to sit (~ 1 h) to allow undissolved cellulose to settle to the bottom of the vial. Analysis was performed using FAAS and metals were quantified using a matrix-matched external calibration curve. The results for several oil and water based paints are presented in Tables 3.3.1 and 3.3.2. It is important to note that the results indicate the maximum percentage of metal that was recovered from the mass of the original paint weighed into the vial, not the efficiency of paint digestion. Watercolour paints consist of one or more pigments and contain varying concentrations of the following: brighteners, which are transparent (white) crystals that increase the chroma of dried paint; plasticizers (e.g. glycerin) are added to soften the binder; humectants help the paint retain moisture; extenders (e.g. dextrin) thicken the paint without affecting the colour. Manufacturing additives such as dispersants and fungicides may also be included[3]. Similarly, oil paint contains varying amounts of pigment most commonly mixed with cold-pressed linseed oil and stabilizers (e.g. aluminum stearate). The proportion of pigment to medium in artist paints depends on the pigment and specific recipes vary for each brand. As a result of the varying amounts of pigment in the dried paints it was only possible to compare the maximum digestion efficiency of each acid to determine the most appropriate digestion procedure.

Table 3.3.1: Optimizing a digestion procedure for various watercolour artist paints.

Acid	Weight percent of pigment metal (wt %)				
	Co	**Cr**	**Cd**	**Fe**	**Zn**
3 ml HNO_3 + 1 ml H_2SO_4	3.7 ± 0.6	2.3 ± 1.2	24.0 ± 5.5	7.8 ± 0.9	25.6 ± 4.3
2 ml HNO_3 + 2 ml H_2SO_4	4.1 ± 1.1	0.9 ± 0.1	24.0 ± 6.8	7.6 ± 1.9	25.4 ± 5.7
4 ml HNO_3	4.0 ± 0.3	2.4 ± 0.9	27.0 ± 2.8	7.9 ± 0.1	26.9 ± 4.2
3 ml HCl + 1 ml HNO_3	2.0 ± 0.1	0.4 ± 0.1	28.0 ± 8.1	9.4 ± 2.4	21.9 ± 5.9
4 ml HCl	0.5 ± 1.2	0.3 ± 0.1	24.0 ± 9.7	8.5 ± 1.7	22.9 ± 9.2
2 ml HF + 2 ml HNO_3	3.3 ± 0.3	0.2 ± 0.1	23.9 ± 3.6	10.8 ± 0.5	23.4 ± 7.6

n = 4

Table 3.3.2: Optimizing a digestion procedure for various oil-based artist paints.

Acid	Weight percent of pigment metal (wt %)				
	Co	**Cr**	**Cd**	**Zn**	**Pb**
3 ml HNO_3 + 1 ml H_2SO_4	10.8 ± 0.5	6.9 ± 2.0	13.0 ± 2.0	38.7 ± 2.0	3.7 ±1.2
2 ml HNO_3 + 2 ml H_2SO_4	12.9 ± 1.2	7.9 ± 0.9	13.0 ± 2.6	50.9 ± 10	7.0 ± 2.8
4 ml HNO_3	5.0 ± 0.2	5.0 ± 2.5	11.6 ± 3.8	44.5 ± 8.9	63.3 ± 8.9
3 ml HCl + 1 ml HNO_3	3.9 ± 1.7	3.7 ± 2.6	18.3 ± 3.2	43.2 ± 7.1	49.4 ± 6.7
4 ml HCl	2.9 ± 0.7	0.3 ± 0.1	17.2 ± 1.0	45.0 ± 17	26.8 ± 17
2 ml HF + 2 ml HNO_3	5.8 ± 0.7	0.06 ± 0.05	8.9 ± 3.1	48.9 ± 5	38.0 ± 6

n = 4

The results illustrate that HNO_3 was an effective compromise to obtain maximum decomposition of pigments in a wide range of commercially available artist paints. It is important to note that the blank prepared with HNO_3 was clear and free of cotton residue, unlike blanks prepared from the other acid mixtures. Contrary to our hypothesis, HF did not significantly improve the decomposition of Cr and Co pigments. Hydrofluoric acid should also be avoided in the future as up to 1 mg of material was lost from the glass vial, which could lead to sample contamination. Digestions using HCl did not completely decompose the cotton bud and a dark brown suspension was present in

solution after dilution. Although the blank measurements for the HCl digestion were comparable to the blank measurements for HNO_3, HCl was avoided because dissolved cellulose may create matrix effects. Also, the addition of H_2SO_4 appeared to be unnecessary as it did not significantly improve metal recovery and the additional acid may complicate analysis by increasing spectral and chemical interferences.

The results from this investigation are in agreement with the results reported by Paudyn and Smith[1] for microwave assisted acid digestion. There was a possibility of contamination when the vials are left uncovered in the fume hood during decomposition. The contamination problem was accounted for by preparing several blanks for each trial and maintaining a clean laboratory atmosphere.

3.4 Raman Investigations

Studying pigments in painted artwork, especially oil paintings, using Raman can be difficult because varnish layers and binder-rich media surrounding the pigment grains can fluoresce which may obscure Raman signals and complicate spectra[54,90]. Using a baseline correction minimizes this effect. It is also important to note that library spectra present Raman signals from pure mineral crystals using a Raman spectrometer equipped with a microscope probe. The Raman spectra obtained for this study were collected directly from painted surfaces and as a result the spectra may have suffered from particle size effects and fluorescence from the binder. Surface heterogeneity and surface unevenness also affected the quality of the spectra. For non-invasive, in-situ, analysis the Raman spectrometers were transported to the object and samples were not removed.

When analyzing coloured pigments, the choice of exciting radiation can be important because absorption of the scattered light by the sample may reduce the quality of the spectrum. There must be a net change in permanent dipole moment during the vibration[89]. The excitation wavelength should fall outside the contour of the electronic absorption bands of the pigment. For example, red pigments (e.g. vermillion and red ochre), yield small signals when excited with green light but do give strong spectra when irradiated with red light. Several examples are illustrated in Figures 3.4.1 through 3.4.6. Factors such as laser power, pigment particle size and paint layer thickness may have affected the quality of Raman spectra and this should be considered when comparing spectra from Raman libraries.

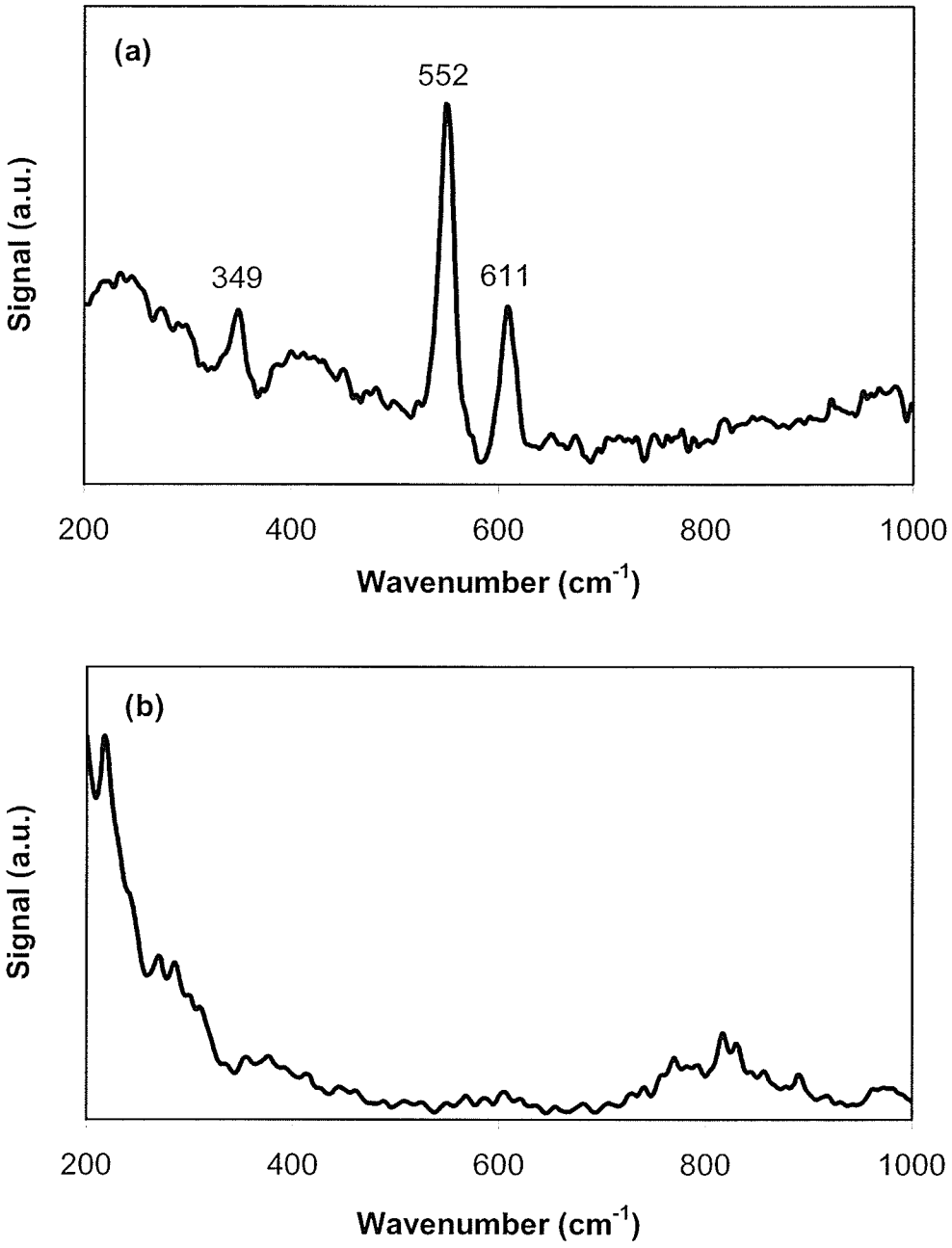

Figure 3.4.1: Raman spectrum of Olive Green (Cr_2O_3) watercolour paint using (a) Rockhound™ (100 mW) and (b) Advantage 200A™ (3 mW).

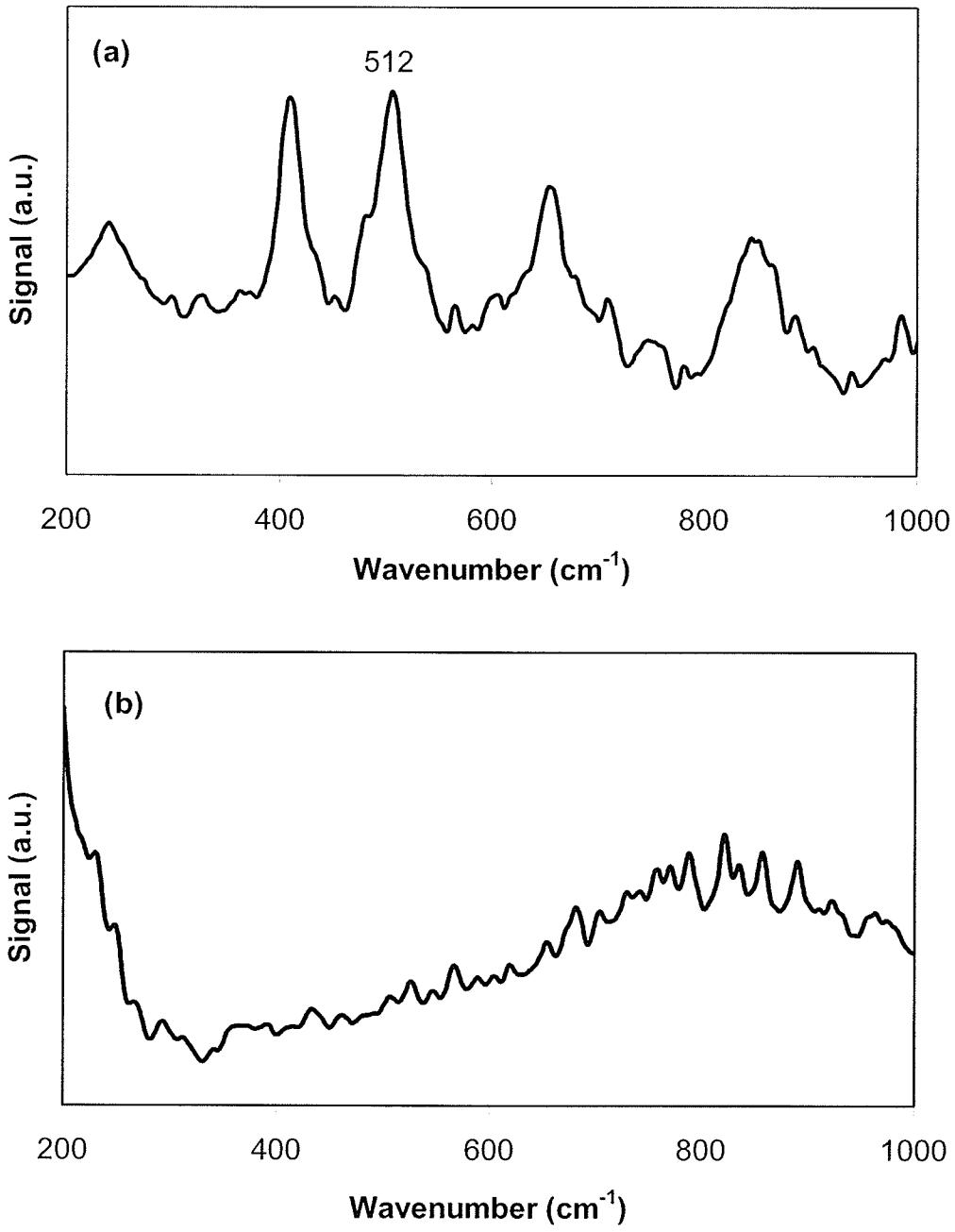

Figure 3.4.2: Raman spectrum of Cobalt Blue ($CoO{\cdot}Al_2O_3$) watercolour paint using (a) Rockhound™ (100 mW) and (b) Advantage 200A™ (3 mW).

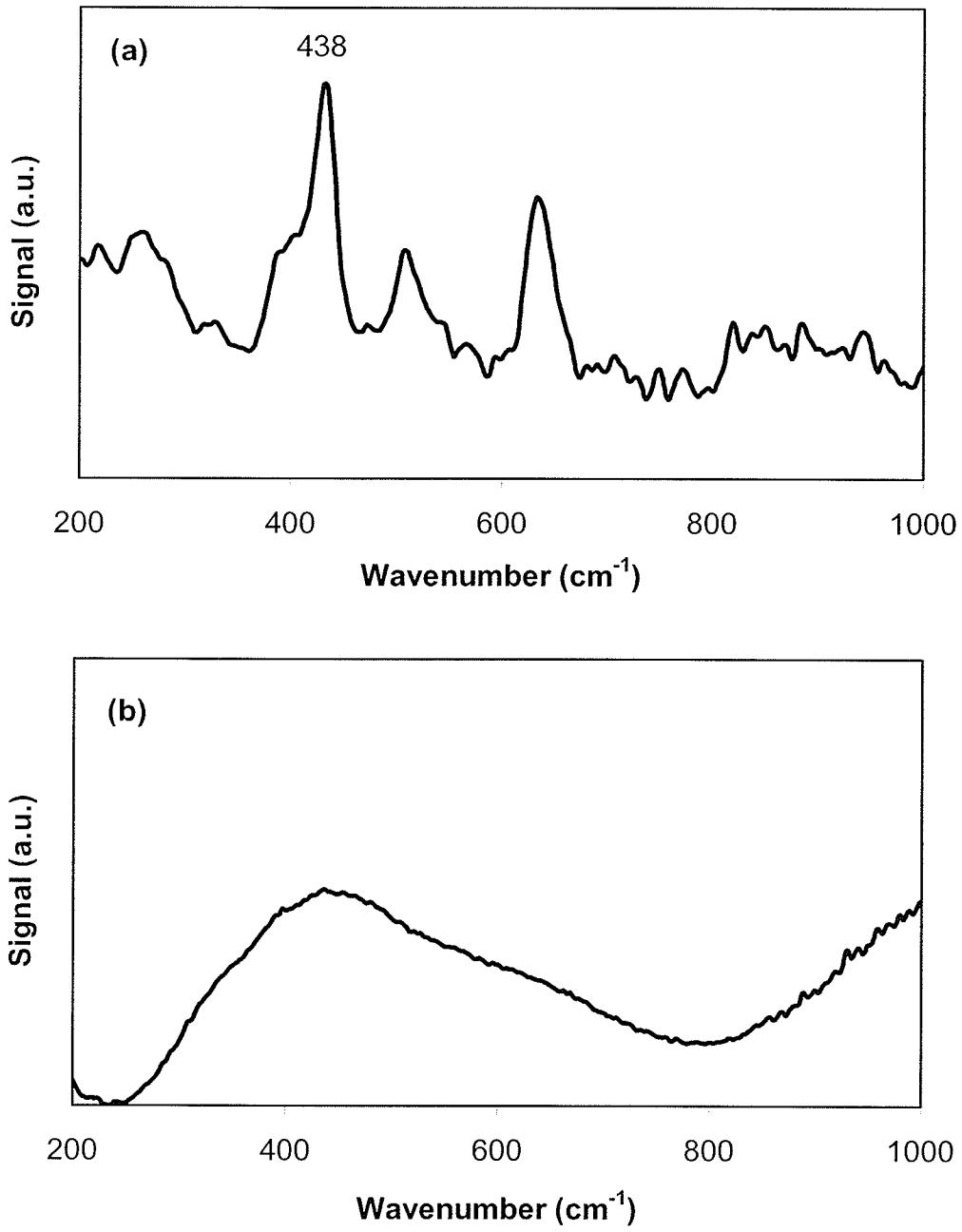

Figure 3.4.3: Raman spectrum of Chinese White (ZnO) watercolour paint using (a) Rockhound^{TM} (100 mW) and (b) Advantage 200A^{TM} (3 mW).

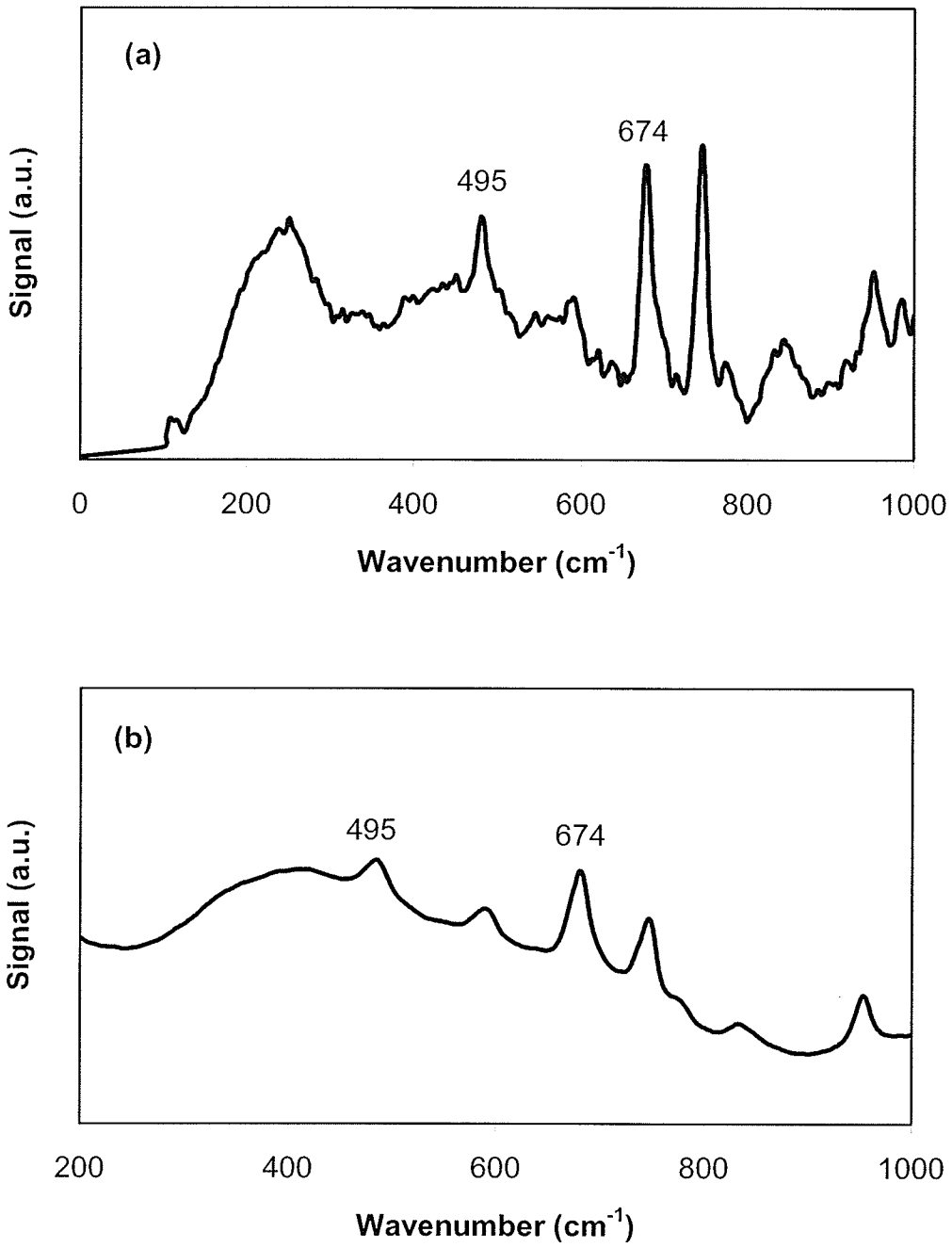

Figure 3.4.4: Raman spectrum of Cerulean Blue ($CoO{\cdot}nSnO_2$) oil paint using (a) Rockhound™ (100 mW) and (b) Advantage 200A™ (3 mW).

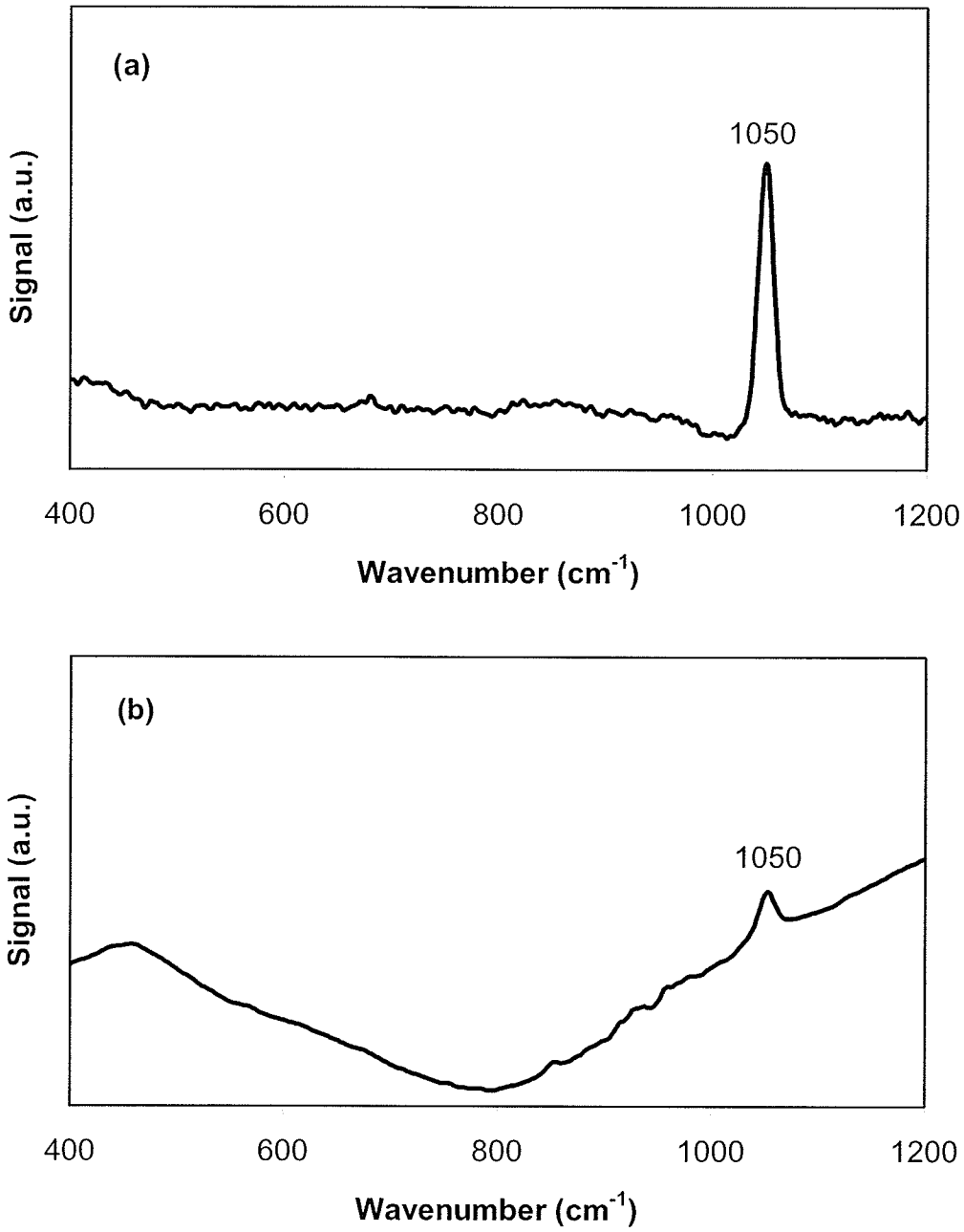

Figure 3.4.5: Raman spectrum of Flake White ($PbCO_3$) oil paint using (a) Rockhound™ (100 mW) and (b) Advantage 200A™ (3 mW).

In general, the Advantage 200A appeared to suffer from more fluorescence but this instrument was useful in cases where the spectrum extended beyond 2000 cm^{-1} for example, Prussian Blue (Fig. 3.4.6).

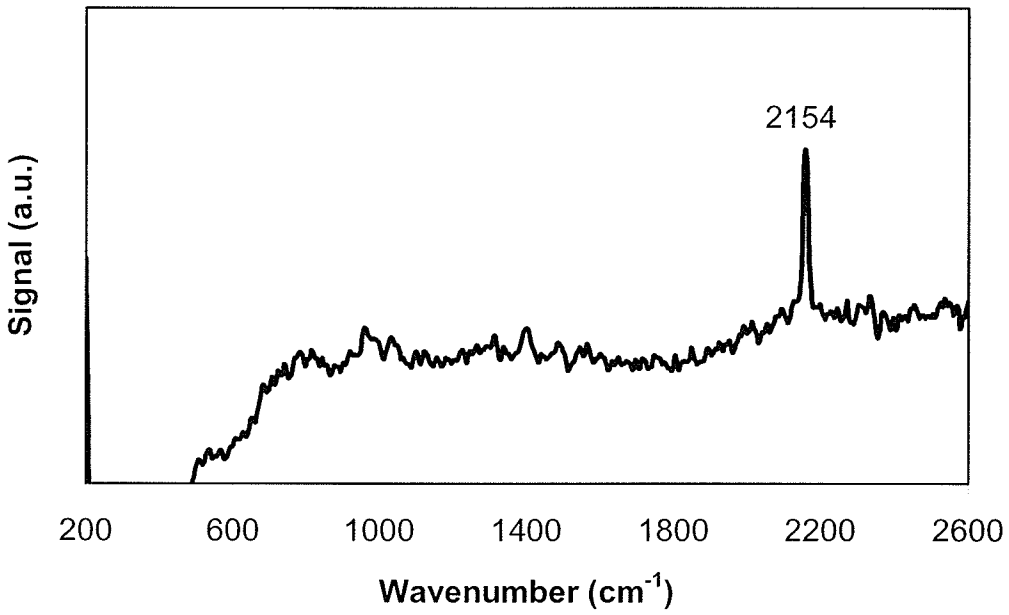

Figure 3.4.6: Raman spectrum of Prussian Blue ($Fe_4[Fe(CN)_6]_3 \cdot 14\text{-}16H_2O$) oil paint using the DeltaNu Advantage 200A™ (3 mW).

3.5 Mixed Pigment Analysis

Previous studies in our laboratory demonstrated the feasibility of using a cotton bud by sampling a watercolour painting entitled 'Hilled Dusk', by the Canadian artist Robert Sinclair and an oil painting entitled 'Redwoods', by Nell Edwards[92]. The results illustrated that identifying the metal using GFAAS and visually inspecting the colour of the paint can allow the analyst, by elimination, to make an educated guess about the identity of a pigment, however, identification of metals alone was not a guarantee for accurate pigment identification. Goltz et al.[89] combined GFAAS with Raman spectroscopy to identify the surface pigment as well as the presence of other pigments, which were mixed with the primary pigment. This study led to the investigation of mixed pigments using GFAAS and Raman spectroscopy.

In a recent review, Vandenabeele et al[95] reported that in-situ investigations represent a difficult analytical challenge as the samples are often complex. It had previously been suggested by Devos et al.[10] that mixing proportions of pigments cannot be determined by Raman spectroscopy. While investigating pigments using XRF, Ferrero et al.[56] report that they limited their analysis to qualitative and semi-qualitative estimations due to mixtures of pigments in the painted objects. According to Clark[9], when dealing with mixtures of pigments it is necessary for the technique to give results from a single grain. They suggest that samples should be removed from the bulk artwork; however, this is not always possible. The Raman spectrometer used for this study was not capable of focusing on single pigment grains. Spectra were obtained from several locations on the surface and represent an area approximately 1 mm^2 of the paint;

this is illustrated in Figures 3.5.1 through 3.5.6. Several experiments were designed to determine whether mixing proportions could be estimated using *in-situ* Raman spectroscopy and sampling with a cotton bud.

Paint mixtures (oil or water) were prepared by mass and applied to the surface of microscope slides (Table 3.5.1). Pigments were chosen based on conventional paint-mixing techniques capabilities of the Raman spectrometers used in this experiment. Historically, darker colours, such as Cobalt Blue, can be lightened using a white pigment such as Flake White or Chinese White[89]. It is important to detect the primary pigment as well as the lightener because white pigments, such as Flake White and Lithopone, are known to darken[3]. A mixture of two white pigments, Chinese White and Flake White, was also prepared to determine the effect of colour on the quality of Raman spectra. Raman spectra for each slide were obtained using either the Advantage 200A™ or the Rockhound™. Samples were also collected by contacting the surface with a cotton bud, which were then digested in concentrated HNO_3 prior to analysis with GFAAS. Factors such as pigment content, particle size and percent metal in the pigment prevented quantification using GFAAS. The paint mixtures were prepared by mass but the amount of pigment present in each paint was not known. As a result, a 1:1 mixture of two pigments was not equivalent to a 1:1 ratio of metals; therefore, determining the metal ratio could not be used to determine the pigment ratios.

Table 3.5.1: Prepared slides of mixed oil paints in ratios ranging from 1:1 to 1:5.

Paint 1	Paint 2	Target Metals	Raman Peaks[a] (cm^{-1})
Flake White	Olive Green	Pb, Cr	552, 611, 1050
Flake White	Cobalt Blue	Pb, Co	512, 1050
Flake White	Cerulean Blue	Pb, Co	674, 1050
Flake White	Chinese White	Pb Zn	438, 1050
Chinese White	Olive Green	Zn, Cr	438, 552, 611
Chinese White	Cobalt Blue	Zn, Co	438, 512
Chinese White	Cerulean Blue	Zn, Co	438, 674

[a]Major peak assignments: 1050 cm^{-1} $(CO_3)^{2-}$; 438 cm^{-1} Zn-O; 512, 552 cm^{-1} Co-O

Figures 3.5.1 through 3.5.6 present Raman spectra obtained from the mixed paints listed in Table 3.5.1. As previously demonstrated, Raman spectrometers behave differently for different pigments and it is desirable to understand the capabilities and limitations of the Raman spectrometer used for the analysis. For example, Cobalt Blue did not have a strong Raman signal (Fig. 3.4.2) and as a result the signal appeared weak in the mixed paint analysis (Fig. 3.5.4). Since the behaviour of Cobalt Blue was known prior to the mixed paint analysis it was possible to interpret the spectra based on the appearance or disappearance of the stronger Flake White signal. The ability to obtain an optimal spectrum was also dependent on the distance between the sample and the

spectrometer and this should be determined prior to in-situ analysis. The experiments did indicate that more than one pigment could be identified by Raman spectroscopy even when a large surface area was analyzed. The Raman spectra were reproducible when spectra were obtained from several spots that were similar in appearance. Raman was also able to identify inorganic pigments when the target metal could not be determined using GFAAS. For example, Cerulean Blue is a Co-containing pigment but the Co is present in small quantities in an alumina glass matrix and as a result it is undetectable when sampled with a cotton bud; however, the Raman spectrum of the same paint sample yielded a typical Cerulean Blue spectrum (Fig. 3.5.6). In this example, the Flake White was identified by determining the presence of Pb and confirmation by Raman spectroscopy, whereas Cerulean Blue was identified only by Raman spectroscopy. The lack of Cr or Cu in the GFAAS analysis ruled out the possibility of other blue coloured pigments. Preparing standards that represent the approximate colour appearance of the suspected pigments, based on GFAAS analysis, may allow for estimation of the mix ratios because a comparison could be made under the same sampling conditions using the same instrument. Paint colour (e.g. dark or light) did not appear to affect the ability to detect pigments using Raman spectroscopy. The Raman spectrometer, laser wavelength and target pigment should all be considered when attempting to estimate mix ratios. Guineau et al.[96] have suggested that using standards that closely resemble the object can be used to compare Raman spectra. In general, the results illustrated that Raman spectroscopy could not determine mixing ratios without the aid of standards.

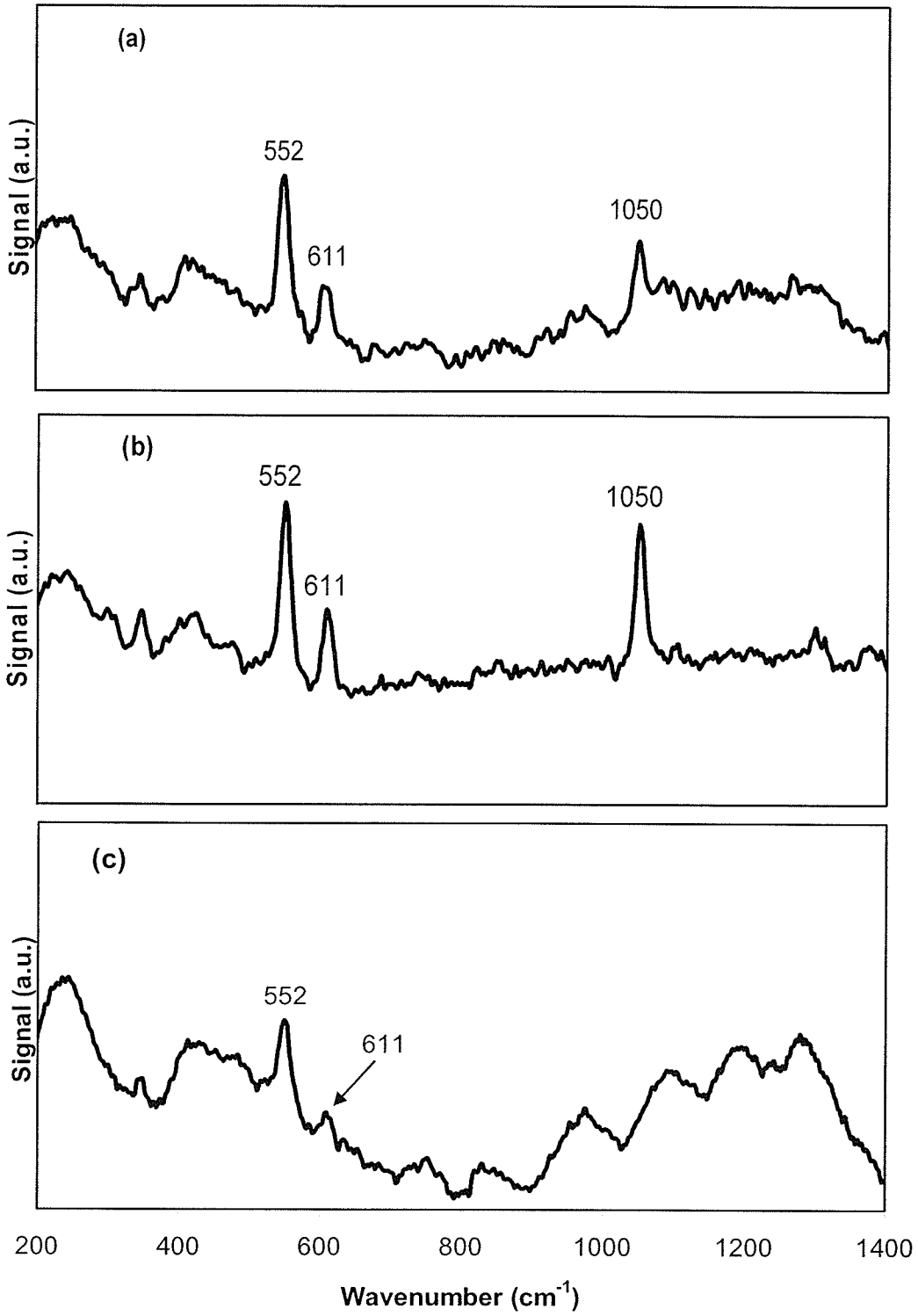

Figure 3.5.1: Raman spectra obtained from various mix ratios of Olive Green and Flake White oil paint, Cr_2O_3: $PbCO_3$ (a) 1:1, (b) 1:5, (c) 5:1 using Rockhound™.

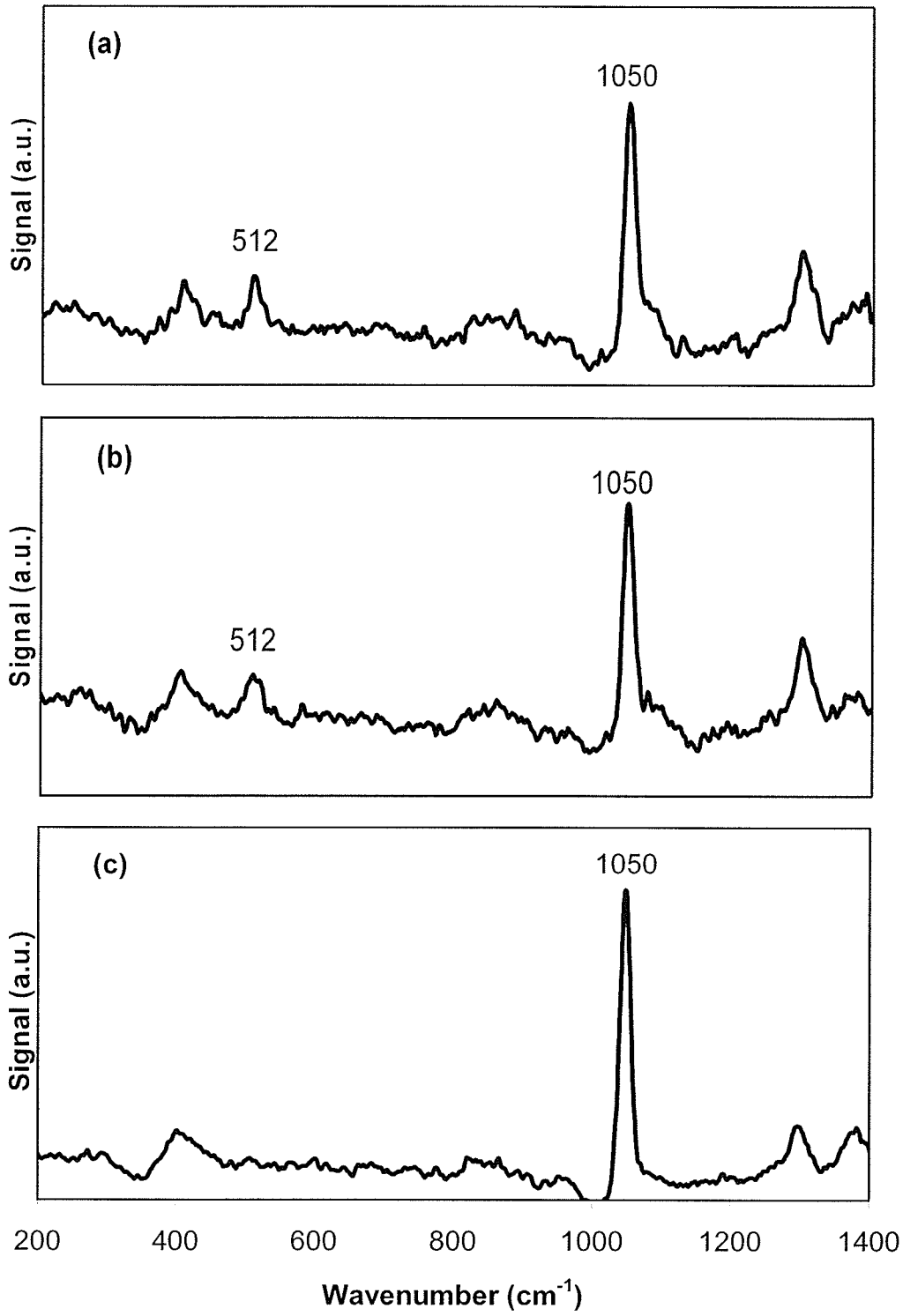

Figure 3.5.2: Raman spectra obtained from various mix ratios of Cobalt Blue and Flake White oil paint, $CoO \cdot Al_2O_3$: $PbCO_3$ (a) 1:1, (b) 5:1, (c) 1:5 using Rockhound™.

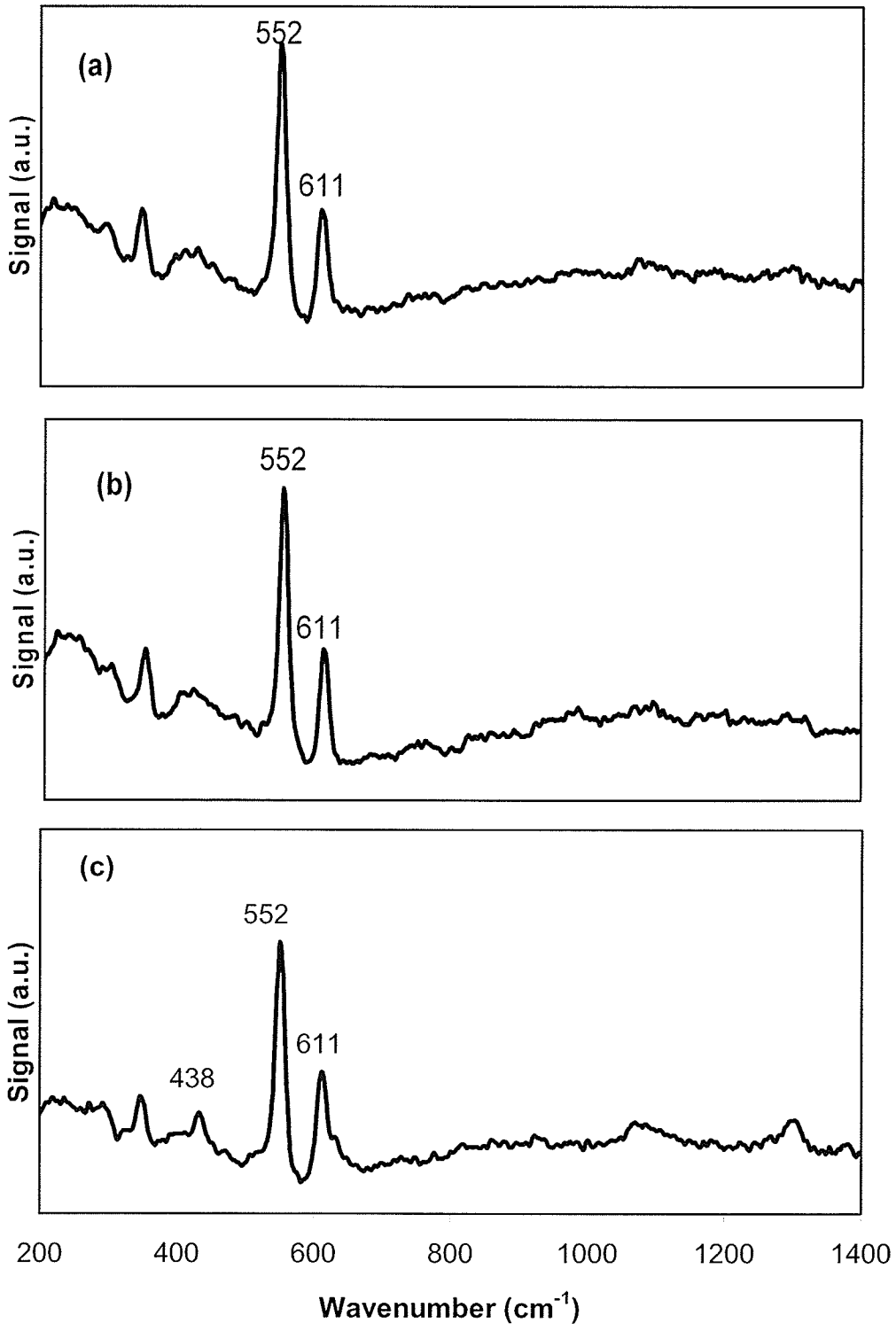

Figure 3.5.3: Raman spectra obtained from various mix ratios of Olive Green and Chinese White oil paint, Cr_2O_3: ZnO (a) 1:1, (b) 5:1, (c) 1:5 using Rockhound™.

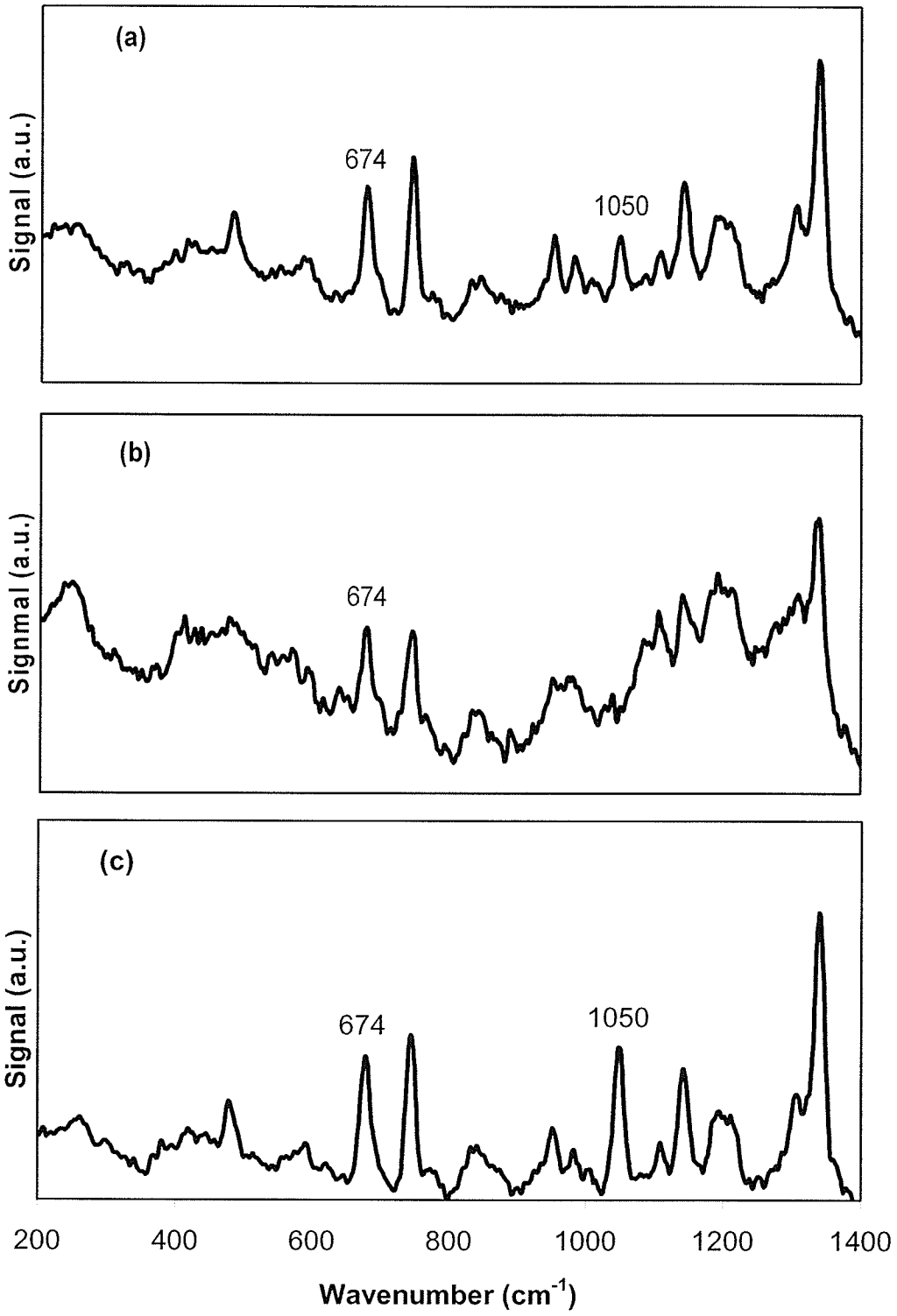

Figure 3.5.4: Raman spectra obtained from various mix ratios of Cerulean Blue and Flake White oil paint, $CoO\cdot_nSnO_2$: $PbCO_3$ (a) 1:1, (b) 5:1, (c) 1:5 using Rockhound™.

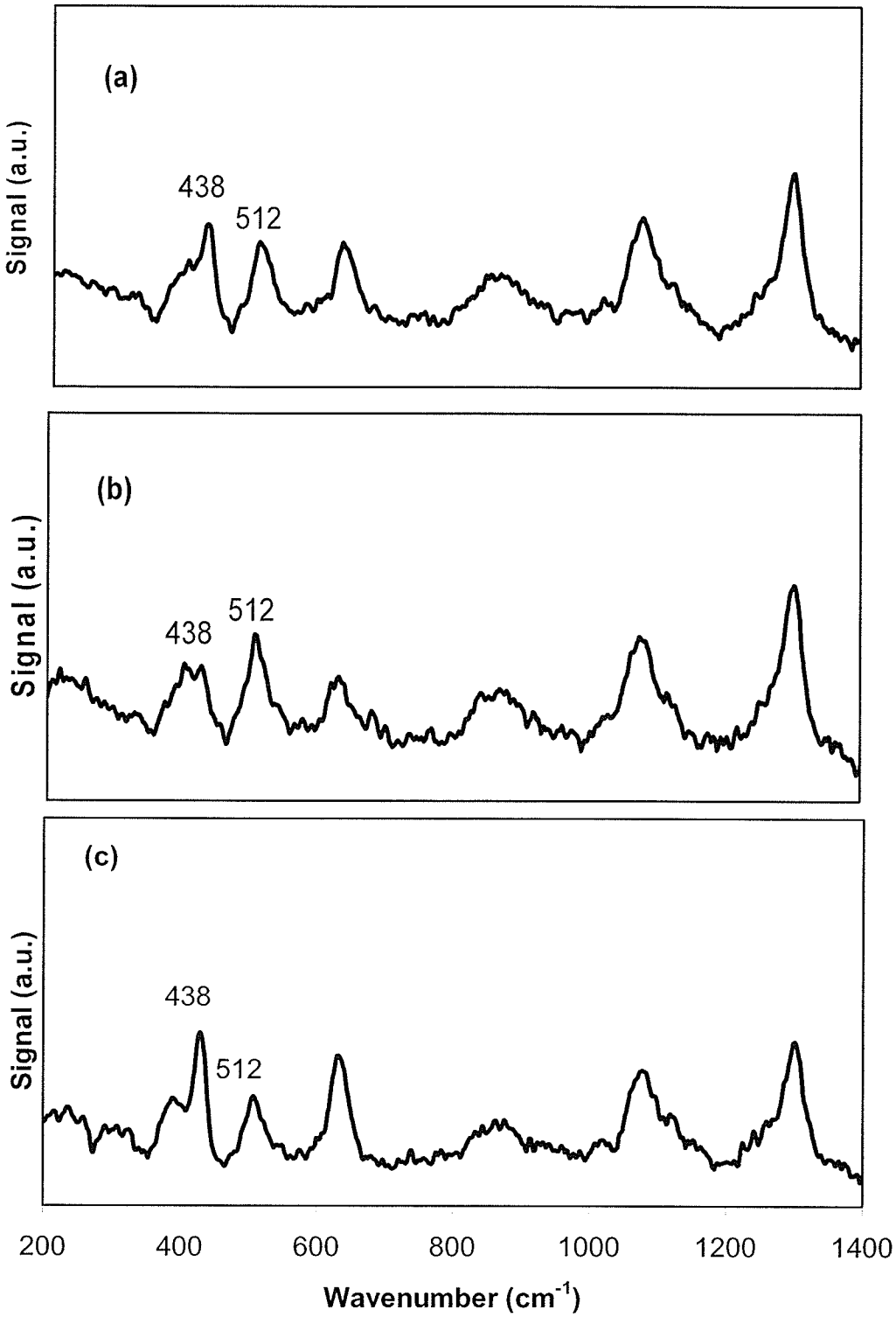

Figure 3.5.5: Raman spectra obtained from various mix ratios of Cobalt Blue and Chinese White oil paint, $CoO \cdot Al_2O_3$: ZnO (a) 1:1, (b) 5:1, (c) 1:5 using Rockhound™.

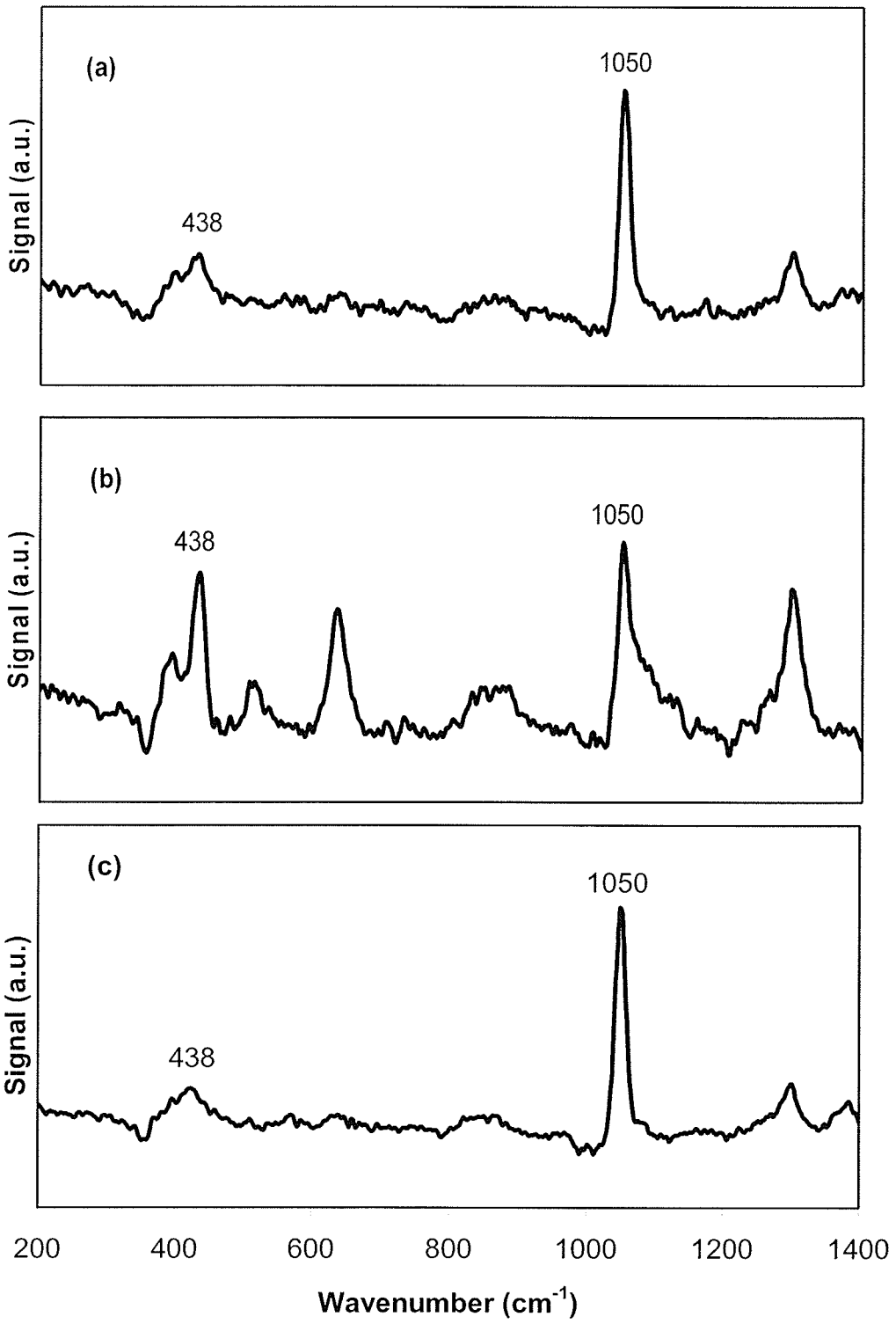

Figure 3.5.6: Raman spectra obtained from various mix ratios of Chinese White and Flake White oil paint, $PbCO_3$: ZnO (a) 1:1, (b) 1:5, (c) 5:1 using Rockhound™.

3.6 Case Studies

Two case studies were considered for this research: a painting on canvas and a map. The objective of each study was to identify pigments that had darkened in order to determine proper conservation and restoration methods. The first object that was examined was a painting, 'untitled – Arctic Spring' (1950), by George Swinton (Fig. 3.6.1). Swinton (1917-2002) was a respected Canadian artist and collector of Inuit artwork in the province of Manitoba, Canada. The problem with 'Arctic Spring' is that it has darkened noticeably since it was created. Areas of paint that were originally white in appearance have become either grey or dark grey in appearance over time. Identifying the white pigments in this painting was a logical first step toward understanding why darkening has occurred. Pigment discolouration may also lead to incorrect pigment identification, which may negatively affect the storage and conservation of the object.

Figure 3.6.1: Colour photograph of Untitled (Arctic Spring), 1958 by George H. Swinton (Canadian, 1917-2002). Gouache on paper: 50.5x76.2 cm. Collection of The Winnipeg Art Gallery; Gift of the Women's Committee (Accession # G-58-8). Photo by Cathy Collins.

A number of areas in 'Arctic Spring' were sampled using a cotton bud with the goal of detecting the pigment metals for the purpose of identifying both the white pigment and possibly the cause of the darkening of the paint in this piece. Figure 3.6.2 shows transient signals obtained from GFAAS analysis. This can be a time consuming approach because the signals for each metal must be collected separately. Absorbance signals for a number of metals that are typically associated with white pigments were measured, including: Ti, Ba, Zn, Pb and Ca. Of these, the largest signals were for Ba and Zn, which indicated that the important white pigment in this piece was probably Lithopone ($BaSO_4$, ZnS). A second approach that was explored for metal identification was ETV-ICP-MS. With this technique, the sample is vaporized in much the same manner as GFAAS. The vaporized pigment metals are ionized in the ICP prior to entering the mass spectrometer. The advantage of using this approach is that multiple signals can be acquired in a single firing of the furnace. Although typically 6 – 7 masses were monitored per ETV firing, other workers have shown that as many as 20 – 25 masses can be measured with quadrupole based instruments[97,98]. In practice, fewer masses are monitored because quadrupole-based instruments (the most commonly used mass spectrometer in ICP-MS instrumentation) operate in a sequential mode, transmitting only one mass-to-charge ratio at each moment (dwell time ~ 10 ms) and they have a poor suitability to deal with the transient signals generated by the ETV.

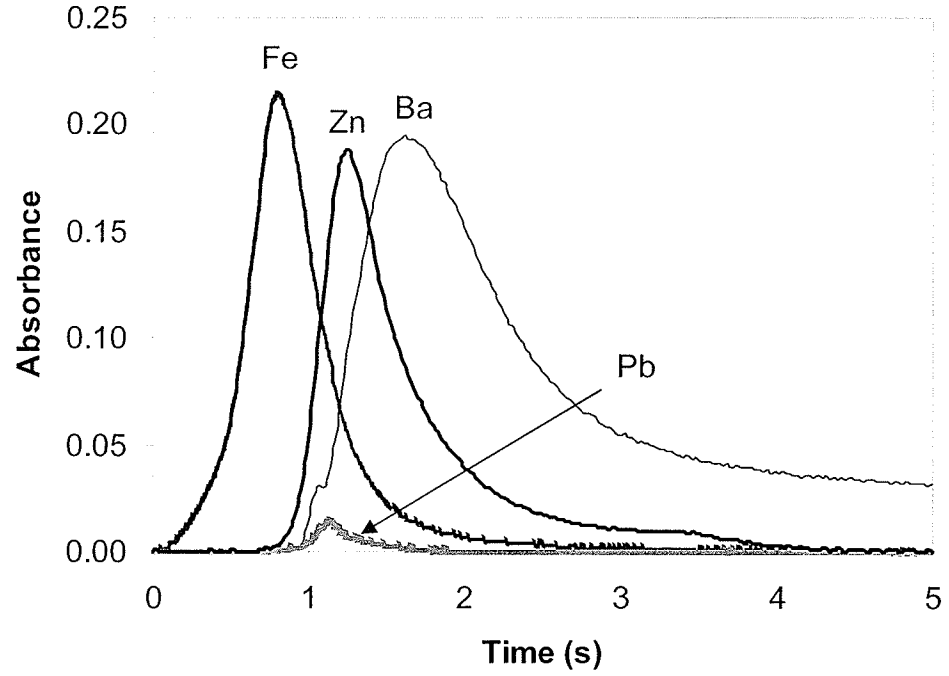

Figure 3.6.2: GFAAS signals of pigment extracted from darkened area of 'Artic Spring'.

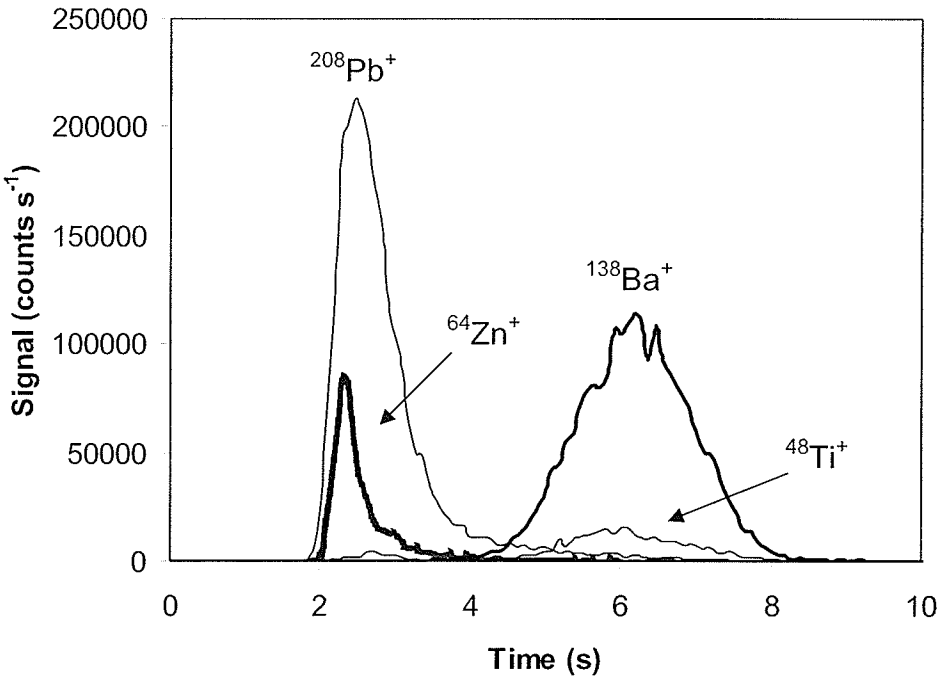

Figure 3.6.3: ETV-ICP-MS signals of pigment extracted from darkened area of 'Arctic Spring'.

Figure 3.6.3 shows the transient signals of metals from a darkened area of 'Arctic Spring'. As with the GFAAS determinations, the presence of large amounts of $^{64}Zn^{+}$ and $^{138}Ba^{+}$ were detected using ICP-MS, again indicating that the darkened pigment was Lithopone. With the ETV-ICP-MS, trace amounts of other metals such as Cd and Ti were detected. Surprisingly large signals for Pb were also observed using both GFAAS and ETV-ICP-MS. The higher sensitivity of EVT-ICP-MS for ^{208}Pb is also illustrated in the Figure.

Solution nebulization ICP-MS is extremely useful for obtaining information regarding the elemental abundance for most of the elements in the periodic table. For example, a more complete estimation of the elemental distribution of metals in different pigments is easily achieved by performing a mass scan. This can provide useful information on both pigment metals and other metals, which may be present either as impurities or as a result of mixing 2 or more pigments. Figure 3.6.4 shows the elemental composition of different areas (Dark, Light, Paper) of 'Arctic Spring'. The darkest areas labelled as 'Dark' and areas that had darkened, but were lighter in appearance, are labelled as 'Light'. For comparison a small area on the painting that was white in appearance is also shown as 'Paper' in this Figure. In Figure 3.6.4 the presence of large amounts of $^{64}Zn^{+}$ and $^{138}Ba^{+}$ were detected in all areas of the darkened white pigment, which is consistent with the pigment Lithopone. Low concentrations of $^{114}Cd^{+}$, $^{88}Sr^{+}$ and $^{208}Pb^{+}$ were also detected, possibly as impurities. The small area that was white in appearance ('Paper') contained significant amounts of $^{44}Ca^{+}$ and much less $^{64}Zn^{+}$ or $^{138}Ba^{+}$, which may indicate that a Ca containing pigment (e.g. $CaCO_3$) was used as a ground layer.

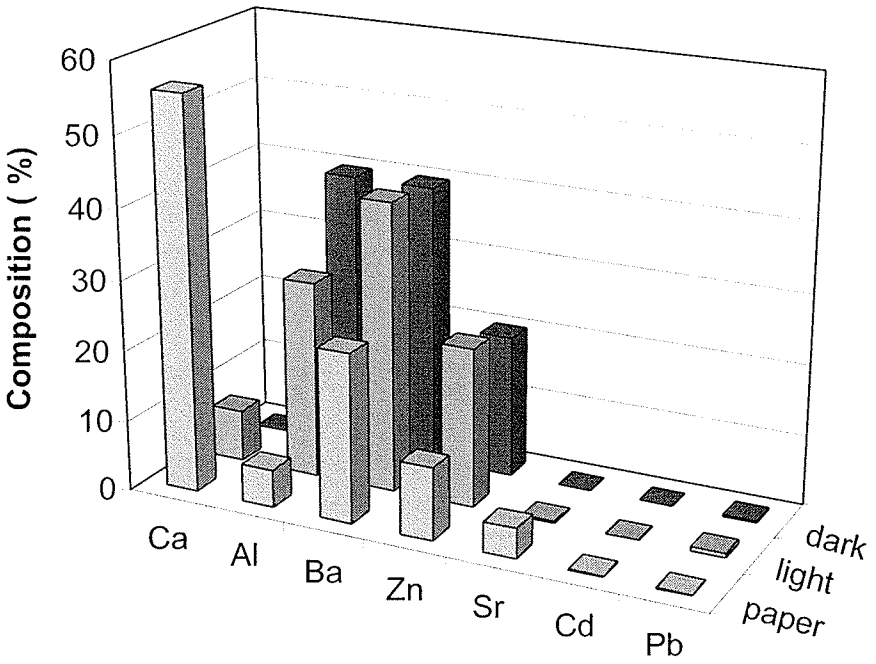

Figure 3.6.4: Mass Scan of white and darkened areas of Swinton's 'Arctic Spring'.

The questionable permanence of Lithopone has been known for a long time and its problems as a modern pigment are well documented[99,100]. Exposure to sunlight and atmospheric levels of oxygen are known to darken this pigment especially in the presence of moisture. The darkening of Lithopone is attributed to the photochemical reduction of the ZnS (white) to elemental Zn (dark), which results in a darkened appearance on the paint surface. Early in its history, manufacturers became aware of this problem as well as its reversibility when it is stored in the dark. A number of approaches have been developed to prevent the darkening such as adding magnesium or even coating it with varnish[101].

Apart from positively identifying the darkened pigment, an interesting outcome of this work was the identification of other metals such as Pb and Fe in the Lithopone. The concentrations of Pb and Fe were further quantified using GFAAS to determine if the concentrations of these metals varied with the extent of darkening. The concentration of Pb and Fe were both found to be approximately the same in areas of the painting that were darker as shown in Table 3.6.1. Because of their low concentrations relative to Ba and Zn, it would be difficult to suggest that Pb or Fe contributed significantly to the darkening of Lithopone. At present, there is no experimental evidence to confirm why Lithopone has darkened in 'Arctic Spring' other than the photochemical reduction of Zn.

Table 3.6.1: Summary of quantitative analysis of selected elements in 'Arctic Spring'.

	Concentration (nM)			
	Pb	**Ba**	**Zn**	**Fe**
Dark gray	0.04 ± 0.01	6.77 ± 3.77	2.61 ± 0.45	0.18 ± 0.02
Light gray	0.06 ± 0.06	7.77 ± 10.1	3.22 ± 2.68	0.28 ± 0.12

n = 3

The second object investigated, 'Mapp or Generall Carte of the World' (circa 1669), provided a similar challenge in terms of pigment identification. This map of the world is part of the holdings in the Hudson Bay Archives (Accession Number: 1987/199) and is housed in the Archives of Manitoba (Winnipeg, Canada). The map, shown in Figure 3.6.5, is an engraved map that was executed in black ink on laid paper during the time of King Charles the Second (1660-1685). It is a map of the world, drawn in ink by Monsieur Sanson as two hemispheres. It was rendered into English and illustrated with

figures by Richard Blome. As such, some portions of the map are coloured in blue, yellow and red pigments. The problem of darkening of the red pigments became apparent while the map was undergoing cleaning by a conservator. Pigments that were initially red in appearance, such as the decorative flowers, appear to have darkened to a brown colour. In some places the red appearance of this pigment is still evident, but most areas containing the red pigment have a darkened appearance to some degree. Figure 3.6.5 also shows the areas of the map that were sampled with a cotton bud. Solution nebulization ICP-MS was used to obtain mass scans of the blue and red pigments found in the map. Electrothermal vaporization ICP-MS was again used to detect a number of metals in the blue pigment of the oval shaped seal as well as in the red pigment used to colour the decorative flowers. Transient signals for the most important metals detected are shown in Figures 3.6.6 and 3.6.7. Figure 3.6.6 shows the ETV-ICP-MS signals obtained from the red pigment. Other than trace amounts of $^{52}Cr^{+}$, the element that was in the highest concentration was $^{208}Pb^{+}$. In this experiment, the large $^{208}Pb^{+}$ signal relative to the blank clearly indicated that this was a Pb containing pigment. Figure 3.6.7 shows transient signals obtained from ETV-ICP-MS for the blue coloured pigment. It was apparent from this experiment that relatively high concentrations of $^{63}Cu^{+}$ were detected as well as other metals including $^{138}Ba^{+}$, $^{52}Cr^{+}$ and $^{75}As^{+}$ in varying concentrations. The transient signals obtained using ETV-ICP-MS were useful for identifying the metals present. The lack of standards prevented accurate quantification of the relative concentration of metals, which would be required for pigment identification if a mixture of pigments was present.

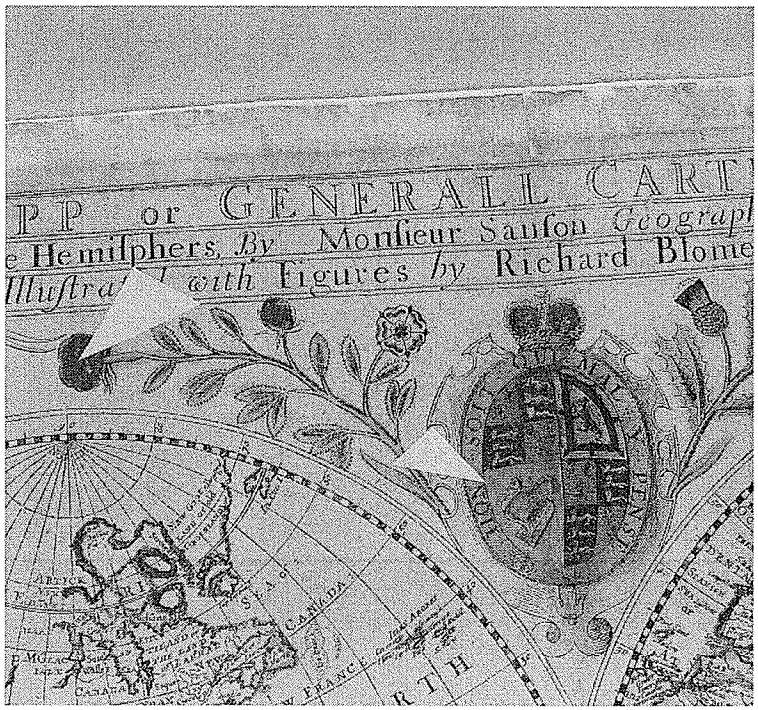

Figure 3.6.5: Colour photograph of a portion of the 'Mapp or Generall Carte of the World Designed in two Plaine Hemisphers' by Monsieur Sanson, Hudson's Bay Company Archives (Accession Number: 1987/199).

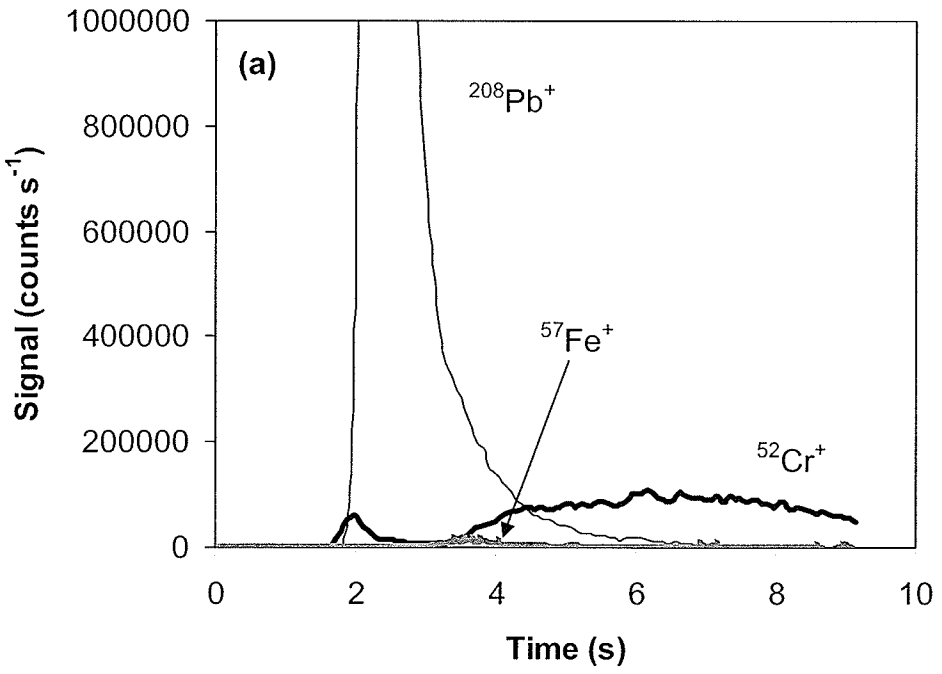

Figure 3.6.6: ETV-ICP-MS signals of darkened red pigment in the 'Generall Carte of the World'.

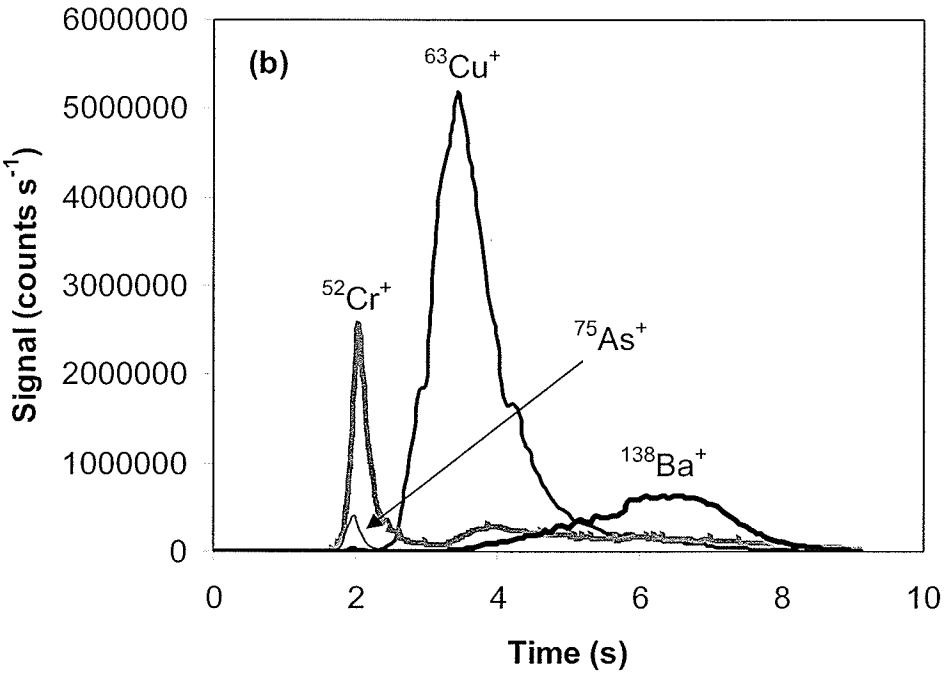

Figure 3.6.7: ETV-ICP-MS signals of blue pigment in the 'Generall Carte of the World'.

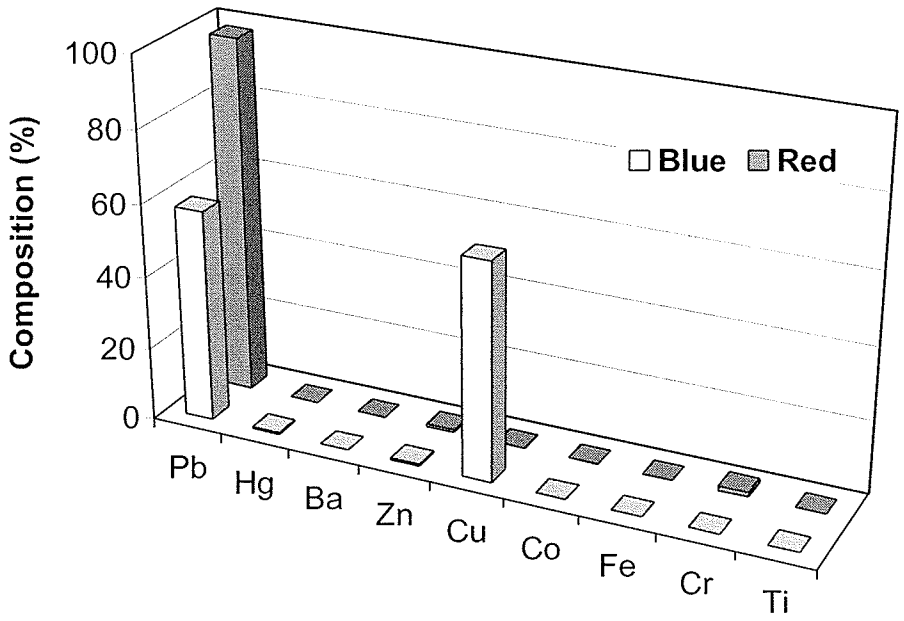

Figure 3.6.8: Mass Scan of blue and darkened red pigments in the 'Generall Carte of the World'.

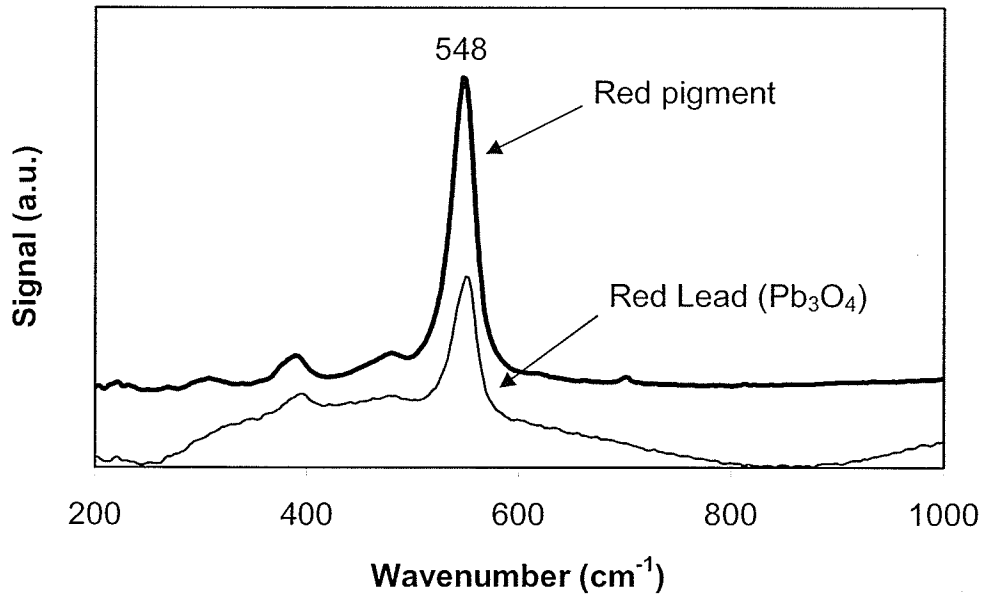

Figure 3.6.9: Raman Spectra of darkened pigment of the 'Generall Carte of the World'.

Solution nebulization ICP-MS was used for quantitative analysis of the red and blue pigments (Fig. 3.6.8). The purity of the pigments used to colour portions of this map became evident by the relative absence of metals other than the pigment metals. Apart from some degree of fading with the blue pigment, the colour of this pigment was still apparent and had not degraded. The relative absence of Cr and the high concentration of Cu, suggests that this pigment was most likely copper carbonate. The basic form of copper carbonate, $CuCO_3 \cdot Cu(OH)_2$, is a pigment obtained from the mineral azurite. It was not possible to obtain a Raman spectrum from the blue pigment because the paint layer was both too thin and somewhat transparent.

The absence of Fe or Hg indicated that neither Red Ochre (Fe_2O_3) nor Cinnabar (HgS) was used in this object. Since it had a very high concentration of Pb, the most likely identity of the red pigment could be Chrome Red ($PbO{\cdot}PbCrO_4$), Molybdate Red ($7PbCrO_4{\cdot}2PbSO_4{\cdot}PbMoO_4$) or Red Lead ($Pb_3O_4$). The Advantage 200A^{TM} Raman spectrometer was used to confirm the structure of the darkened pigment. This was necessary because both Cr and Mn were detected in measurable quantities with the ICP-MS. Figure 3.6.9 shows a Raman spectrum of the darkened pigment. For comparison, a Raman spectrum of pure Pb_3O_4 is also shown and indicates that the darkened pigment is consistent with Red Lead. The absence of CrO_4^{2-} or MoO_4^{-} modes in the Raman spectrum indicates that Cr and Mn are present as impurities in the darkened pigment.

Red lead is a pigment that is known to darken over time as a result of oxidation of the Pb(II) atoms in Pb_3O_4 to PbO_2 (Pb(II and IV)), which is dark brown in appearance[102]. Platternite (PbO_2) appears to have been detected in wall paintings using X-ray diffraction, however, a more recent study used Raman spectroscopy for identifying degradation products of lead pigments[52]. This work presented a reasonable degradation pathway for red lead Pb_3O_4 to PbO (litharge, tetragonal) which will ultimately form PbO (massicot, orthorhombic). Unfortunately the detection of PbO_2 in painted objects using Raman spectroscopy is difficult at best since PbO_2 is a weak Raman scatterer.

The most important advantage of using the cotton bud was the relative ease with which a surface layer of paint could be sampled, and it worked equally well when either oil or water was used as the binding agent. This approach was limited to sampling only the surface, and a protective layer of varnish would have certainly diminished the

usefulness of microsampling with a cotton bud. For older cultural objects that have not been stored properly, dirt or soot accumulated on the surface would certainly affect the observed elemental composition. The magnitudes of the AAS or ICP-MS signals, obtained from the metal-containing pigments, were usually large enough that small amounts of dirt or soot should not interfere with pigment identification. This may not be the case for metals that are present in pigments in low concentrations, such as when pigments are mixed.

4.0 CONCLUSION

Sampling with a cotton bud allows for the analysis of small quantities of paint with minimal damage to the surface of an object. The small sample size requirement (1 μg or less) of GFAAS and ETV-ICP-MS makes them very powerful techniques for detecting small quantities of metals. In many ways the multi-technique approaches used in this study were complimentary to each other. If one instrumental technique gave unsatisfactory results, it was replaced with another. For example, elements such as $^{56}Fe^{+}$ and $^{52}Cr^{+}$ which have spectral interferences with $^{40}Ar^{16}O^{+}$ and $^{40}Ar^{12}C^{+}$ can be problematic for the ICP-MS user. These problems were easily overcome by using GFAAS for these metals. The Raman spectrometer was capable of identifying individual pigments in a mixture; however, it was suggested that standards representing the suspected pigment mixture should be prepared and used as a guide to estimate the pigment ratio. The high sensitivity of ETV-ICP-MS and GFAAS for most metals allows the user to determine if more than one pigment is present. Since detecting only the metals present was insufficient at times for identifying a pigment, the use of Raman spectroscopy was essential for confirming the chemical structure of the pigment.

5.0 RESULTS AND DISCUSSION CHAPTER 2: LOW POWER ELECTROCORROSION FOR METAL IDENTIFICATION USING SPECTROSCOPY

A number of different alloys were used as test materials including brass, steel, aluminum and silver. The electrocorrosion process for oxidizing and removing a small amount of metal sample appeared to work equally well for all of the alloys tested. For example, it was found that 316L Steel would generate a Cr absorbance comparable to a 40 ppb standard after 10 s of electrocorrosion. Figure 5.0.1 is an example of an absorbance signal from a sample that was obtained using 316L steel. The results yielded absorbance peaks for Cr (16 – 18%) and Ni (10 – 14%) while the signal for Cd (0%) was essentially baseline, demonstrating that this technique can be used for qualitative and semi-quantitative analysis of alloys to determine their metal content.

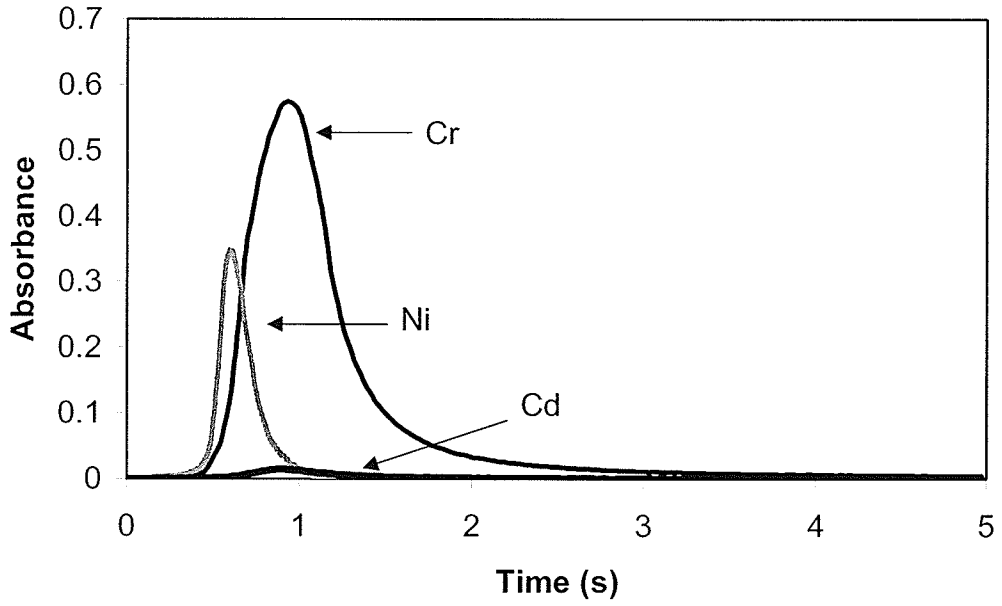

Figure 5.0.1: Typical absorbance signals generated using a 316L Steel sample.

5.1 Sample Preparation

For low power electrocorrosion to be used for the analysis of valuable objects, it would be advantageous to be able to obtain a sample without pre-treatment of the surface. As a result, an experiment was performed to determine if it was necessary to file or polish the metal rod between samples. A set of 9 trials were prepared using an electrode that was pre-soaked in 0.05 M NaCl solution prior to corrosion for 10 s with 9 V applied potential. Samples were obtained from 316L Steel in series without polishing.

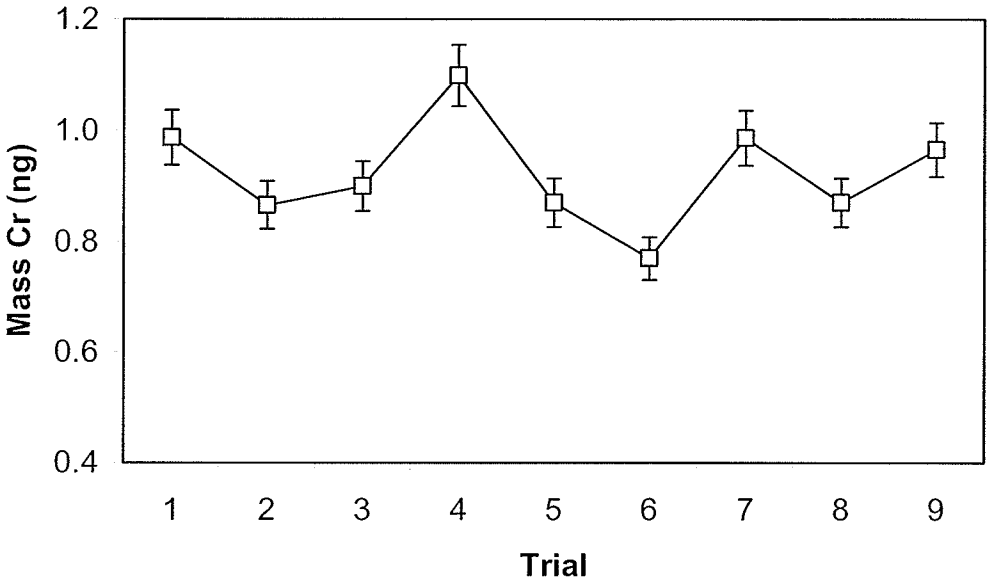

Figure 5.1.1: Absorbance of Cr in 9 trials sampled and analyzed in sequence without filing the metal rod in between samples.

Figure 5.1.1 illustrates that there was no trend when 9 samples were prepared and analyzed in sequence. Error bars on the vertical axis represent the measurement uncertainty of the instrument (i.e. ± 5%). The results indicate that polishing the metal rod between samples was an unnecessary step and could be omitted at least for Cr in 316L Steel. All subsequent analyses were performed without polishing or treating the metal between corrosion experiments.

5.3 Optimization of Metal Extraction

Several experiments were performed to determine the precision of the sampling technique and it was found that the percent relative standard deviation (% RSD) ranged between 30 – 35%. It was hypothesized that complete extraction was not occurring because the metals may have been interacting with the cotton. If the reactions suggested by Stansbury and Buchanan[41] occur for low power electrocorrosion then the electrons in the cellulose may be interacting electrostatically with the oxidized metal species. In order to determine if the cotton bud was contributing to poor signal reproducibility as a result of incomplete metal extraction an experiment was performed to isolate the extraction efficiency of metal from the cotton bud. A known amount of standard Ag solution was injected onto the cotton bud in a 1.5 ml polystyrene cup. The cotton was then digested for 5 minutes in 200 µl concentrated HNO_3 and the cup was filled with de-ionized water (~ 1.5 ml). Two control trials were prepared by adding a known aliquot of the Ag standard directly to a polystyrene cup without the cotton bud. Analysis was performed using GFAAS and the extraction efficiency was calculated using the controls as 100% recovery. It is important to note that aqueous solution was not added to the cotton bud prior to analysis because it was not possible to inoculate the cotton while it was saturated with solution.

It was found that the extraction efficiency of the Ag standard from the cotton was 102 ± 6%, indicating complete recovery and disproving the hypothesis that the metal was interacting with the cotton in such a way as to inhibit extraction. This established that the extraction step probably did not introduce significant error.

Low power electrocorrosion was applied to several other metals under various conditions to establish sampling precision and it was found that precision did not improve. Given that quantitative metal recovery was occurring it was necessary to develop a new sampling method. Filter paper was substituted for the cotton bud because it made a flexible electrode, and was found to be relatively free of transition metal contamination relative to the blank. The extraction efficiency experiment was repeated for the filter paper to determine if it would yield results that were comparable to the cotton bud. Two metals were used for the filter paper experiment to demonstrate that the method would apply to more than one type of metal; Co and Ag were chosen because they have different chemical and physical properties such as oxidation states, standard reduction potentials and reactivity. A set of samples were prepared with a Ag and Co standard spike. Table 5.2.1 shows that the extraction efficiency from filter paper was similar to the extraction efficiency from the cotton bud and therefore, switching to filter paper would not interfere with metal recovery.

Table 5.2.1: Extraction efficiency of Ag and Co from filter paper.

	Co Extraction Efficiency (%)	**Ag Extraction Efficiency (%)**
Average	101.2 ±1.36	99.97 ±3.18

n = 10

Since it was established that quantitative recovery of the metal was possible, it was necessary to determine whether an acid digestion step was required. Acid digestion is typically employed to ensure that there is complete matrix dissolution in order to obtain a homogeneous sample[28]. For the purpose of this study acid dissolution was used to release metal from the cellulose electrode. It was possible that the addition of acid was unnecessary if de-ionized water was capable of extracting the metal from the cellulose. If possible, it is useful to avoid the addition of reagents to the sample as they could be a source of metal contamination. Acid may contribute to higher signals for blanks, and it is advisable to limit the quantity of strong acids used during the digestion and dissolution process as they may contribute to matrix effects[28]. The experimental method employed was similar to the procedure used to determine extraction efficiencies. Several acid digestion controls were prepared and analyzed and the results were compared to several trials that were performed without an acid digestion step. Quantitative extraction was obtained from the acid control group, whereas an extraction efficiency of less than 15% was achieved when no acid was present (Table 5.2.2) demonstrating that extraction with acid was required. Nitric acid was used in all subsequent analyses unless otherwise stated.

Table 5.2.2: Extraction efficiency of Ag with and without concentrated HNO_3.

	Extraction Efficiency (%)	
	Acid (n = 5)	**No acid (n = 10)**
Average	103.9 ± 0.8	13.42 ± 5.26

It was practical to determine the time required for complete metal extraction from cellulose. Long digestions allow more time for possible contamination to occur and it was useful to have a rapid dissolution technique for higher sample throughput. The experimental method was similar to the procedure used to determine extraction efficiencies. Filter paper was 'spiked' with a Ag and Co standard and 150 µl of concentrated HNO_3 was added. The results demonstrated that the addition of acid to the sample was sufficient to achieve complete recovery (Table 5.2.3).

Table 5.2.3: Extraction efficiency of Co and Ag from cellulose extracted for various amounts of time.

Time (s)	Ag Extraction Efficiency (%)	Co Extraction Efficiency (%)
0	101.3 ± 1.65	101.2 ± 2.07
30	103.9 ± 1.46	102.0 ± 3.11
60	101.9 ± 2.74	103.1 ± 1.71
90	98.94 ± 1.29	104.4 ± 2.12

n = 5

In order to minimize the amount of acid added to the samples an experiment was performed to determine the optimal acid volume required for complete extraction (Table 5.2.4).

Table 5.2.4: Extraction efficiency of Co and Ag from cellulose extracted with various volumes of HNO_3.

Volume HNO_3 (µl)	Cr Extraction Efficiency%	Co Extraction Efficiency %
0	6.010 ± 1.71	5.689 ± 1.45
50	105.0 ± 2.18	99.78 ± 2.68
100	101.9 ± 1.35	100.3 ± 2.42
150	98.93 ± 2.36	101.1 ± 2.01
200	100.9 ± 4.51	102.9 ± 1.89

n = 8

The results show that at least 50 µl of HNO_3 must be added for complete extraction of the metal from the filter paper. For all subsequent analyses 100 µl of HNO_3 was used for metal extraction.

5.3 Effect of Corrosion Time

A number of experimental parameters affect the quantity of metal that is electrocorroded from the surface of an alloy, including sampling time, applied potential and ionic strength. Figure 5.3.1 and 5.3.2 show the corroded mass of Cr, Ni, Cu, and Mn from various alloys. The samples presented in Figure 5.3.1 were sampled using 9 V of applied potential and a cellulose electrode that was pre-soaked in 0.05 M NH_4NO_3. For Figure 5.3.2 the samples were electrocorroded using 18 V of applied potential and a cellulose electrode that was pre-soaked in 0.6 M NH_4NO_3 and 0.125 M HNO_3. For short sampling times (< 2 minutes) the mass corroded appeared to increase linearly. For SRM

663 steel the relative masses of metal removed were consistent with the composition of the steel alloy, Mn (1.50%), Cr (1.31%), Ni (0.32%) and Cu (0.098%). This is consistent with the results reported by Boileau et al.[37] for high power electrocorrosion in solution. Boileau et al.[37] reported that different corrosion rates could be explained by the varying alloy compositions. This experiment illustrates that for metals in high concentrations (%), there was the possibility of obtaining a representative sample and performing semi-quantitative analysis after only 60 s.

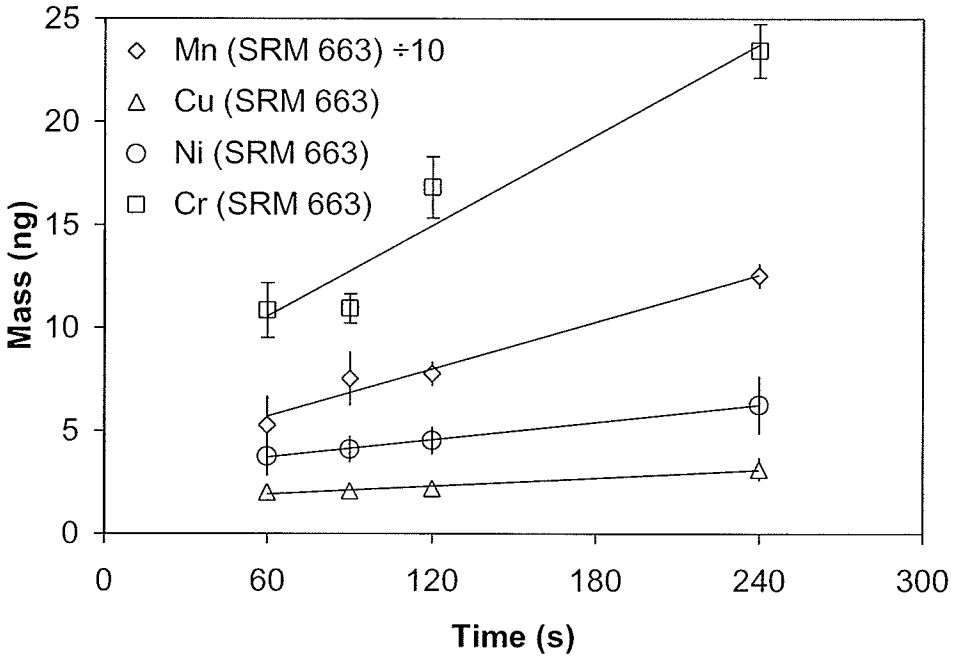

Figure 5.3.1: Mass of Cu, Cr, Mn and Ni removed from SRM 663 Steel at various sampling intervals (n = 6).

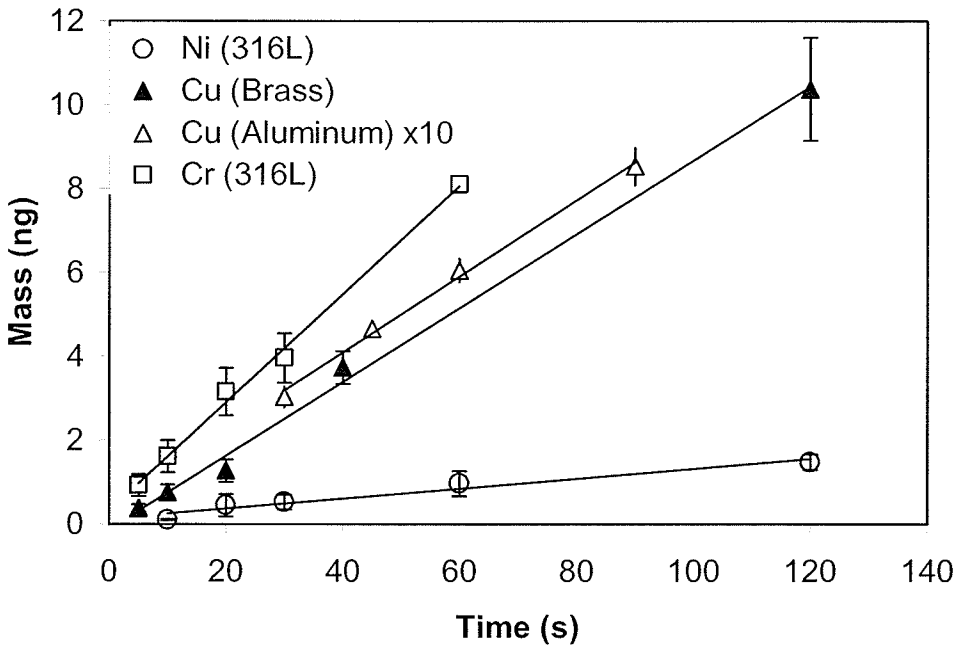

Figure 5.3.2: Amount of analyte corroded over time; Cr, Ni (316L Steel) and Cu (Brass and 2xxx Aluminum) in 0.05M NH_4NO_3 with a 9-V battery (n = 6).

The rates of metal corrosion for SRM 663 and various other alloys were plotted for each time interval and the results are shown in Figures 5.3.3 and 5.3.4. These figures show that the corrosion rates for each metal in the alloy decrease as soon as potential is applied. The decrease in rate of electrocorrosion eventually levels off after longer time intervals (> 2 minutes). A logical explanation for the decrease in rate would likely be physical (evaporation) and chemical changes (oxidation on the metal surface). The maximum corrosion rate for each metal decreased from 870 to 125 pg s^{-1} for Mn and from 34 to 5 pg s^{-1} for Cu in SRM 663. Depending on the composition of the alloy under investigation, optimal sampling times for most metals range from 10 – 120 s; collecting sample for longer periods did not significantly increase the amount of metal removed.

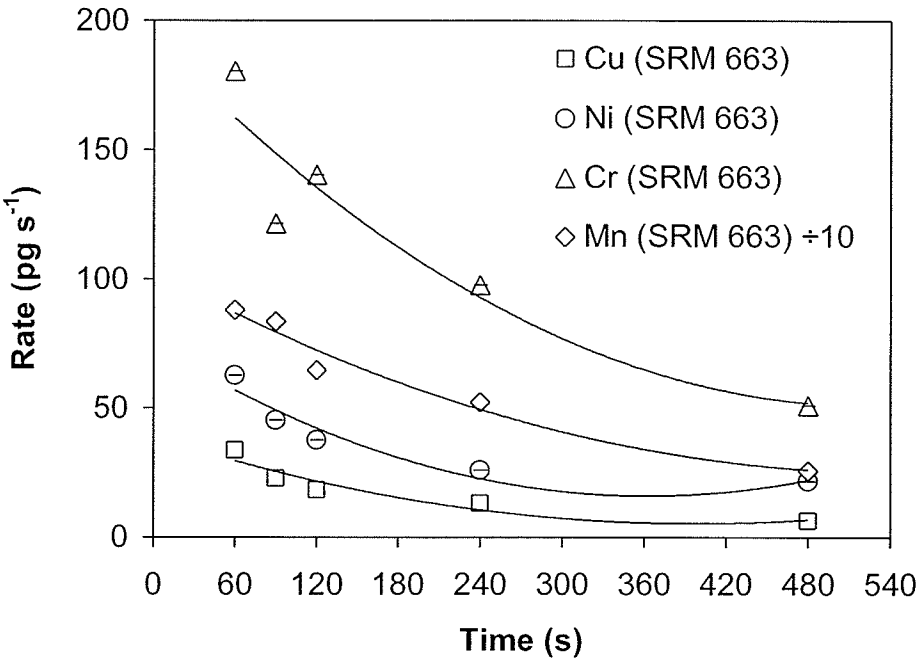

Figure 5.3.3: Rate of metal removal as a function of sampling time (n = 6).

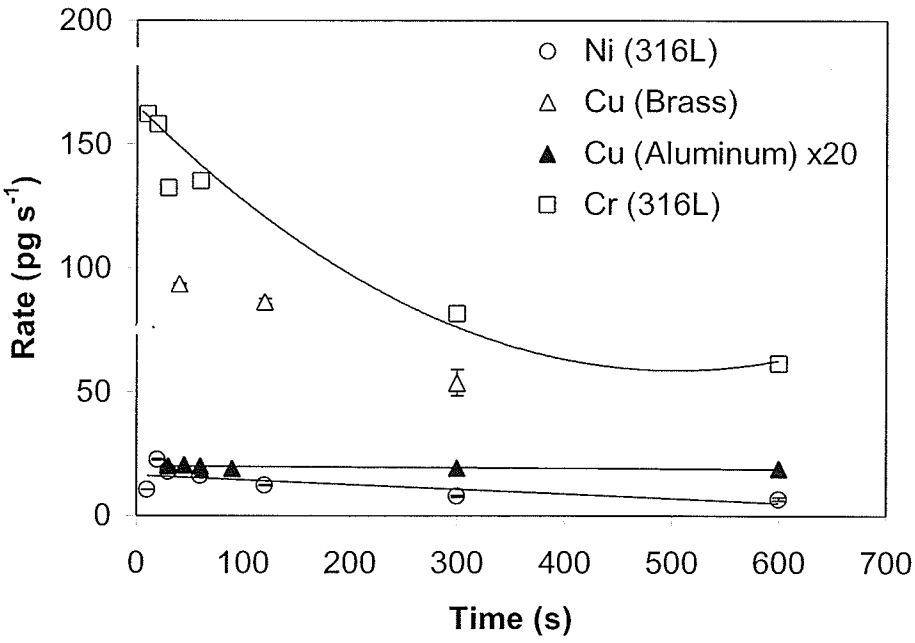

Figure 5.3.4: Rate of electrocorrosion of Cr, Ni (316L Steel) and Cu (Brass and 2xxx Aluminum) in 0.05M NH_4NO_3 with a 9-V battery (n = 6).

High power electrocorrosion is based on the same principals as low power electrocorrosion because it also uses electrolysis to achieve metal oxidation[37]. For high power (10 – 30 W) electrocorrosion the samples are immersed in an aqueous solution, which affects the corrosion behavior with regards to the sampling parameters such as corrosion time. During high power electrocorrosion the rate of dissolution increases over time as a result of increasing conductivity of the surrounding aqueous solution. Goltz et al.[103] found that the rates of corrosion of Fe in steel increased over time as a result of increased solution conductivity and increased spark gap when using high power electrocorrosion. The conductivity increases as a result of contributions from the dissolved metal and from increasing temperature (molar conductivities increase with temperature). The difference between the corrosion rates of low power electrocorrosion using a cellulose electrode and high power electrocorrosion in solution suggests that physical changes such as evaporation of the aqueous solution played a significant role in the low power electrocorrosion process since the mechanism of metal oxidation is similar.

5.4 Effect of Applied Potential

The effect of increasing applied potential on the mass corroded at specific time intervals was examined. Figure 5.4.1 shows the relationship between applied voltage (1.5 – 27 V) and mass corroded for both ferrous and non-ferrous alloys. In this experiment the applied voltage was increased by using additional batteries in series. For consistent electrocorrosion and reproducible sampling of the metals, exact duplication of experimental conditions was required. This was important because resistance of the filter

paper increased significantly with distance from the electrical contact and highest concentrations of corroded metal were at the metal-electrode interface. The rate of metal corrosion in both ferrous and non-ferrous metals increased linearly with applied potential. In this experiment the Cu content in 2xxx Aluminum was much lower (4 – 6%) compared to that in Brass (30 – 60%) and therefore a longer electrocorrosion time was used for the aluminum alloy. Unlike Cr in 316L Steel, the mass and therefore rate of electrocorrosion of Ni did not increase linearly with applied potential. One possibility was that saturation of the cellulose electrode with Ni was occurring, however this can be probably ruled out since it was not observed with Cr. For steel, a black film was visible on the surface after electrocorrosion, which indicated that an oxide species, possibly NiO, may have formed[104]. Formation of a stable oxide layer could have changed the conductivity which likely affected the rate of corrosion of some metals on the sample surface. Furthermore, some metal oxides may be quite stable and difficult to oxidize.

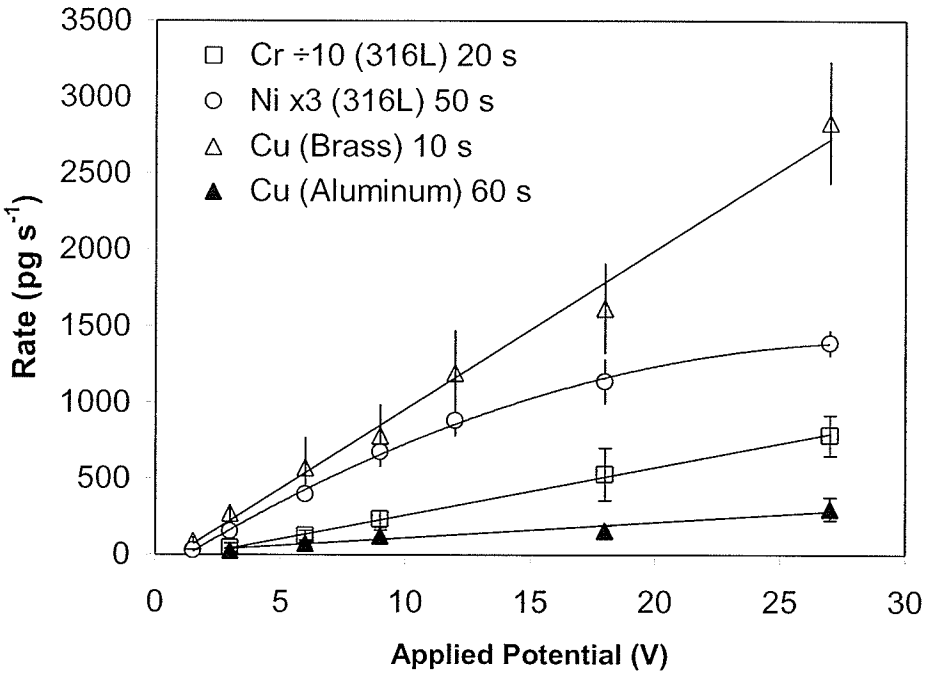

Figure 5.4.1: Rates of Cr and Ni removal from 316L Steel, Cu from Brass and Cu from Aluminum 6061 as a function of applied potential (n = 6).

5.5 Effect of Ionic Strength

Prior to electrocorrosion of a sample, the cellulose electrode was soaked in an aqueous salt solution in order to facilitate the movement of charge and hence oxidation of the metal surface. It was previously observed that the concentration of the salt solution affected the rate of corrosion. Consequently, experiments were carried out to observe the effect of aqueous strength of the solution on the rate of metal corrosion. It was hypothesized that increasing the aqueous strength would increase the conductivity which would increase the mass corroded. Experiments were performed using either NH_4NO_3 or KCl in concentrations ranging from 0.3 M to 3.0 M and acidified with 0.125 M HNO_3. These experiments are similar to work done in previous studies[35,39], where higher

concentrations of HNO_3 were added to the solution as a supporting electrolyte prior to analysis. Figure 5.5.1 shows the rates of corrosion of Cr and Ni from 316L Steel (Fig. 5.5.1a) and Cu and Mn from SRM 663 (Fig. 5.5.1b) with various concentrations of NH_4NO_3 when 18 V was applied for 10 s. Figure 5.5.2 shows the rates of corrosion when the aqueous solution was KCl. As expected the rate of metal removal increased as the aqueous strength increased when the electrode was soaked in either NH_4NO_3 (Fig. 5.5.1) or KCl (Fig. 5.5.2). The rates of corrosion of either Ni, Cr, Cu or Mn were not significantly affected by the type of electrolyte when a high ionic strength solution was used (2.4 – 3.0 M); however, the corrosion behavior appears to be affected at low ionic strength. For example, the ratio of Cr to Ni is 2:1 in 316L Steel which was observed at high concentrations of electrolyte but preferential corrosion of Ni appeared to be occurring when low ionic strength solutions of NH_4NO_3 were used. This did not appear to be the case when KCl was used. A similar trend was observed for Cu and Mn in SRM 663 where Mn appears to be preferentially corroded (Fig. 5.5.1b and 5.5.2b).

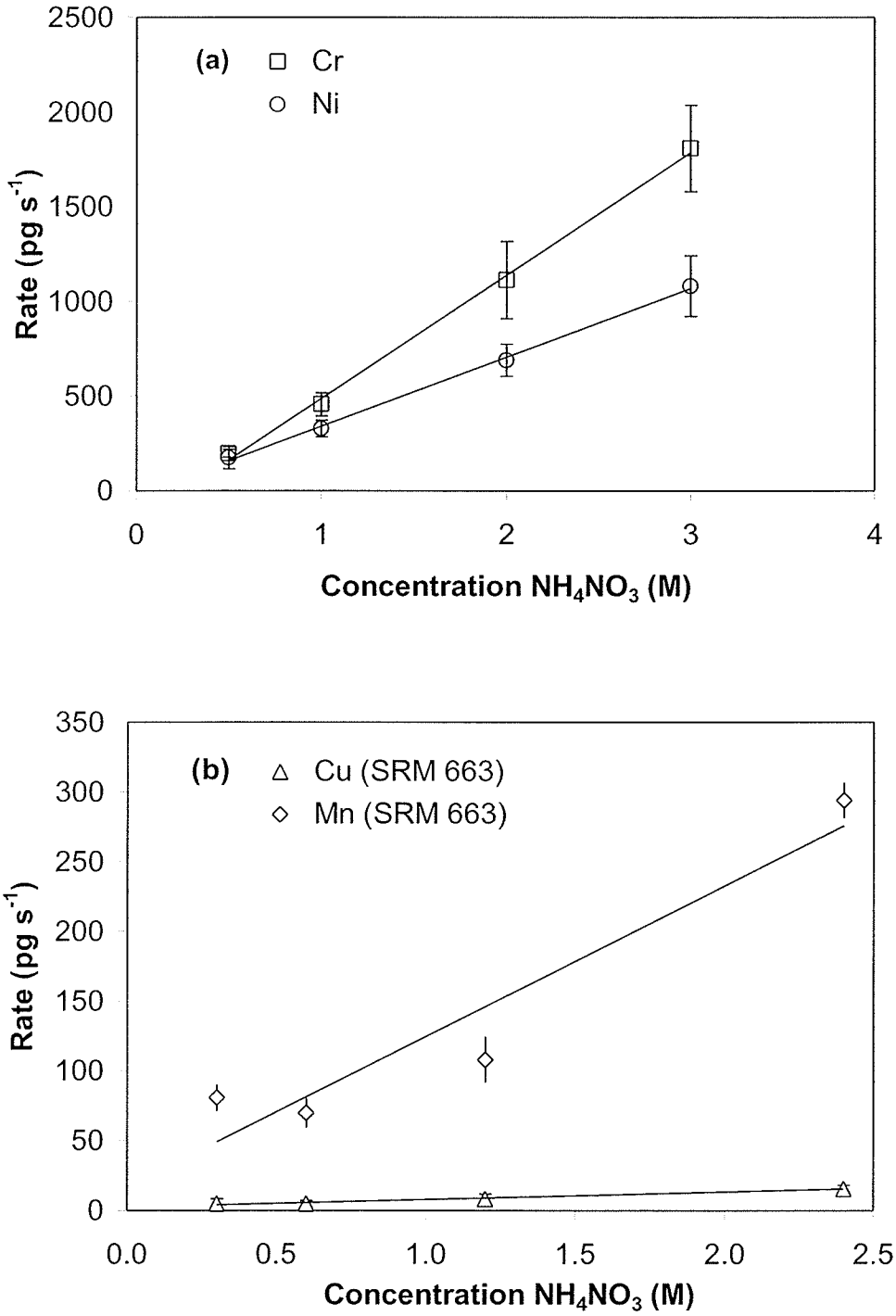

Figure 5.5.1: (a) Rate of Cr and Ni removal from 316L Steel and (b) rate of Cu and Mn removal from SRM 663 as a function of concentration of NH_4NO_3 (n = 6).

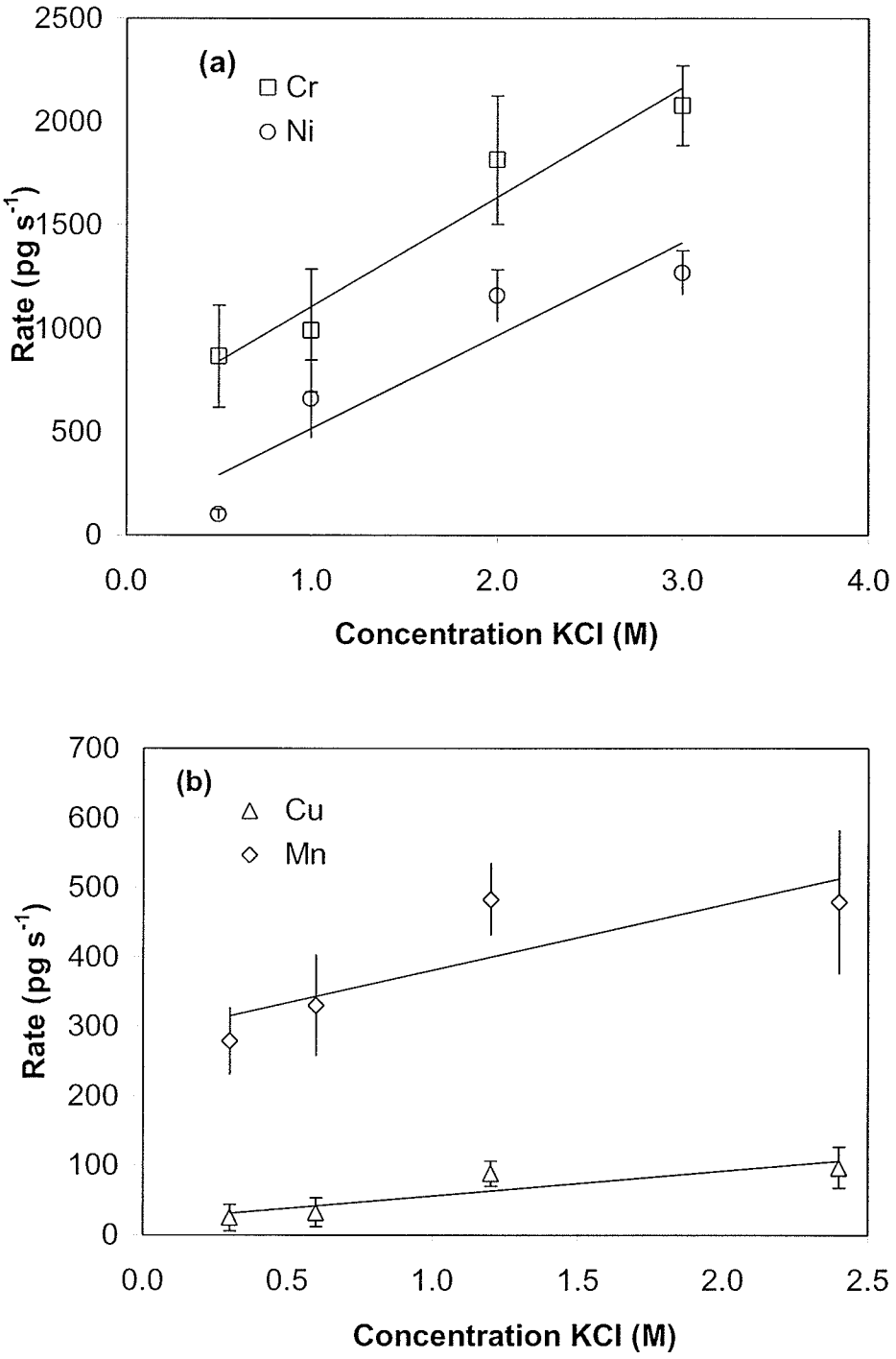

Figure 5.5.2: (a) Rate of Cr and Ni removal from 316L Steel and (b) rate of Cu and Mn removal from SRM 663 as a function of concentration of KCl (n = 6).

5.6 Preferential Corrosion

One fundamental question that required examination was whether one metal was preferentially corroded relative to another in an alloy. If preferential corrosion does occur during electrocorrosion experiments, quantitative analysis would not be possible and the overall effect would be equivalent to incomplete acid digestion. Figure 5.6.1 shows a plot of the mol % of corroded Cr with respect to Ni in sample 316L. For this experiment the metal was corroded at 10, 20, 30, and 60 s using an electrode soaked with 2.4 M NaCl. The slope of the curve is in agreement with the expected ratio (2:1) of Cr to Ni in this steel (16-18 % Cr, 10-14 % Ni). The high degree of linearity (r^2 = 0.999) suggests that neither Cr nor Ni was removed preferentially under these conditions. To verify that preferential corrosion was not occurring several metals in SRM 663 were analyzed to determine if the ratio of each metal pair agreed with certified values. The steel was sampled with an applied potential of 9 V using an electrode soaked in 3 M NH_4NO_3 or KCl in 0.125 M HNO_3. Each alloy was sampled six times each at 40, 60 and 90 s. Tables 5.6.1 and 5.6.2 show the expected and experimental ratios of Cu, Cr, Mn and Ni corroded over time from SRM 663 steel using electrodes soaked in either KCl (Table 5.6.1) or NH_4NO_3 (Table 5.6.2). The ratio of each metal did not change significantly over time. For this experiment shorter time intervals were avoided because of sampling uncertainty due to the small sample size. For all metals, Mn, Cr, Cu and Ni, the expected ratio was within the standard deviation of the experimentally determined value at longer sampling intervals (> 40 s). Unlike NH_4NO_3, when KCl was used it appeared that, relative to other metals, more Ni was corroded than expected. This indicated that preferential corrosion of Ni may have occurred; however, it should

also be noted that the precision was considerably worse for all of the metals with KCl. This was partly due to the matrix effect of Cl^- in the graphite furnace[108] and partly due to random sampling errors (e.g. corrosion time). As such, the magnitudes of the expected ratios of all the metals were still within one standard deviation of the experimentally determined ratios. In general, preferential corrosion should not occur provided that a sufficient ionic strength solution, sampling time and potential are used. This was consistent with results reported by groups studying electrodissolution for metal sample preparation. For example, Souza et al.[45] and Bergamin et al.[43] report that electrodissolution sensitivity is related to current density, electrolyte and sample composition. That preferential corrosion did not occur is significant as it validated this technique for determining approximate elemental ratios for characterizing and identifying alloys. It is also important to note that increasing the amount of metal removed did not have a significant impact on the surface and the technique could still be considered minimally-invasive.

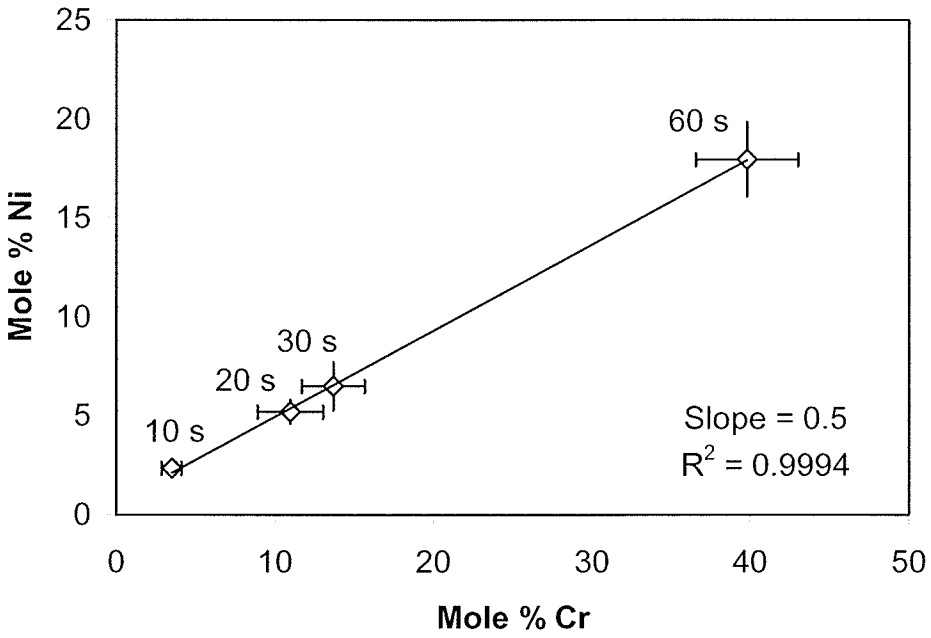

Figure 5.6.1: Mole % Ni plotted against the mole % Cr removed during low power electrocorrosion of 316L Stainless Steel (n = 6).

Table 5.6.1: Ratios of Cu, Cr, Ni and Mn from the corrosion of 663 SRM Steel using cellulose soaked in 3 M KCl and 0.125 M HNO_3 (n = 6).

Time (s)	3 M KCl					
	Cu/Ni	**Cu/Cr**	**Mn/Cu**	**Ni/Cr**	**Mn/Ni**	**Mn/Cr**
30	0.32 ± 0.11	0.07 ±0.04	15.5 ± 6.11	0.22 ± 0.11	4.99 ± 1.36	1.08 ± 0.53
40	0.21 ± 0.06	0.11 ± 0.04	15.4 ± 5.33	0.53 ± 0.18	3.30 ± 0.92	1.75 ± 0.60
60	0.19 ± 0.04	0.10 ± 0.03	15.9 ± 3.04	0.54 ± 0.16	2.97 ± 0.69	1.61 ± 0.46
90	0.15 ± 0.04	0.09 ± 0.03	13.81 ± 4.73	0.60 ±0.23	2.07 ± 0.45	1.24 ± 0.39
Expected	**0.31**	**0.07**	**15.3**	**0.24**	**4.69**	**1.15**

Table 5.6.2: Ratios of Cu, Cr, Ni and Mn from the corrosion of 663 SRM Steel using cellulose soaked in 3 M NH_4NO_3 in 0.125 M HNO_3 (n = 6).

Time (s)	3 M NH_4NO_3					
	Cu/Ni	**Cu/Cr**	**Mn/Cu**	**Ni/Cr**	**Mn/Ni**	**Mn/Cr**
30	0.44 ± 0.18	0.17 ±0.08	8.72 ± 3.77	0.39 ± 0.17	3.80 ± 1.07	1.48 ± 0.48
40	0.43 ± 0.05	0.16 ± 0.02	15.3 ± 3.61	0.37 ± 0.05	6.52 ± 1.53	2.38 ± 0.57
60	0.46 ± 0.09	0.17 ± 0.04	14.1 ± 3.26	0.36 ± 0.08	6.51 ± 1.59	2.34 ± 0.63
90	0.45 ± 0.04	0.12 ± 0.02	14.1 ± 1.72	0.27 ±0.05	6.35 ± 0.54	1.69 ± 0.29
Expected	**0.31**	**0.07**	**15.3**	**0.24**	**4.69**	**1.15**

5.7 Scanning Electron Microscopy

Prior to applying electrocorrosion to valuable samples, examination of the corroded surface of test samples was performed using microscopy. Since optical microscopy did not provide satisfactory detail of the corroded surface, SEM was used. Figures 5.7.1 and 5.7.2 show images of Aluminum 6061 after low power electrocorrosion was applied to the surface. The alloy was corroded for 1 s with a 9 V battery and a cellulose electrode soaked with 3 M NH_4NO_3 in 0.125 M HNO_3 (Fig. 5.7.1). The same spot was then corroded for another 30 s and the sample was imaged again (Fig 5.7.2). At 40x magnification some pitting was observed and is represented by the lighter regions on the left side of the image (indicated by A). At higher magnification (Fig. 5.7.3), it became apparent that the majority of the corrosion occurred at the point of closest contact between the power supply and the metal sample. This area is located on the light

side of the boundary in this image and corresponds to the area of greatest current density in the cellulose that makes contact with the sample. Measurements with a voltmeter indicated that this area with the greatest corrosion corresponded to the lowest resistance between the metal sample and the cellulose. Resistance between the cellulose and the metal sample increased significantly with distance from the point of contact of the cellulose. This coincided with areas on the metal surface with decreasing corrosion. Another interesting feature was that in addition to pitting, there also appeared to be individual grains and clumps of particles breaking apart, or perhaps precipitating, from the surface (indicated by B).

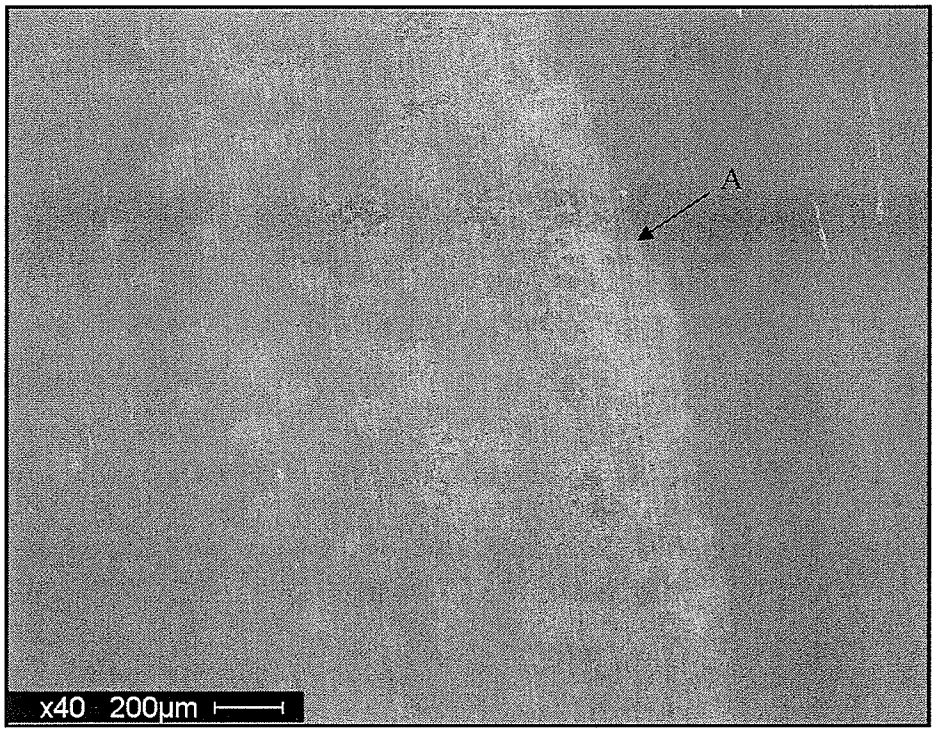

Figure 5.7.1: SEM image of Aluminum 6061 40 x magnification after low power electrocorrosion (1 s).

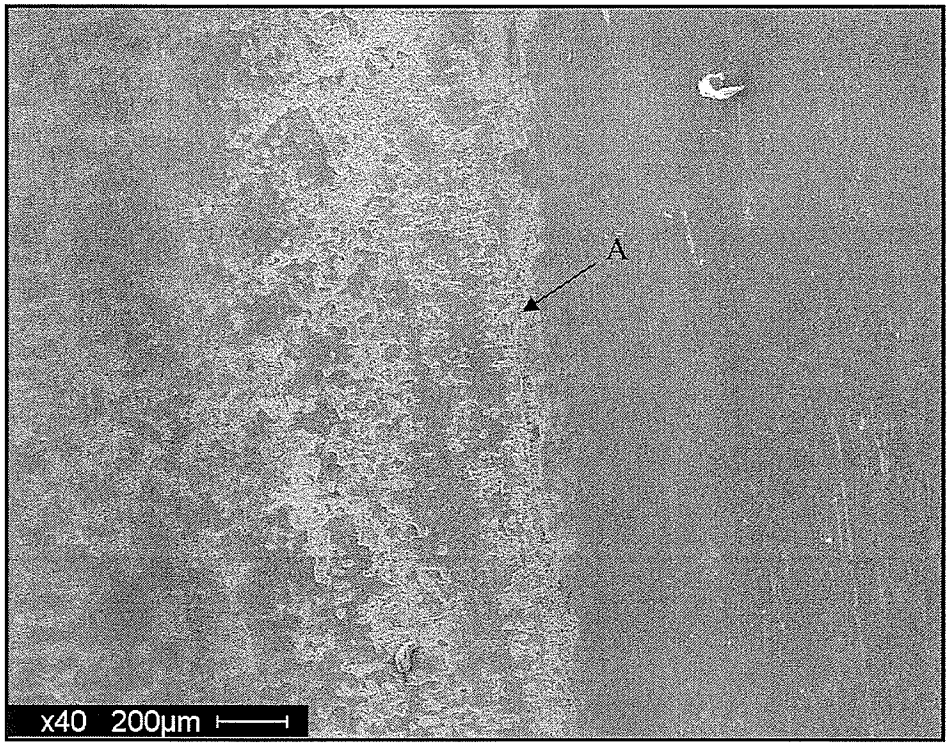

Figure 5.7.2: SEM image of Aluminum 6061 40 x magnification after low power electrocorrosion (30 s).

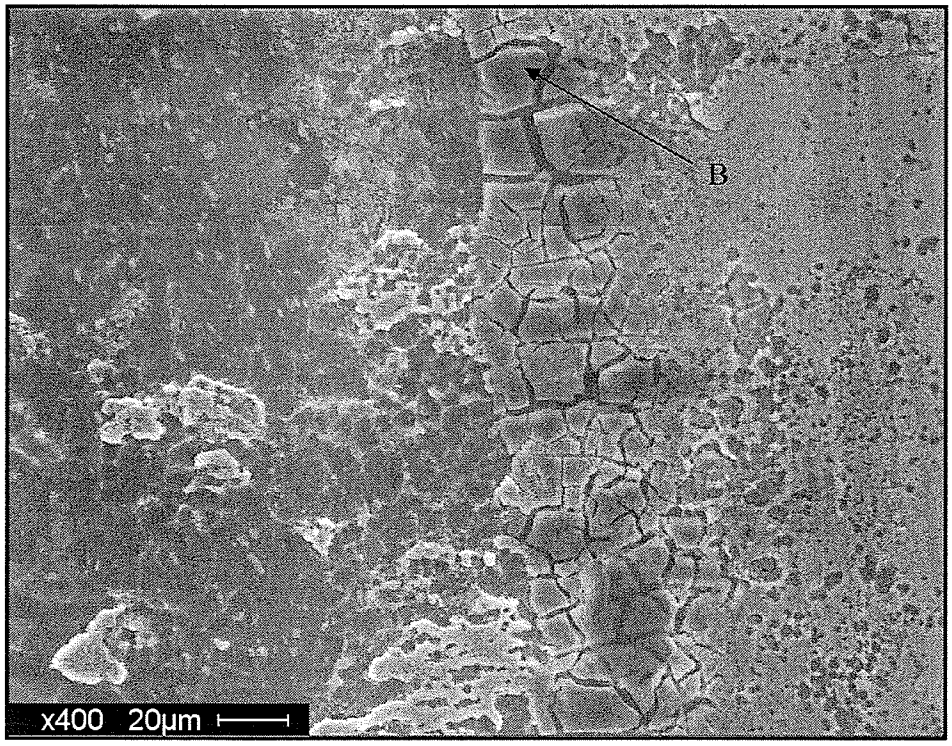

Figure 5.7.3: SEM of Aluminum 6061 400 x magnification after low power electrocorrosion (30 s).

For comparison, an identical experiment was performed using 304L Stainless Steel. This alloy was chosen because, in contrast to the aluminum, it is a harder alloy that might be expected to be less susceptible to corrosion under similar experimental conditions. For shorter time intervals (1 s) very little corrosion was observed on the surface with the unaided eye. At longer time intervals (20 s) some corrosion could be observed; however, the effects of corrosion were much less damaging when compared to Aluminum 6061. Figures 5.7.4 and 5.7.5, showing the pitting (indicated with C) in the 304L Steel after 20 s and 40 s exposures, confirm this observation. In these images the cellulose electrode contact was on the right side and pitting is represented by the lighter regions. The amount of pitting was only marginally increased after 40 s. Pitting of the surface should create a larger surface area, which should also cause the corrosion rate to increase with time. In reality, the rate of corrosion tended to decrease with time, which suggested that formation of stable oxides, evaporation of the aqueous solution and saturation of the cellulose likely had greater effects on the rate of corrosion.

Goltz et al.[105] illustrated surface damage by high power electrocorrosion in solution with SEM images and speculated that, because the surface is damaged by homogeneous porous micro-pitting, electrocorrosion removes metal predominantly by redox type reactions. This is in contrast to spark ablation in solution where the metal is removed primarily as a result of mechanical ablation from the high current. It is interesting to note apart from the work published by Goltz there is little work to illustrate the type of damage that occurs during electrodissolution: However, other research groups do not use electrodissolution for the study of valuable objects. Typically, SEM imaging is conducted to verify the presence of oxide films and passivation layers.

Figure 5.7.4: SEM of 304L Steel 200 x magnification after low power electrocorrosion (20 s).

Figure 5.7.5: SEM of 304L Steel 200 x magnification after low power electrocorrosion (40 s).

5.8 Analysis of a Museum Object

During this study our research group received a metal fork from a local conservator in Manitoba (Parks Canada). The fork had a missing tine and the composition of the alloy was required in order to repair it. Prior to analysis, several experiments were conducted to estimate the fork's composition. The fork did not display magnetic properties, which eliminated Fe as a major component. The fork was also examined under a microscope to confirm that the object was not plated. Images were collected using SEM and energy dispersive XRF (EDXRF) was used for non-destructive analysis of the fork. Analysis by EDXRF indicated it was a Ag-Cu alloy (Figure 5.8.1). Traditional methods for direct, non-destructive, sample analysis such as XRF and SEM/EDXRF lack sensitivity in the lower $\mu g\ g^{-1}$ range[48]. In most cases silver objects, such as utilitarian items, are too large to fit into the sample chambers of these instruments and sensitivity is significantly reduced for portable instruments[48]. Other trace elements may not be detected due to high background induced by electron bombardment. Previously, EDXRF has been applied to the investigation of antique silverware and currency[57,67]. Milazzo et al.[59] investigated quantitative EDXRF for the analysis of ancient metallic objects. They reported two main difficulties. First, the irregular shapes and reliefs required mathematical correction factors. Second, there were no standards available that matched the objects under investigation. They specifically examined coins and decided that representative samples could be made from the original coins and the results can be compared to correct for surface irregularities. They concluded that XRF analysis of coins in this manner would not be practical because the quality of the analytical information did not justify removing samples from the objects. Similarly, for

this investigation the irregular shape and lack of standards eliminated the possibility of quantitative analysis using EDXRF. Therefore, electrocorrosion was used for sample preparation prior to analysis using FAAS, ICP-MS and GFAAS. For this experiment a 9 V potential was applied between the fork and the cellulose electrode, which was soaked with 3 M NH_4NO_3 and 0.125 M HNO_3.

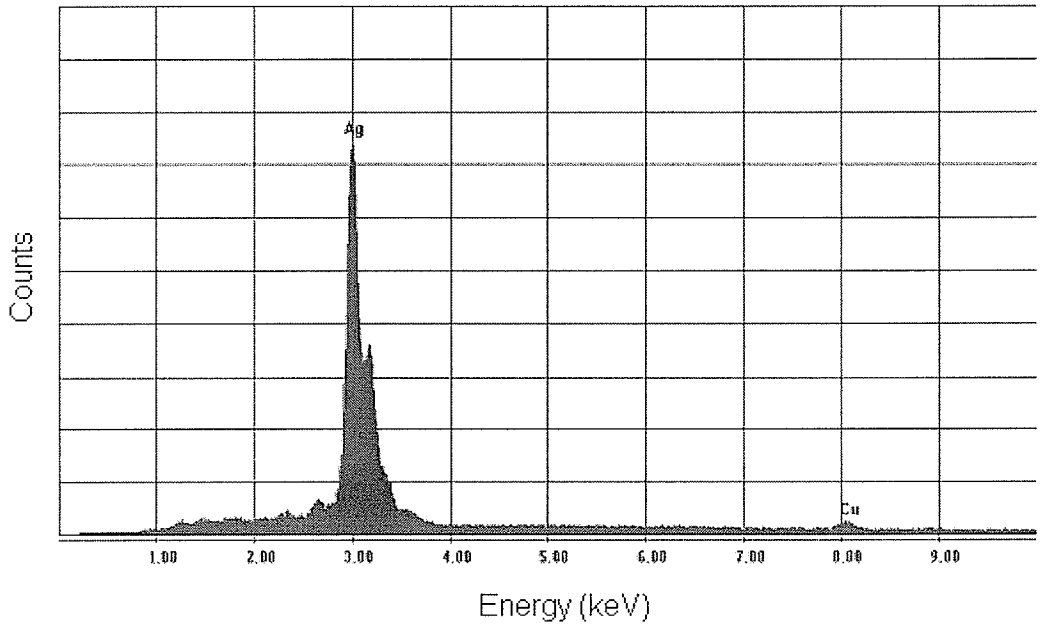

Figure 5.8.1: EDXRF analysis of the fork.

Several literature references state that there are interferences associated with determination of Ag when Cl^- is present in the furnace[106,107]. For example, Sramkova et al.[106] examined signal depression of Ag in the presence of HCl. Bulska and Ortner[108] report that halogens may become intercalated in the graphite furnace at low temperatures. At high temperatures only a portion of these intercalated compounds are removed and the remaining halogens will influence many atomization reactions

especially when halogen solutions are used. For this reason, a furnace that had never been used for samples with a Cl-containing matrix was used for determinations involving Ag in order to avoid potential interferences.

To establish that representative sampling could be achieved with electrocorrosion, a silver alloy that was similar in composition was analyzed. The alloy was purchased locally and was not a reference material, but its composition was determined by obtaining a much larger sample size using acid dissolution with concentrated HNO_3. Acid dissolution is a common method used to confirm results from new sampling methods. For example, Packer et al.[39] used acid digestion to confirm the results of their electrodissolution procedure. The solution was analyzed by FAAS using an external calibration curve prepared with matrix matched standards. To compare the two approaches, this Ag alloy was then analyzed by GFAAS after sample preparation using low power electrocorrosion. The results of this analysis, presented in Table 5.8.1, illustrated the similarity of the ratios of Ag to Cu when samples were prepared using either acid digestion or electrocorrosion. A t-test at the 95% confidence level also confirmed this result statistically.

Table 5.8.1: Analysis of a silver alloy using electrocorrosion and acid digestion.

	Ag (ng)	Cu (ng)	Ratio Ag:Cu
Electrocorrosion (GFAAS)	10 ± 1	2.0 ± 0.5	5 ± 1
Acid Digestion (FAAS)	$20 \times 10^5 \pm 4 \times 10^5$	$40 \times 10^4 \pm 8 \times 10^4$	5 ± 1

n = 8

Table 5.8.2 shows the ratio of Ag to Cu in the fork when electrocorrosion was used for sample preparation. For FAAS an external calibration curve was used and the Ag to Cu ratio was found to be 3.6 ± 0.2. Longer sampling intervals were used which yielded representative samples. This is reflected in the precision of the data. While FAAS gave satisfactory data for Ag and Cu, it lacked the sensitivity required for trace analysis. Therefore, SN-ICP-MS was used to identify trace metals. With this technique, the sample is aspirated as an aerosol using a nebulizer prior to ionization in the ICP. The ions are separated in a mass spectrometer. The ratio of Ag to Cu was found to be 3.8 ± 0.2, which is similar to the results obtained using FAAS.

Table 5.8.2: Analysis of fork of unknown composition using electrocorrosion.

	Ag (ng)	Cu (ng)	Ratio Ag:Cu
FAAS	399 ± 17	111 ± 6	3.6 ± 0.2
SN-ICP-MS	377 ± 12	97 ± 4	3.8 ± 0.2
GFAAS	33 ± 1	13 ± 2	2.6 ± 0.9

n = 8

The most important advantage of using ICP-MS was that the elemental abundance for most of the elements could be obtained by performing a mass scan. The mass scan did not reveal any other major elements; traces of ^{51}V, ^{208}Pb, ^{27}Al and ^{66}Zn were detected but not quantified. One of the limitations of ICP-MS is isobaric interferences. For example, elements such as $^{56}Fe^{+}$, $^{52}Cr^{+}$ and $^{75}As^{+}$ overlap with $^{40}Ar^{16}O^{+}$, $^{40}Ar^{12}C^{+}$ and

$^{40}Ar^{35}Cl^{+}$ respectively. The large sample size requirements for FAAS and ICP-MS are also a disadvantage because of potential damage to the surface. For this reason, the fork was also analyzed using GFAAS, because of the small sample size requirement (< 20 µl) and high sensitivity of this technique. The GFAAS analysis of the fork (Table 5.8.2), gave a ratio of 2.6 ± 0.9 for Ag to Cu. Although this result is lower, the relative standard deviation from the GFAAS analysis is quite large, 34% compared to 5% for both ICP-MS and FAAS. The main reason for the poor precision is likely the small sample size. The results of the analyses by ICP-MS, FAAS and GFAAS overlap within standard deviation. Other metals, such as Al and Pb, were also detected by GFAAS, but not quantified as they were found to be present in trace amounts (< 0.1%).

6.0 CONCLUSIONS

In the absence of a portable XRF, low power electrocorrosion with GFAAS could be a useful alternative to identify metals and alloys. Damage to the surface was minimal when the corrosion was applied for 10 – 30 s. The filter paper was an easily manoeuvred and flexible electrode that could be used for irregularly-shaped or large objects. Solution nebulization ICP-MS provided a mass scan with greater sensitivity than SEM for identifying alloy metals that were present in low concentrations. The drawback of SN-ICP-MS is that it requires a large sample volume and some elements can have spectral interferences. Graphite furnace AAS offers the possibility of determining small quantities of material, which makes it a very powerful technique for detecting trace levels of metals. Successive measurements did not give increasing amounts of Cu indicating that a Ag enriched patina was not present in detectable amounts.

Multiple techniques were used in this study to obtain both quantitative and qualitative information about the unknown composition of the fork. It was possible to use FAAS for this object because a large quantity of material could be removed; however, FAAS and SN-ICP-MS may not be feasible approaches for more valuable objects because of their large sample size requirements and low sensitivity. Although the small sample size requirement for GFAAS solves this problem, a small sample size may not be representative of the sample which can limit the accuracy of a quantitative analysis.

7.0 SUMMARY

The objective of this work was to study microsampling for sample preparation of valuable objects and to enhance the present capabilities by developing minimally-invasive microsampling techniques for metals in alloys and pigments in painted artwork. The microsampling techniques were developed to take advantage of the small sample size requirements and sensitivity of GFAAS. It was advantageous to use multiple complementary spectroscopic approaches to analyze a single sample. The techniques presented in this work were not a replacement for traditional approaches but they were convenient for small museums and archives that did not have direct access to sophisticated analytical equipment.

8.0 REFERENCES

1. Paudyn, A.M.; Smith, R.G. *Fresenius J. Anal. Chem.* **1993**, 345, 695-700.

2. Speed, H.; Oil Painting Techniques and Materials; Dover Publications Inc.: New York, 1987; pp 228-229

3. *Artist's Pigments A Handbook of Their History and Characteristics*; Roy, A.; Oxford University Press: New York, 1993, Vol. 2.

4. *Artist's Pigments A Handbook of Their History and Characteristics*; Fitzhugh, E.W.; Oxford University Press: New York, 1997, Vol. 3.

5. *Artist's Pigments A Handbook of Their History and Characteristics*; Feller, R.L.; Oxford University Press: New York, 1986, Vol. 1.

6. Ciliberto, E.; Spoto, G. in *Modern Analytical Methods in Art and Archeology,* ed. J.D. Winefordner; Chemical Analysis Series; John Wiley and Sons, Inc.: New York, NY, 2000, vol. 155.

7. Lahanier, Ch.; Preusser, F.D.; Van Zelst, L. *Nucl. Instrum. Meth B* **1986**, 14, 1-9.

8. Klockenkamper, R.; von Bohlen, A.; Moens, L. *X-Ray Spectrom.* **2000**, 29, 119–129.

9. Clark, R.J.H. *C. R. Chimie*, **2002**, 5, 7-20.

10. Devos, W.; Moens, L.; von Bohlen, A.; Klockenkamper, R. *Stud. Cons.* **1995**, 40, 153-162.

11. Vittiglio, G.; Janssens, K.; Vekemans, B.; Adams, F.; Oost, A. *Spectrochim. Acta B* **1999**, 541, 1697-1710.

12. Adams, F.; Adriaens, A.; Aerts, A.; De Raedt, I.; Janessens, K.; Schalm, O. *J. Anal. At. Spec.* **1997**, 12, 257–265.

13. Gonsior, B.; Roth, M. *Talanta* **1983**, 30, 385-400.

14. Malmqvist, K.G. *Nucl. Instr. and Meth. in Phys. Res. B* **1986**, 14, 86-92.

15. Johansson, E-M.; Johansson, S.A.E.; Malmqvist, K.G.; Wiman, I.M.B. *Nucl. Instr. and Meth. in Phys. Res. B* **1986**, 14, 45-49.

16. Ortega-Aviles, O.; Vandenabeele, P.; Tenorio, D.; Murillo, G.; Jimenez-Reyes, M.; Gutierrez, M. *Anal. Chim. Acta* **2005**, 550, 164–172.

17. Daniilia, S.; Bikiaris, D.; Burgio, L.; Gavala, P.; Clark, R.J.H.; Chryssoulakis, Y. *J. Raman Spectrosc.* **2002**, 33, 807-814.

18. Andalo, C.; Bicchieri, M.; Bochini, P.; Casu, G.; Galleti, G.C.; Mando, P.A.; Nardone, M.; Sodo, A.; Zappala, M.P. *Anal Chim Acta* **2001**, 429, 279-286.

19. Paternoster, G.; Rinzivillo, R.; Felici, A.; Fronterotta, G.; Nicolais, C.; Piacentini, M.; Scuiti, S.; Venditelli, M. *J. Cult. Heritage* **2005**, 6, 21-26.

20. Janssens, K.; Vittiglio, G.; Deraedt, I.; Aerts, A.; Vekemans, B.; Vincze, L.; Wei, F.; Deryck, I.; Schalm, O.; Adams, F.; Rindby, A.; Knochel, A.; Simionovici A.; Snigirev, A. *X-Ray Spectrom.* **2000**, 29, 73–91.

21. Knapp, G. *Mikrochim acta.* **1991**, 11:445-455.

22. Goltz, D.M.; Hinds, M.; Coombs, J.; Jagdeo. A.; Craig, D. *J. Anal. At. Spectom.* **2002**, 17,395-399.

23. Perez-Jordan, M.Y.; Salvador, A.; delaGuardia, M. *Anal. Lett.* **1998**, 31, 867-877.

24. Chakraborty, R.; Das, A.K.; Cervera, M.L.; delaGuardia, M. *Anal. Lett.* **1997**, 30, 283-303

25. Wen, X.H.; Wu, L.Z.; Zhang, Y.; Chu, Y. *Fresenius J. Anal. Chem.* **1997**, 357, 1111-1115.

26. SenGupta, J.G.; Bertrand, N.B. *Talanta* **1995**, 45, 1947-1957.

27. Fadda, S.; Rivoldini, A.; Cau, I. *Geostand. Newslett.* **1995,** 19, 41-54.

28. Somenath, M.; *Sample Preparation Techniques in Analytical Chemistry,* John Wiley & Sons Inc.: NJ, 2003.

29. Halmos, P.; Borszeki, J.; Gegus, E. *Magy. Kem. Foly.* **1993,** 99, 420-423.

30. Ashley, K. *Electroanalysis.* **1995**, 7, 1-4.

31. Mamba, S.; Kratochvil, B. *Int. J. Environ. Anal. Chem.* **1995**, 60, 295-302.

32. Borszeki, J.; Halmos, P.; Gegus, E. *Talanta* **1994**, 41, 1089-1095.

33. Hinds, M.W.; Littau, S.; Moulinie, P. *Analyst* **1990**, 236, 399-408.

34. Saraswati, R.; Vetter, T.W.; Watters, R.L. *Analyst* **1995**, 120, 95-99.

35. da Silva, J.B.B.; Giacomelli, M.B.O.; de Souza, I.G.; Curtius, A.J. *Talanta* **1998**, 47, 1191-1198.

36. Bendicho, C. *Fresen. J. Anal. Chem.* **1994**, 348, 353-355.

37. Boileau, M.; Goltz, D.; Hinds, M. *Can. J. Anal. Sci. Spec.* **2004**, 49, 185-192.

38. Berglund, B.; Fernando, C. Anal Chim Acta **1990**, 236, 399-408.

39. Packer, A.P.; Gervasio, A.P.G.; Miranda, C.E.S.; Reis, B.F.; Menegario, A.A.; Gine, M.F. *Anal. Chim. Acta,* **2003**, 485, 145-153.

40. Ogle, K.; Weber, S. *J. Electrochem. Soc.* **2002**, 147, 1770-1777.

41. Stansbury, E.E.; Buchanan, R.A. Fundamentals of Electrochemical Corrosion; ASM International, Materials Park: Ohio, 2000.

42. Kondo, H.; Aimoto, M.; Ono, A.; Chiba, K. *Anal. Chim. Acta.* **1999**, 394, 293-240.

43. Bergamin, H.; Krug, F.J.; Zagatto, E.A.G.; Arruda, E.C.; Courinho, C.A. *Anal. Chim. Acta*. **1986**, 190, 177-181.

44. Flock, J.; Ohls, K. *Fresen. Z. Anal. Chem.* **1988**, 331, 408-412.

45. Souza, I.G.; Bergamin, H.; Krug, F.J.; Nobrega, J.A.; Oliveira, P.V.; Reis, B.F.; Gine, M.F. *Anal. Chim. Acta.* **1991**, 245, 211-216.

46. Yuan, D.; Wang, X.; Yang, P.; Huang, B *Anal. Chim. Acta*. **1991**, 243, 65-69.

47. Gervasio, A.P.G.; Luca, G.C.; Menegario, A.A.; Bergamin, H. Anal. Chim. Acta 2000, 405, 213-219.

48. Devos, W.; Moor, C.; Lienemann, P. *J. Anal. At. Spectrom.* **1999**, 14, 621-626.

49. Anglos, D.; Couris, S.; Fotakis, C. A*ppl. Spectrosc.* **1997**, 51, 1025-1030.

50. Castillejo, M.; Martin, M.; Oujja, M.; Silva, D.; Torres, R.; Domingo, C.; Garcia-Ramos, J.V.; Sanchez-Cortes, S. *Appl. Spectrosc.* **2001**, 55, 992-998.

51. Melessanaki, K.; Papadakis, V.; Balas, C.; Anglos, D. *Spectrochim. Acta Part B* **2001**, 56, 2337-2346.

52. Burgio, L.; Clark, R.J.H.; Firth, S. *Analyst*, **2001**, 126, 222-227.

53. Bicchieri, M.; Nardone, M.; Russo, P.A.; Sodo, A.; Corsi, M.; Cristoforetti, G.; Palleschi, V.; Salvetti, A.; Tognoni, E; *Spectrochim. Acta Part B* **2001**, 56, 915-922.

54. Burgio, L.; Clark, R.J.H.; Sheldon, L.; Smith, G. *Anal. Chem.* **2005**, 77, 1261-1267.

55. Colao, F.; Fantoni, R.; Lazic, V.; Spizzichino, V. *Spectrochim. Acta Part B* **2002**, 57, 1219–1234.

56. Ferrero, J.L.; Roldan, C.; Ardid, M.; Navarro, E. *Nucl. Inst. Meth. Phys. Res. A* **1999**, 422, 868-873.

57. Wei, C.L.; Fan, Q.M.; Liu, Y.W.; Li, D.L. *X-Ray Spectrom.* **1990**, 25, 138-139.

58. Swann, C.P.; Caspi, S.; Carlson, J. *Nucl. Instrum. Meth B* **1999**, 150, 571-575.

59. Milazzo, M.; Cicardi, C. *X-Ray Spectrom.* **1997**, 26, 211-216.

60. Moens, L.; Devos, W.; Klockenkamper, R.; von Bohlen, A. *J. Trace and Microprobe Tech.* **1995**, 13, 119-139.

61. Aloupi, E.; Karydas, A. G.; Paradellis, T. *X-Ray Spectrom.* **2000**, 29, 18–24.

62. Fairman, B.; Hinds M.W.; Nelms, S.M.; Penny, D.M.; Goodall, P. *J. Anal. At. Spectrom.* **2000**, 15, 1606-1631.

63. Civici, N.; Demko, O.; Clark, R.J.H. *J. Cult. Heritage* **2005**, 6, 157-164.

64. Van Hooydonk, G.; De Reu, M.; Moens, L.; Van Aelst, J.; Milis, L. *Eur. J. Inorg. Chem.* **1998**, 639-634.

65. Klockenkamper, R.; von Bohlen, A. *J. Anal. At. Spectrom.* **1992**, 7, 273-279.

66. Hajivaliei, M.; Garg, M.L.; Handa, D.K.; Govil, K.L.; Kakavand, T.; Vijayan, V.; Singh, K.P.; Govil, I.M. *Nucl. Instrum.Meth. B* **1999**, 150, 645-650.

67. Linke, R.; Schreiner, M.; Demortier, G.; Alram, M. *X-Ray Spectrom.* **2003**, 32, 373-380.

68. Abraham, M.H.; Grime, G.W.; Northover, J.P.; Smith, C.W. *Nucl. Instrum.Meth. B* **1999**, 150, 651-655.

69. Gyodi, I.; Demeter, I.; Hollos-Nagy, K.; Kovacs, I.; Szokefalvi-Nagy, Z. *Nucl. Instrum. Meth B* **1999**, 150, 605-610.

70. Demortier, G.; Fernandez-Gomez, F.; Ontalba Salamanca, M.A.; Coquay, P. *Nucl. Instrum. Meth. B* **1999**, 158, 275-280.

71. Demortier, G.; Morciaux, Y.; Dozot, D. *Nucl. Instrum. Meth. B* **1999**, 150, 640-644.

72. Swann, C.P.; Fleming, S.J. *Nucl. Instr. Meth. Phys. Res. B* **1990**, 49, 65-69.

73. Swann, C.P. *Nucl. Instr. Meth. Phys. Res. B* **1982**, 197, 237-242.

74. Fleming, S.J.; Swann, C.P. *Nucl. Instr. Meth. Phys. Res. B* **1992**, 64, 528-537.

75. Swann, C.P. *Nucl. Instr. Meth. Phys. Res. B* **1995**, 104, 576-583.

76. Swann, C.P. *Nucl. Instr. Meth. Phys. Res. B* **1997**, 130, 289-296.

77. Weber, G.; Guillaume, J.; Strivay, D.; Garnir, H.P.; Marchal, A.; Martinot, L. *Nucl. Instr. Meth. Phys. Res. B* **2002**, 12, 724-729.

78. Panczyk, E.; Ligeza, M.; Walis, L. *J. Radioanal. Nucl. Chem.* **2000**, 244, 543-551.

79. Zaidi, J.H.; Waheed, S.; Ahmed, S. *J. Radioanal. Nucl. Chem.* **1999**, 242, 259-263.

80. Carrot, F.; Dardenne, C.; Deschamps, N.; Lahanier, C.; Revel, G. *J. Radioanal. Nucl. Chem.* **1993**, 168, 287-296.

81. Clark, R.J.H. *Chem. Soc. Rev.* **1995**, 24, 187-196.

82. Edwards, H.G.M.; Farwell, D.W.; Perez, F.R.; Villars, S.J. *J. Raman Spectrosc.* **1999**, 30, 307–311.

83. Gardiner, D.J.; Bowden, M.; Graves, P.R.; Thompson, R.B. Phil. Trans. R. Soc. Lond. A **1986**, 320, 295-306.

84. Clark, R.J.H.; Gibbs, P.J. *J Raman Spectrosc.* **1997**, 28, 99-103

85. Clark, R.J.H.; Gibbs, P.J.; Seddon, K.R.; Brovenko, N.M; Petrosyan, Y.A. *J Raman Spectrosc.* **1997**, 28, 91-94.

86. Gilbert, B.; Denoel, S.; Weber, D.; Allart, D. *Analyst*, **2003**, 28, 1213-1217.

87. Bell, I.M.; Clark, R.J.H.; Gibbs, P.J. *Spectrochim Acta Part A* **1997**, 53A, 2159-2179.

88. Bruni, S.; Cariati, F.; Consolandi, L.; Galli, A.; Gugliemi, V.; Ludwig, N.; Milazzo, M. *Appl. Spec.* **2002**, 56, 827-833.

89. Best, S.P.; Clark, R.J.H.; Withnall, R. *Endeavor.* **1992**, 16, 66-73.

90. Davey, R.; Gardiner, J.B.; Singer, B.W.; Spokes, M. *J. Raman Spectrosc.* **1994**, 25, 53-57.

91. Byrne, J.P.; Lamoureux, M.M.; Chakrabarti, C.L.; Ly, T.; Gregroire, D.C. *J. Anal. Atom. Spectrom.* **1993**, 8, 599-609.

92. Goltz, D.M.; Coombs, J.; Marion, C.; Cloutis, E.; Gibson, J.; Attas, M.; Choo-Smith, L.P.; Collins, C. *Talanta* **2004**, 63, 609-616.

93. Goltz, D.M.; Charleton, K.; Cloutis, E.; Grinberg, P.; Collins, C. *J. Anal. At. Spectrom.* **2007**, 22, 140-146.

94. Coedo, A.G.; Dorado, M.T.; Padilla, I.; Alguacil, F.J. *J. Anal. At. Spectrom.* **1998**, 13, 1193–1197.

95. Vandenabeele, P.; Edwards, H.G.M.; Moens, L. *Chem. Rev.* **2007**, 107, 675-686.

96. Guineau, B. *J. Forens. Sci.* **1984**, 29, 471-485.

97. Resano, M.; Verstraete, M.; Vanhaecke, F.; Moens, L. *J. Anal. At. Spectrom.* **2001**, 16, 1018–1027.

98. Venable, J.D.; Langer, D.; Holcombe, J.A. *Anal. Chem.* **2002**, 74, 3744–3753.

99. Maass, E.; Kempf, R. *Agnew. Chem.* **1923**, 36, 293-297.

100. Goshorn, J.H.; Black, C.K. *Ind. Eng. Chem.* **1929**, 21, 348-349.

101. Eibner, E. *Chem. Ztg.*, **1923**, 47, 13-16.

102. Gettens, R.J.; Kuhn, H.; Chase, W.T.; *"Lead White", in Artists' Pigments- A Handbook of Their History and Characteristics*, A. Roy, Oxford University Press: New York, NY, 1993, vol. 2, pp. 367.

103. Goltz, D.M.; Kostic, G.; Reinfelds, G. *Talanta* **2000**, 52, 1131-1138.

104. Abd El Aal, E.E. *Corr. Sci.* **2003**, 45, 641-658.

105. Goltz, D.M.; Boileau, M.; Plews, I.; Charleton, K.; Hinds, M.W. *Spectrochim Acta Part B* **2006**, 61, 817-823.

106. Sramkova, J.; Kotrly, S.; Peknikcova, M. *Analysis* **1999**, 27, 839-846.

107. Kumar, S.; Sanglikar, M.B.; Shaikh, M.S.; Sudersanan, M. *Indian J. Chem. Technol.* **2004**, 11, 170-177.

108. Bulska, E.; Ortner, H.M. *Spectrochim. Acta Part B*, **2000**, 55, 491-499.